DTU Library

Aeroelastic model field validation and performance state estimation of wind turbine active flaps

Gamberini, Andrea

Link to article, DOI:
10.11581/DTU.00000290

Publication date:
2023

Document Version
Publisher's PDF, also known as Version of record

SIEMENS Gamesa
RENEWABLE ENERGY

DTU Wind and Energy Systems

Aeroelastic model field validation and performance state estimation of wind turbine active flaps

Andrea Gamberini

PhD Thesis

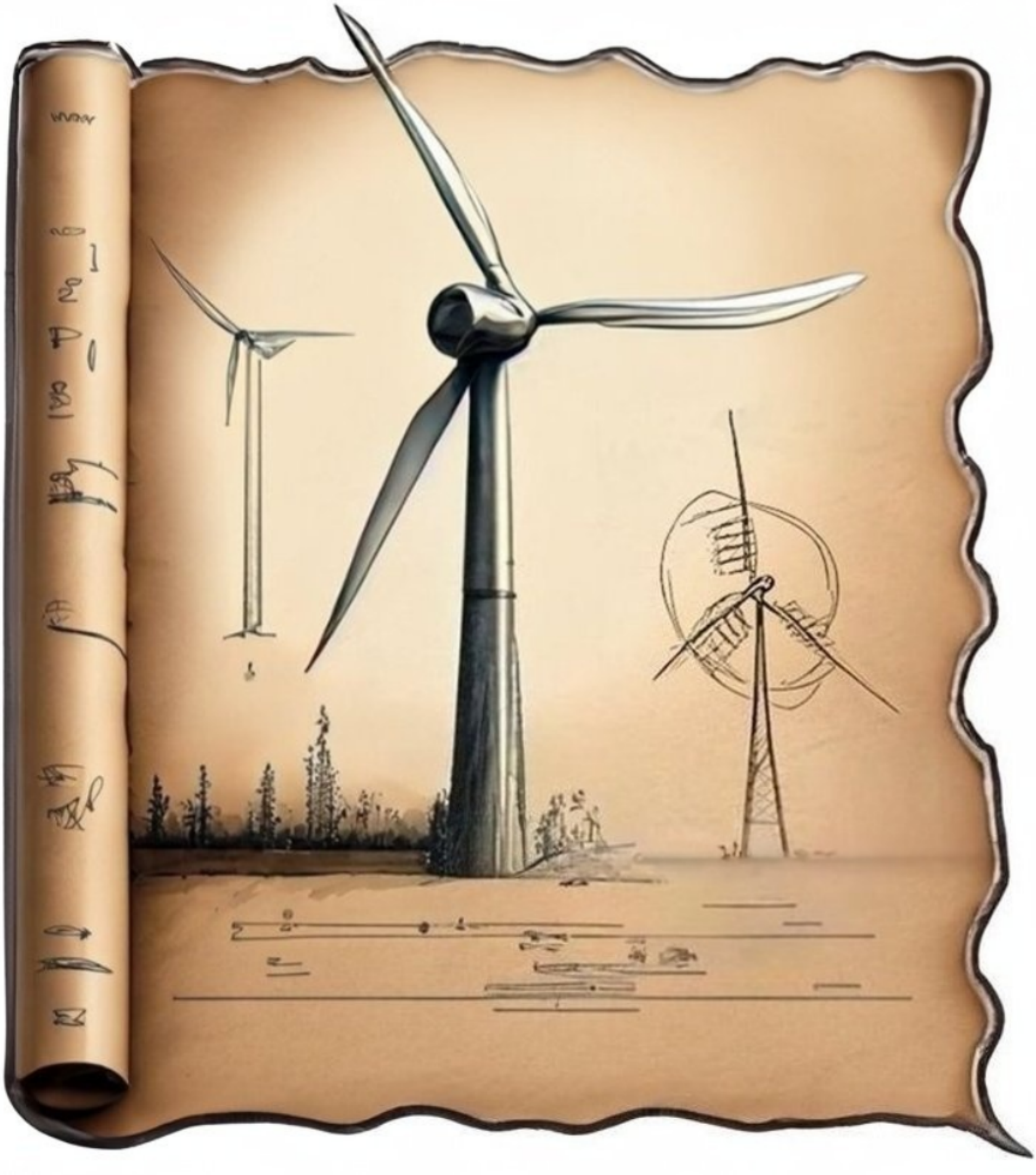

Aeroelastic model field validation and performance state estimation of wind turbine active flaps

PhD Thesis
July, 2023

By
Andrea Gamberini

Cover photo: Photo create with the AI tool Adobe Firefly (Beta Version) from Adobe Inc. and manually edited.

Published by: DTU Wind and Energy Systems, DTU Risø Campus, Frederiksborgvej 399, Building 1144000 Roskilde, Denmark
`wind.dtu.dk`

DOI: 10.11581/DTU.00000290

Preface

This thesis presents a summary of research findings on the field validation of aeroelastic models of active trailing edge flaps for wind turbines and the estimation of the flap performance state with machine learning. The thesis consists of a collection of papers integrated with a supplementary study.

The present thesis was submitted to the Department of Wind and Energy Systems at the Technical University of Denmark (DTU) as part of the requirements for earning a Doctor of Philosophy in Wind Energy. The research was conducted within the framework of an Industrial PhD project, a collaboration between Siemens Gamesa Renewable Energy (SGRE) and DTU. SGRE, Danmarks Innovationsfond (Case no. 9065-00243B), and Otto Mønsteds Fond (application file no. 22-70-0210) funded the project.

The research was conducted from May 2020 to July 2023 at the Design and Validation team of the SGRE Turbine Load and Control section, wherein I was employed, and at the Airfoil and Rotor Design Section of the DTU Wind Turbine Design division. Furthermore, a collaboration with the Chair of Structural Mechanics and Monitoring at the Department of Civil, Environmental and Geomatic Engineering of the Swiss Federal Institute of Technology in Zürich (ETH Zurich) allowed a three-months research visit at ETH Zurich that resulted in one of the publications presented in this thesis.

The research was supervised by Alejandro Gomez Gonzalez (SGRE) and Thanasis Barlas (DTU) with co-supervision from Helge Aagaard Madsen (DTU) and Bjarne Skovmose Kallesoee (SGRE).

Andrea Gamberini

Abstract

This PhD thesis summarizes research findings on the field validation of aeroelastic models of active trailing edge flaps for wind turbines and on the estimation of the flap performance state with machine learning.

As wind energy plays a fundamental role in achieving a climate-resilient future, the wind power sector must advance wind turbine technology to cope with the escalating demand. A promising technology is active trailing edge flaps, devices placed at the trailing edge of the wind turbine blades to control the local aerodynamic forces acting on the blades. They have the potential to control and reduce wind turbine loads while enhancing overall performance. As the aeroelastic modeling has a fundamental role in the design of wind turbines, the accuracy and reliability of active flap aeroelastic models are paramount for the design soundness of commercial wind turbines equipped with active flaps. The active flap aeroelastic models have been only limitedly validated, mainly due to the scarcity of full-scale experimental data. Therefore, more validation is needed to fully integrate active flaps in the design of commercial wind turbines. This integration also requires the development of systems to detect, monitor, and quantify any potential fault or performance degradation of the flap system to avoid jeopardizing the wind turbine's safety and performance.

The aims of this industrial PhD thesis are *the validation of the aeroelastic models of active trailing edge flap with full-scale field measurements* and *the development of an application to estimate the performance state of the active flap system*. To achieve them, two research questions are investigated: 1) *Do the aeroelastic models of wind turbines equipped with active trailing edge flaps estimate accurately and reliably the loads and behavior of an actual commercial-scale wind turbine?* and 2) *Can a machine learning model estimate the flap performance states of a wind turbine to improve the reliability of the active flap system design?*

Regarding the first question, a major outcome of this industrial PhD thesis is the validation of the flap models implemented in the two cutting-edge aeroelastic codes BHawC and HAWC2 with full-scale measurement data from a commercial wind turbine (4.3 MW rated power, 120 m diameter, 20 m flap length). The validation shows that the flap models accurately and reliably model the impact of the flap actuation on the wind turbine's aerodynamic, loading, and operational parameters. The study also highlights that modeling and tuning the flap actuator and the flap aerodynamic properties are crucial elements for correctly modeling active flaps in wind turbine aeroelastic codes. Finally, the study suggests that the capability of the active flap model to estimate the unsteady effect on the aerodynamic forces due to the flap motion would become relevant at high flap actuation frequencies.

Regarding the second question, an application has been developed for the first time to estimate the flap performance states for asymmetric faults. The application has remarkable precision, higher than 90%, and is based on a simple and well-proven machine learning technique. Furthermore, it requires only input signals commonly available on commercial wind turbines, simplifying its possible implementation in future wind turbines.

The findings of this PhD research project have significantly contributed to increasing the accuracy and reliability of the active flap aeroelastic tools and the capability of detecting active flap system faults. These contributions are essential milestones to enable the safe and reliable design of future wind turbines equipped with active flaps.

Resumé

Denne ph.d.-afhandling opsummerer forskningsresultater om feltvalidering af aeroelastiske modeller af aktive bagkant-flaps til vindmøller samt estimering af operationelle tilstande af bagkant-flaps ved hjælp af maskinlæring.
Da vindenergi spiller en afgørende rolle for at opnå en klimarobust fremtid, må vindenergisektoren udvikle vindmølleteknologien for at kunne klare den stigende efterspørgsel. En lovende teknologi er aktive bagkantsklapper, der placeres ved bagkanten af vindmøllevingerne for at kontrollere de lokale aerodynamiske kræfter, der virker på vingerne. De har potentiale til at kontrollere og reducere vindmøllens belastninger og samtidig forbedre den samlede ydeevne. Da den aeroelastiske modellering spiller en fundamental rolle i designet af vindmøller, er nøjagtigheden og pålideligheden af de aeroelastiske modeller for aktive flaps altafgørende for, om designet af kommercielle vindmøller med aktive flaps er forsvarligt. De aeroelastiske modeller for aktive flaps er kun blevet valideret i begrænset omfang, primært på grund af manglen på eksperimentelle data i fuld skala. Derfor er der behov for mere validering for fuldt ud at integrere aktive flaps i designet af kommercielle vindmøller. Denne integration vil også kræve udvikling af systemer til at opdage, overvåge og kvantificere enhver potentiel fejl eller forringelse af flap-systemets ydeevne for at undgå at bringe vindmøllens sikkerhed og ydeevne i fare.
Formålet med denne erhvervs-ph.d.-afhandling er *valideringen af de aeroelastiske modeller for aktive bagkant-flaps med feltmålinger i fuld skala* og *udviklingen af en applikation til estimering af aktive flap-systemers operationelle tilstande*. For at opnå dem undersøges to forskningsspørgsmål: 1) *Estimerer de aeroelastiske modeller af vindmøller udstyret med aktive bagkant-flaps nøjagtigt og pålideligt belastningerne og opførslen af en kommerciel vindmølle?* og 2) *Kan en maskinlæringsmodel estimere flap-systemers operationelle tilstande for en vindmølle for at forbedre pålideligheden af designet af det aktive flap-system?*
Hvad angår det første spørgsmål, er et vigtigt resultat af denne erhvervs-ph.d.-afhandling valideringen af de flap-modeller, der er implementeret i de to førende aeroelastiske koder BHawC og HAWC2, med måledata i fuld skala fra en kommerciel vindmølle (4.3 MW nominel effekt, 120 m diameter, 20 m flap-længde). Valideringen viser, at flap-modellerne nøjagtigt og pålideligt modellerer flap-aktiveringens indvirkning på vindmøllens aerodynamiske, belastnings- og driftsparametre. Undersøgelsen fremhæver også, at modellering og indstilling af flap-aktuatoren og flaps aerodynamiske egenskaber er afgørende elementer for korrekt modellering af aktive flaps i vindmøllers aeroelastiske koder. Endelig tyder undersøgelsen på, at den aktive flap-models evne til at estimere den ustabile effekt på de aerodynamiske kræfter på grund af flap-bevægelsen vil blive relevant ved høje flap-aktiveringsfrekvenser.
Hvad angår det andet spørgsmål, er der for første gang blevet udviklet et program til at estimere operationelle tilstande for flaps for asymmetriske fejl. Programmet har en bemærkelsesværdig præcision, højere end 90 %, og er baseret på en enkel og velafprøvet maskinlæringsmetode. Desuden kræver den kun indgangssignaler, der er almindeligt tilgængelige på kommercielle vindmøller, hvilket forenkler dens mulige implementering i fremtidige vindmøller.
Resultaterne af dette ph.d.-forskningsprojekt har bidraget væsentligt til at øge nøjagtigheden og pålideligheden af de aeroelastiske værktøjer til aktive flaps og evnen til at opdage fejl i aktive flap-systemer. Disse bidrag er vigtige milepæle for at muliggøre et sikkert og pålideligt design af fremtidige vindmøller udstyret med aktive flaps.

Acknowledgements

I would like to express my sincere appreciation and gratitude to all the people who have helped and supported me during the long and challenging journey of my PhD.

First and foremost, I thank Anna, my partner and my rock, for having supported and *"sopported"* me from the moment the crazy idea of starting a PhD came into my mind until today. Without her, I would have never started and managed to conclude this industrial PhD.

I want to thank my supervisors, Alejandro Gomez Gonzales and Thanasis Barlas, for their constant presence, invaluable guidance, and unwavering support. Their patience, expertise, and constant feedback have shaped my research experience. I would also like to thank my co-supervisors, Helge Aagaard Madsen, Bjarne Skovmose Kallesoee, and Peder Bay Enevoldsen, for their broad and overall perspective that has greatly helped the development of the PhD project.

I will be forever grateful to the Siemens Gamesa Turbine Loads sections that financially supported this project. I am thankful to the managers, Kristian Markussen, Rune Rubak, and Vladimir Leble, that believed in me and in this PhD, granting me their trust and the freedom to run this project independently. Also, I cannot forget all the SGRE colleagues and friends that helped me in overcoming the everyday challenges of modeling and running simulations (Peter Fisker Skjoldal, Anders Kjaer Lomholt, and Jose Fernandez Bolanos Maya), acquiring measurement data (Soeren Markkilde Pedersen, Soeren Olesen Furbo, and Srikar Vulli), solving tool and random IT issue (Josep Fernandez Gausach and Thomas Kofoed Nielsen), managing the prototype controller (Gustav Hoegh, Daniel Sale, and Anthony Brill), investigating ML application (Laurent Beaudet, Bastien Duboc and Paul Deglaire), decrypting the blade structural properties (Gregory Hesler) and keeping the positive mood in the office (Oscar Ramirez, Albert Meseguer Urban, Erik Steven Hauger, Morten Hansen, and Anders Riis Soerenses).

I am grateful to the Airfoil and Rotor Design Section of the DTU Wind Turbine Design division for providing me with the support and resources to utilize the HAWC2 code. In particular, I would like to thank Riccardo Riva and Georg Pirrung for their help in dealing with the HAWC2 modeling challenges.

I am also grateful to Eleni Chatzi for hosting me at the Chair of Structural Mechanics and Monitoring of the Department of Civil, Environmental, and Geomatic Engineering of the Swiss Federal Institute of Technology in Zürich (ETH Zurich). During this research visit, I significantly enhanced my knowledge of machine learning applications for wind turbines, bringing a valuable addition to my thesis, mainly thanks to the formidable assistance of Imad Abdallah and Gregory Duthé.

I am extremely thankful to my family, back in Italy, and my friends scattered in Europe, that had always supported me, my passions and interests, even if they brought me far from them.

Finally, I would like to acknowledge all the fellow PhD students I have met along the way. Their support in the daily struggles of the PhD life and their valuable tips and tricks have helped me navigate the academic world without sinking. I want to especially thank Heloisa Mendonca, the best buddy I could have hoped for in the industrial PhD "basement" office, Jenna Iori, the advocate of the industrial PhD cause, and Kristian Ladefoged Ebbehoej, my student companion at SGRE. They significantly enriched this PhD journey.

To all of you, thank you for being a part of my PhD adventure and helping me accomplish this important milestone.

Contents

Chapter 1

Introduction

1.1 Motivation

Climate change poses unprecedented risks to our planet's ecosystem. The path to overcoming the climate change crises requires immediate greenhouse gas emissions reductions in all sectors, aiming to reach global net zero CO2 emissions by early 2050 [1]. Wind energy is a fundamental player in achieving a climate-safe future, as up to a third of global energy is expected to be generated from wind power alone in 2050 [2]. The wind power industry faces unprecedented challenges to meet the growth the climate targets require while providing secure and affordable energy supplies [3]. The challenges include a paradigm shift in electrical grid design, and advancements in manufacturing and logistics, meanwhile maintaining the ongoing decrease in the cost of wind energy.

Following the historical trend, the need for wind energy cost reduction will lead to an increase in the size of wind turbines. This increase requires significant and continuous technology developments in several fields: new materials with higher mechanical properties and lower weight, new blade designs optimizing the balance between performance and weight, improved efficiency in generation and power transmission, and advanced control techniques to mitigate the wind turbine loading in all environmental conditions. Active flaps are a promising technology for controlling and reducing wind turbine loads meanwhile enhancing performance.

Active Trailing Edge Flaps (ATEF) are devices placed at the trailing edge of the wind turbine blades that actively adjust the shape or curvature (or both) of the blade section profile to control the aerodynamic forces acting on the blades. This concept originated from flaps and ailerons used in airplanes and has been proposed in several designs, ranging from a rigid aerodynamic surface hinged to the blade trailing edge near the blade tip to multiple flexible trailing edge flaps spread along the outer part of the blade (Figure 1.1). Compared to the standard pitch control, where the whole blade is rotated to control the wind turbine, active flaps enable a distributed control that modifies the aerodynamic loading as needed at different blade sections.

The contribution of active trailing edge flaps to the wind turbine design has been extensively investigated, as described in details in Section 2.1, showing significant potential reduction of extreme [4] and fatigue loads [5] on several wind turbine components. Such load reductions can be leveraged to decrease the components' cost [6] or to increase the energy production of the wind turbines[7]. Despite these potential benefits, the design of an active flap system faces several challenges. The ATEF design has to combine the requirements of a system located in the external outer part of the blade (lightweight, protection from lightning, lifetime comparable to that of wind turbines, and low and easy maintenance) with the complexity of precisely and safely controlling the aerodynamic loading in several locations of the blade. Until

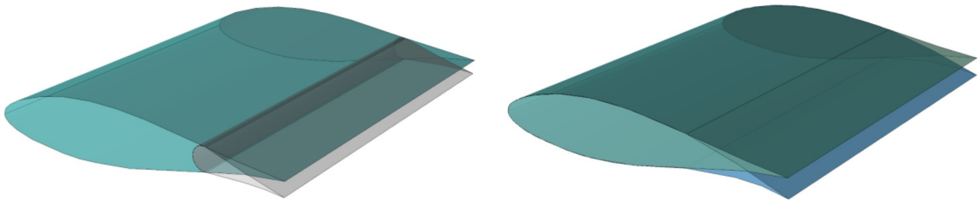

Figure 1.1: Examples of Trailing edge flap designs: rigid hinged flap on the left, flexible morphing flaps on the right.

now, these challenges have overcome the active flap benefits and prevented active flap system applications on commercial wind turbines. However, future wind turbine designs face even more significant challenges [8] that active flaps can contribute to overcoming. The growing size, weight, and flexibility of wind turbine blades, along with the increasing variability of the blade's inflow conditions in a rotation [8], are significant challenges for the conventional pitch control system. Active flaps are an additional control feature to keep blade deflections and wind turbine loading within design limits while ensuring optimal energy production. They have the potential to directly address the variable inflow conditions on the blade, achieving faster and more precise control of the blade loading and deflection than the pitch system. Simultaneously, they can contribute to decreasing the loading at the blade root and then reducing the action required from the pitch control, decreasing the wear and tear of the pitch system.
The challenges in the active flap system design also have implications for the testing and validation of this technology, raising the already significant monetary investment needed for experimental testing activities. As a result, measurements to validate the models of active flap systems, especially for full-scale validation, are limited. Consequently, research efforts to investigate the benefits of active flaps and optimize their design rely on models with limited validation, increasing the uncertainty of the research results. As the accuracy and reliability of flap models are paramount for the soundness of future design and studies concerning active flap systems, this PhD project focuses on the field validation of the active trailing edge flap models.

1.2 Background and research questions of the Industrial PhD project

The current design of commercial wind turbines heavily relies on low-fidelity aeroelastic models for the estimations of design loads and the tuning of the wind turbine controller [9]. However, the aeroelastic models have shortcomings and uncertainties, and their validation with measurements is needed in the certification of commercial wind turbines [10] [11]. To integrate the active trailing edge flap in the design of commercial wind turbines, the accuracy and reliability of their aeroelastic models is paramount for the soundness of the wind turbine design. Furthermore, any integration of new components has to ensure a safe and reliable continuous operation of the wind turbine for the entire turbine lifetime. This mandatory condition requires additional components or systems to detect, monitor, and quantify any potential fault or performance degradation of the flap system that may jeopardize the safety and performance of the wind turbine.
Siemens Gamesa Renewable Energy (SGRE) investigated, developed, and tested an active trailing edge flap system within INDUFLAP2 [12] and VIAs [13] projects. These projects were conducted in collaboration with DTU Wind and Energy Systems Department (DTU), one of the universities leading the research on active flap systems.
The primary objective of this industrial PhD thesis is *the validation of the aeroelastic models*

of active trailing edge flap with full-scale field measurements, validation based on measurements provided by SGRE that will enable the reliable design of future wind turbines equipped with active flap. Furthermore, this industrial PhD thesis aimed to *develop an application to estimate the performance state of the active flap system*, identifying the cases of flaps with faults or with reduced performance.
To achieve the PhD objectives, two key research questions were formulated:

Question 1: *Do the aeroelastic models of wind turbines equipped with active trailing edge flaps estimate accurately and reliably the loads and behavior of an actual commercial-scale wind turbine?*

For a reliable design, the aeroelastic model of the active trailing edge flaps has to correctly estimate the impact of the flap on the aerodynamic properties and loading of the wind turbine. The model has to properly simulate the properties of the flap when it is in a stationary state, like stationary activation, and the aeroelastic dynamic response to the flap motion, whether it is a single-step actuation or a continuous cyclic motion. Chapter 2 provides a description of the validations for two distinct ATEF aeroelastic models. These models vary in complexity and are implemented in two different aeroelastic codes. The validations are based on a field campaign conducted on a 4.3 MW wind turbine prototype equipped with an active trailing edge flap on one blade. Additionally, the investigation of the behavior of the ATEF models for high-frequency cyclic activation provides suggestions on the setup for future validation studies aiming to identify the limit of application of the studied active flap models.

Question 2: *Can a machine learning model estimate the flap performance states of a wind turbine to improve the reliability of the active flap system design?*

Active flaps have several promising applications for reducing wind turbine fatigue and extreme loads as well as increasing wind turbine energy production. All these applications assume that the active flap system can operate with the expected performance for the entire wind turbine lifetime or be repaired when its operability is compromised. Hence, a reliable wind turbine design requires one or more systems to measure or estimate the flap system's performance state, also called health state. A simple but reliable system to estimate the active flap health state, suitable for industrial application and based on machine learning, is described in Chapter 4.2.

1.3 List of articles

In this PhD thesis, objectives and research questions have been addressed in the form of four peer-reviewed articles, either published or under review, and an additional comparative study. The publications are as follows:

- Andrea Gamberini, Alejandro Gomez Gonzalez & Thanasis Barlas. 2022. **Aeroelastic model validation of an Active Trailing Edge Flap System tested on a 4.3 MW wind turbine**. Journal of Physics. Conference Series.
  Published in contribution to the TORQUE 2022 conference in Delft, the Netherlands.
- Andrea Gamberini, Thanasis Barlas, Alejandro Gomez Gonzalez & Helge Aagaard Madsen. 2023. **Validation of aeroelastic dynamic model of Active Trailing Edge Flap system tested on a 4.3 MW wind turbine**. Wind Energy Science. Preprint.
  Under review at the Wind Energy Science journal
- Alejandro Gomez Gonzalez, Peder Enevoldsen, Andrea Gamberini, Athanasios Barlas & Helge Aagaard Madsen. 2023. **Operational experience during a four year test**

program of active flaps on a wind turbine blade. Proceeding of 10th ECCOMAS Thematic Conference on Smart Structures and Materials.
Accepted at the 10th ECCOMAS Thematic Conference on Smart Structures and Materials in Patras, Greece

- Andrea Gamberini & Imad Abdallah. 2023. **Active Trailing Edge Flap System fault detection via Machine Learning**. Wind Energy Science. Preprint.
Under review at the Wind Energy Science journal

1.4 Outline of thesis

The thesis is structured as follows. Chapter 2 focuses on validating the aeroelastic ATEF models, addressing the first research question introduced in Section 1.2. Chapter 3 focused on the estimate of the flap performance states via machine learning, answering the second research question. The outline of the first chapter is as followings. A background is introduced, followed by outlines of the relevant thesis articles and the description of an additional study yet to be published. Finally, the research question is answered in the summary section. The second chapter presents an introduction to the topic, followed by the research's main findings. Finally, the research question is answered in the summary section. Chapter 4 contains concluding remarks and suggestions for future work. The associated research articles are provided in the appendices.

Chapter 2

Validation of aeroelastic active flap models

In the following chapter, an investigation into the first topic of the thesis work, field validation of aeroelastic models of active trailing edge flap, is presented. A background is introduced, followed by outlines of the relevant thesis articles and the description of an additional study yet to be published. Finally, the research question is answered in the summary section.

2.1 Background

Actively controlled flaps located at the blade trailing edge (ATEF) of wind turbine blades are one of the promising technologies to mitigate the challenges arising from the steady growth of the wind turbine size. The integration of ATEF in the wind turbine design has been extensively investigated, from the pioneering works of [14], [15], [16], [17],[18] and [19], to some of the more recent research by [20], [4], [21] and [5]. These studies concluded that ATEF has the potential to reduce extreme and fatigue loads, consequently decreasing the cost of wind turbine components [6] or increasing the energy production of wind turbines[7].

As the current design of commercial wind turbines relies on low-fidelity aeroelastic models, ATEF models have been developed in most of the aeroelastic codes, like HAWC2 [22], FAST [23] or Bladed [24]. The simplest ATEF models compute the steady two-dimensional (2D) aerodynamic properties of the flap blade sections. These properties are calculated at every time step for the instantaneous value of flap angle (or flap state) by interpolating a set of pre-generated 2D steady aerodynamic properties provided for a range of flap angles (or flap states). The aeroelastic code then utilizes the calculated ATEF steady properties to compute the unsteady aerodynamics using the same methodology applied to the remaining blade sections. Instead, more advanced ATEF models directly compute the unsteady 2D aerodynamic properties of the flap profiles, including the unsteady aerodynamic effect of the flap motion.
ATEFlap is the active flap aerodynamic model [25] implemented in HAWC2, the aeroelastic code developed by DTU. ATEFlap is an "engineering" model that provides the unsteady aerodynamic forces and pitching moments for a 2D airfoil section undergoing arbitrary motion and flap deflection. The unsteady dynamics are captured both in attached and stalled flow conditions. ATEFlap describes the dynamic of the forces related to the flow separation and the effects of the vorticity shed into the wake under the assumption of plane wake separation, trailing edge stall separation, and uniform upwash velocity along the chord. The ATEFlap model is obtained by merging the Gaunaa's model for thin airfoil undergoing camber line deformation in potential flow [26], corrected by finite thickness profiles [27], with the Beddoes-Leishmann

type dynamic stall model for a rigid airfoil presented by [28]. The inputs the model requires are steady lift, drag, and moment coefficients as a function of the angle of attack and of the flap angle, pre-processed by the Preproc ATEFlap tool to avoid discontinuities in the dynamic stall model.
To integrate the active trailing edge flap in the design of commercial wind turbines, the reliability of their aeroelastic models is paramount for the soundness of the wind turbine design. However, the experimental validation of these models and their potential load reduction are limited, especially at commercial full-scale. The main reasons are the significant monetary investment needed for experimental testing activities, especially for publicly funded research, and the lack of a reliable active flap system design that limits the interest from the private sector. An approach to partially assess the validity of the aeroelastic codes is to compare them against higher fidelity models, like lifting-line free vortex wake models or Computational Fluid Dynamic (CFD) models. Unlike the aeroelastic "engineering" models, these higher fidelity models directly resolve the three-dimensional flow around the blade geometry, including root and tip regions. This capability increases the models' accuracy, even with some limitations [29], but requires a much higher computational cost than the "engineering" models.
The ATEFlap model was validated [30] by comparing it with two 2D high-fidelity models: EllipSys 2D, a CFD solver, and the viscous-inviscid interaction panel code developed at the National Technical University of Athens. For a NACA 64-418 profile with a 10% chord flap, the ATEFlap model accurately reproduces the dynamics of the unsteady lift force, both for pitch and flap deflection variations, in the condition of attached flow. However, the model slightly overestimated the drag force and aerodynamic moment in response to changes in the angle of attack while closely matching the results for flap deflection. At high angles of attack, due to the complex flow condition derived from the stall, ATEFlap is less accurate but still captures the dynamic characteristics of the flow separation. The validation also highlighted the importance of a reliable input for the steady aerodynamic, which discrepancies might impact the dynamic response at a higher degree than differences in the unsteady force models. Another validation [29] based on the experimental data of the DU95W180 airfoil with a 20% chord flap confirmed the presence of an error in the prediction of unsteady flow effects, more significant for regions of separated flow where the lift variation due to flap oscillation tend to be overestimated.
On a blade, the motion of the flap impacts both the shed and the trailed vorticity. When the flap section moves, additional vorticity is trailed in the wake from its edges, inducing an additional downwash or upwash along the whole blade span. At the same time, the change in flap angle causes a change in the bound circulation at the flap location that generates shed vorticity with an opposed sense of rotation, vorticity that also induces an additional downwash or upwash. These unsteady and viscous three-dimensional (3D) aerodynamic effects significantly reduce the lift amplitude and hysteresis loop due to flap motion compared to the 2D condition [31].
To investigate the impact of the 3D effects on the ATEF aeroelastic models, extensive code-to-code comparisons were performed in [32] and [33]. In the investigation, HAWC2 with ATEFlap was compared with higher fidelity models, including free-wake lifting line (GENUVP) and fully resolved CFD models (MaPFlow and FLOWer). The study concluded that the BEM models fail to accurately replicate the distribution of local thrust and in-plane forces in the proximity of the flap edges because they neglect the 3D effects originated by the shed and the trailed vorticity. The local trust force is overestimated in the flap area, especially near the flap edges, and underestimated in the blade area in the proximity of the flap. The tangential forces are instead consistently overestimated. However, when the oscillating frequency is 1P or lower, these BEM models reasonably estimate the impact of an oscillating flap on the integrated overall thrust, providing a reasonable estimation of the flap impact in the innermost blade

sections. This result can be attributed to the compensation of the over-predicted flap impact in the flap region by the under-predicted impact in the blade regions near the flap edges. At high wind speed (19 $\mathrm{ms}^{-}1$), where the loading of the blade is dominated by the lift increase and the 3D effects due to induced velocity and drag are less intense, the BEM model accuracy improves, but it decreases with increased flap activation frequency. In conclusion, HAWC2 with ATEFlap can still be considered a reliable design tool if the active flap is operated at high wind speed, where most of the currently developed controller operates, at a low activation frequency.
The limitations of BEM models in the design of the flaps can be overcome if the missing 3D vorticity effects can be accounted for with appropriate corrections. The Near Wake model [34] [35] available in HAWC2 (HAWC2_NW) is a simplified lifting line model for the wake in the vicinity of each blade. It can efficiently compute the detailed steady and unsteady induction from the first part of the trailed vorticity behind the individual rotor blades. The trailed vorticity is computed dynamically between all the aerodynamic sections on the blade; thus, the model can capture the vorticity trailed from the edges of the flaps. In the code-to-code validations [32] and [33], HAWC2_NW can accurately predict the local and global impact of the flap on the thrust force for both low and high wind speeds. The provided amplitudes of the sectional thrust force in the middle of the flap section are reduced while the flap influence extends to the blade sections adjacent to the flap edges. The prediction of the driving force is also improved, reproducing the fundamental physical mechanisms of the 3D flow and matching the amplitude variation for 1P flap activation.
The code-to-code validation allows to partially assess the accuracy and reliability of the BEM aeroelastic model. However, more is needed to validate the ATEF model fully. As the CFD calculations still present limitations [29], experimental measurements are necessary to verify that the calculated behavior of the aerodynamic forces reflects reality. Validation of the ATEF subsystem has been carried out through a variety of experimental methods, including wind tunnel tests [36] and outdoor rotating rig experiments [37] [38]. In recent investigations, 3D laboratory-scale tests were performed at the TU Berlin's large wind tunnel on BeRT, a research turbine of 3 m diameter rotor equipped with ATEF on each blade. These tests aimed to assess the ability of different controllers utilizing trailing edge flaps in reducing fatigue [39] and extreme flapwise blade root bending moments [40] while also providing valuable datasets for future validation of numerical models. Regarding full-scale validation, only three field tests have been reported so far. These tests include the Sandia field test conducted on a Micon 65/13 turbine with a capacity of 115 kilowatts [41], the DTU and Vestas test on a V27 turbine with a capacity of 225 kilowatts [42], and the Siemens Gamesa Renewable Energy (SGRE) and DTU tests performed on an SWT-4.0-130 (4.0 MW) turbine as part of the INDUFLAP2 project [37]. While these field tests confirmed the potential of active flaps in controlling aerodynamic loads, they also highlighted the need for further development and validation of aeroelastic ATEF models.

To address the lack of full-scale validation of active flap, from 2019 to 2022, SGRE and DTU carried out the Validation of Industrial Aerodynamic Active Add-ons (VIAs) project [13]. As part of this project, in the Høvsøre Test Centre on the West coast of Jutland, an active trailing edge flap was installed on a single blade of the 4.3 MW SGRE prototype (PT) wind turbine with a 120 m rotor diameter (left picture of Figure 2.2). The active flap system, detailed described by [13], consisted of a 20 meters long flap placed on the blade trailing edge between 64% and 98% of the blade radius, actuated pneumatically by a hose that was connected to a pneumatic supply system located in the hub. A remotely programmable control regulated the pressure in the hose via a pressure valve located in the hub. The displacement of the flap was regulated by the air pressure within the hose, where an increase in pressure corresponded

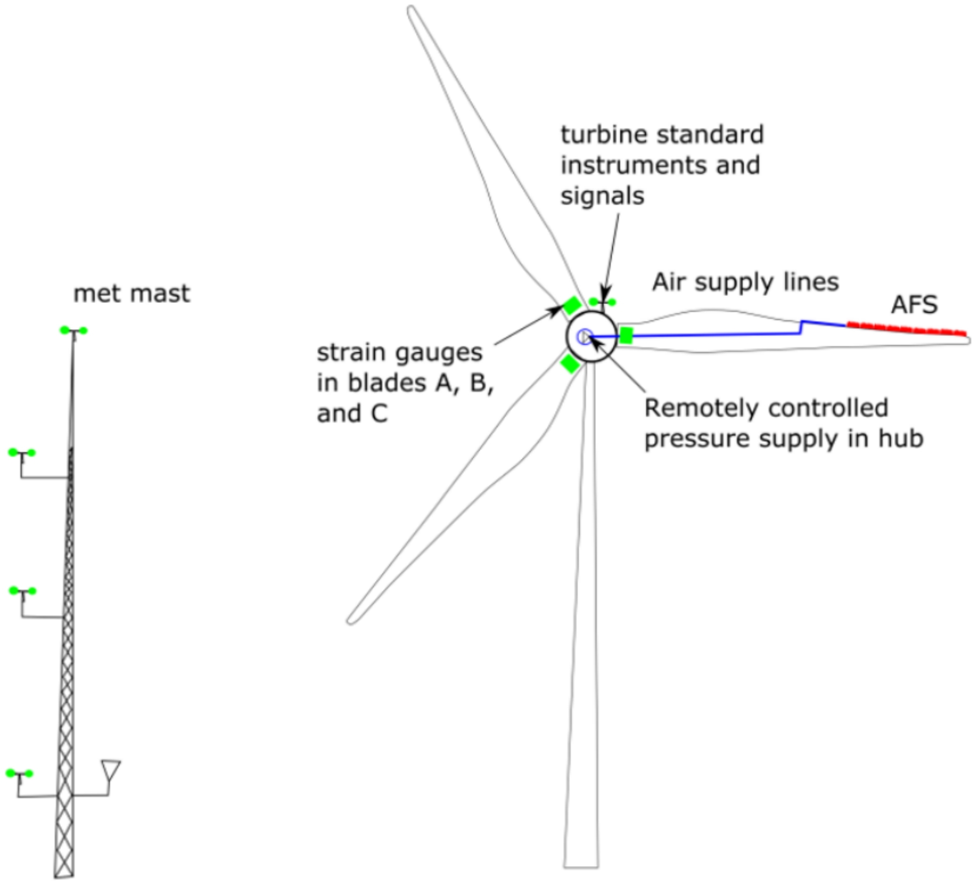

Figure 2.1: Schematic representation of ATEF and instrumentation setup [43].

to an increase in the flap deflection. The deflection of the flap increased the curvature of the profile section, leading to an increase in aerodynamic lift. The left picture of Figure 2.3 shows the lift coefficient for a 21% thickness profile with flap not active (black line) and flap active (red dotted line). A data acquisition system continuously logged PT operational parameters, such as power, pitch, and rotor speed, the pressure at the pressure valve, and the flapwise and edgewise bending moments of all three blades provided by strain gauges located in the blades at 3 m from the root. Atmospheric and wind conditions were instead provided by a met mast located approximately 2.5 D west of the PT. A schematic representation of the ATEF system and the instrumentation setup is shown in Figure 2.1.

In June 2020, an inflow and pressure measurement system was temporarily added to the PT at 50 meter from the hub flange. The measurement system, developed by DTU, measured the aerodynamic properties at the middle section of the ATEF, as described in [45] and showed in the central photo of Figure 2.2. In the same period, two couples of small plastic fins and a camera were briefly installed near the pressure belt location to analyze the ATEF deflection visually (top right photo of Figure 2.2). From May 2020 to February 2021, extensive testing of the active flap was conducted with different actuation strategies and flap actuation pressure. These field tests provided the measurement data necessary for the validation activities performed in this PhD project.

The validation of the ATEF aeroelastic models focused on two different aeroelastic codes:

- **BHawC** [46] is the aeroelastic engineering tool based on BEM developed internally by

Figure 2.2: Left photo: Active trailing edge flap of the SGRE PT installed in Høvsøre (DK). Central photo: Installation of the flyboard and pressure belt in June 2020. Bottom right photo: Close look at the flyboard and the pressure belt. Top right photo: Camera and fins installed to measure the flap deflection. Photos courtesy of SGRE and DTU [44].

SGRE. It includes a Flap Module modeling the steady aerodynamic and the actuator system of the flap.

- **HAWC2** is the aeroelastic engineering tool developed by DTU. Based on BEM, it models the unsteady aerodynamics associated with the active flaps with the Beddoes-Leishman type ATEFlap dynamic stall model. Furthermore, with the Near Wake model enabled, HAWC2 can compute the detailed steady and unsteady induction from the first part of the trailed vorticity behind the individual rotor blades.

The validation process is inspired by the IEC61400-13 guideline [10]. It is performed by comparing the PT measurements with the BHawC and HAWC2 simulation results, where environmental conditions (mean wind speed, mean wind direction, TI, mean wind shear, mean air density) measured on the site are replicated into the simulations setup. The validation consists of three different steps:

1. **Stationary validation**: aims to validate the impact of the stationary flap activation on the PT loads and operative parameters. It requires the initial tuning of the HAWC2 and BHawC models of the PT and allows the identification of the stationary differences between the two aeroelastic codes and their ATEF models.

2. **Dynamic validation**: aims to validate the dynamic response of the blade loads and aerodynamic lift due to the flap activation and deactivation. Based on the results of the stationary validation, it also requires the tuning of the actuator model to match the flap motion's dynamic properly.

3. **Impact of flap unsteady aerodynamic**: investigates how the impact of the unsteady aerodynamics due to flap motion (detailed modeled in the ATEFlap model) evolves as the flap operative condition change. The study compares HAWC2 with ATEFlap and BHawC results for increasing flap activation frequency. Flap activation conditions at which the BHawC and HAWC results diverge could become the target for future flap

model validations.

The remaining content in this chapter is structured as follows. In Section 2.2, the stationary validation is described. Initially, the validation of the BHawC and HAWC2 models with flap not active is described, also focusing on the differences between the results of the two models. Afterward, the validation of the impact of the stationary flap activation computed with the two different aeroelastic codes is presented. Section 2.3 described the dynamic validation. Initially, the tuning of the actuator model is described. Afterward, the validation of the aerodynamic lift transient at the flap's middle section is presented. Finally, the validation of the dynamic of the flap actuation impact on the blade root loads is described. Section 2.4.1 investigates flap operative conditions at which the impact of the unsteady aerodynamics due to flap motion becomes significant and can be validated via measurements. Section 2.5 proposes the setup for future validation of active flap aeroelastic models maturated from experience gained in the previous validation steps. Finally, concluding remarks are made in Section 2.6.

2.2 Stationary validation

This section summarises the research articles titled:
***Aeroelastic model validation of an Active Trailing Edge Flap System tested on a 4.3 MW wind turbine** [47] (See Appendix Article 1).*
***Operational experience during a four year test program of active flaps on a wind turbine blade** [43] (See Appendix Article 3).*

This study validates the ATEF aeroelastic models of the HAWC2 and BHawC codes for the flap in stationary activation and deactivation states. The validation relies on the portion of the VIAs measurement campaign run between May 2021 and February 2022 on the 4.3 MW wind turbine prototype installed in Høvsøre (DK) and equipped with an active flap on one of its blades. In those nine months, the PT operated in normal power production with the flap alternating 10 minutes of constant activation (AFOn) to 10 minutes of constant deactivation (AFOff). Four different pressure levels of flap activation were tested. For the validation, the measurements are filtered to include only normal operation and wind data measurements unaffected by nearby wind turbines' wake or significant wind direction changes. Furthermore, periods with malfunctioning of the ATEFS, the met mast wind sensor, or load sensors are excluded. Among the remaining measurements, only the activation pressure level 3 case has sufficient data for the aeroelastic model validation. The total number of 10 minutes measurements binned per mean wind speed for AFOff and AFOn at pressure level 3 are shown in Table 2.1, limited to the wind speeds with at least ten measurements.

The BHawC model of the PT was provided by SGRE, together with the aerodynamic properties of the active flap of the 21% thickness profile measured in a wind tunnel test. From these properties, the impact of flap activation on other blade profiles was derived, as summarized in Figure 2.3. The HAWC2 model is developed and tuned to match the structural and aerodynamic properties of the BHawC model. Furthermore, it integrates the same controller of the BHawC model. The ATEFlap model is used with the Near Wake model not active. The two models are initially compared for constant wind speeds between 3 to 20 $\mathrm{m\,s^{-1}}$. This

Wind speed [m/s]	7	8	9	10	11	12	13	14	15	16	Total
# AFOff measurements	100	79	56	67	76	77	50	65	36	19	625
# AFOn measurements	15	14	17	19	11	15	25	13	16	15	160

Table 2.1: Number of measurements binned per mean wind speed for AFOff and AFOn at pressure level 3.

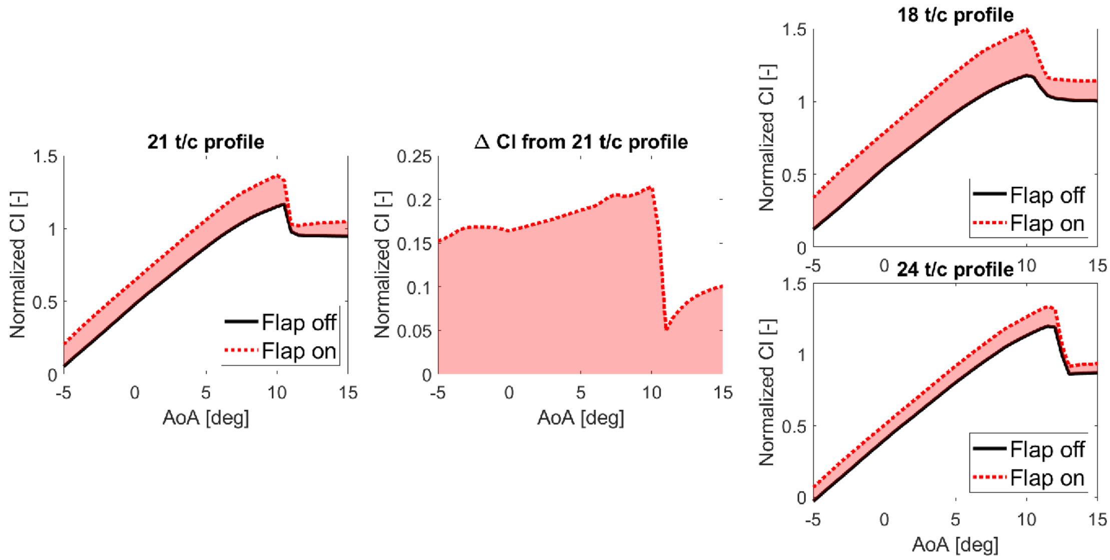

Figure 2.3: Left: Normalized Cl curve of the 21% thickness profile with flap not active (black) and flap active (red dotted line). Center: ΔCl from 21% thickness profile due to flap activation. Right: Normalized Cl curve of 18% (Top) and 24% (Bottom) thickness profile with flap active (red dotted line) obtained by adding the scaled ΔCl from 21% thickness to the curves with flap not active (black lines) [44].

steady-state comparison aims to define the baseline differences between the two aeroelastic tools before including the ATEF models. It also investigates how the differences evolve when the ATEF is included with the active or inactive flap.

The validation with field data is inspired by the IEC61400-13 guideline [10], following the so-called One-to-One approach (O2O). In this approach, every 10 minutes of measured data are reproduced with a 10 minutes simulation where the simulation setup mirrors the measured mean environmental conditions (mean wind speed, mean wind direction, turbulence intensity, mean wind shear, mean air density) and flap state (AFOff or AFOff). The 10 minutes statistics (mean, std, max) of WT operational parameters and blade loads are then binned as a function of the wind speed. The binned value of measurements and simulations are compared for model validation. The same turbulent wind field is recreated in the corresponding aeroelastic simulations of HAWC2 and BHawC to minimize the source of uncertainties in the aeroelastic models' comparison.

The key contributions from the presented article are as follows:

- The BHawC and HAWC2 models of the PT are in good agreement for steady-state simulations (mean power ±1%, mean rotor speed ±0.1 rpm, and mean pitch angle ±0.2 deg). Without ATEF models, HAWC2 provides slightly higher blade root moments (+2% mean and +3% max flapwise, +2% max edgewise). With ATEF models, the difference between flapwise bending moment slightly increases (+3% mean and +3% Max when AFOff, +4% mean, and +4% max when AFOff); meanwhile, edgewise loads are unaffected.

- The BHawC and HAWC2 simulations are in good agreement with the PT measurements (mean power ±3%, mean rotor speed ±0.3 rpm, and mean pitch angle ±0.1 deg), see Figure 2.4a for the power comparison. The simulations slightly overestimate the flapwise bending moment at the blade root (BHawC: +2% both mean and max. HAWC2 +5% mean and +4% max)

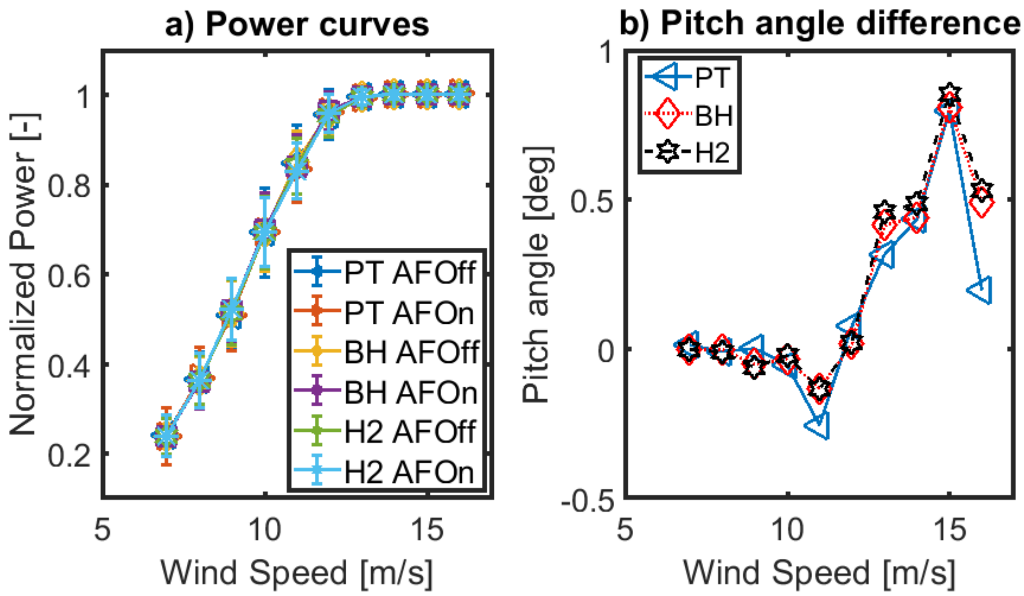

Figure 2.4: a) Power curves comparison. b) Pitch angle differences due to ATEF activation.

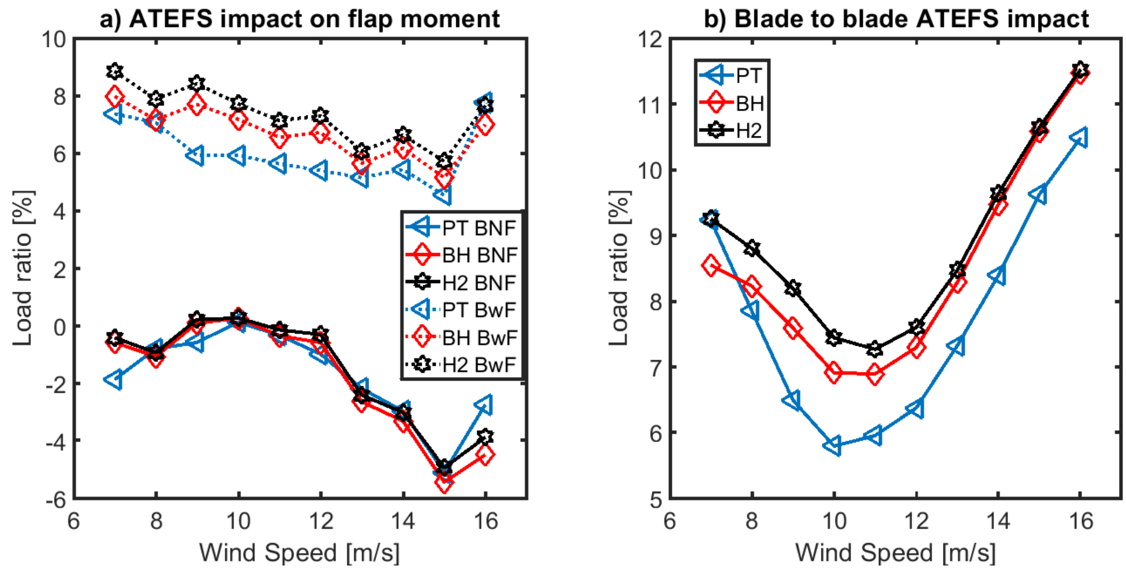

Figure 2.5: a) Variation of flap bending moment on the blade with flap (BwF) and on the blades without flap (BNF) due to ATEF activation measured on the prototype (PT) or simulated with BHawC (BH) and HAWC2 (H2). b) Blade to Blade load variation due to ATEF activation.

- The ATEF models of the two aeroelastic codes well captured the impact of the flap activation on the PT operative conditions, like the increase of pitch angle operated by the controller to balance the increase in torque due to the flap activation, see Figure 2.4b. Also, the impact on the flapwise bending moment is accurately reproduced on the blades without flap and on the blade with flap (Figure 2.5a), with the aeroelastic codes slightly overestimating the increase on the blade with flap (BHawC: +0.5% mean, 1% max. HAWC2: +1% mean, +2% max). A detailed blade-to-blade load increase on the flapwise bending moment due to flap activation is shown in Figure 2.5b.

2.3 Dynamic validation

*This section summarises the research article titled: **Validation of aeroelastic dynamic model of Active Trailing Edge Flap system tested on a 4.3 MW wind turbine** [44] (See Appendix Article 2).*

This study describes the validation of the dynamic response of the ATEF aeroelastic models of the HAWC2 and BHawC codes to the flap actuation. The study relies on the same HAWC2 and BHawC models and setups validated in Section 2.2. In addition, the HAWC2 with Near Wake model enabled (HAWC2_NW) is also added to the comparison. For the validation of the dynamic properties of the aeroelastic ATEF models, the modeling and tuning of the flap actuator system are crucial, as the actuator dynamic directly impacts the simulated flap motion and the related dynamic of the aerodynamic properties. The flap actuator model is included in the AETF aeroelastic model of the BHawC and HAWC2 codes, as shown in Figure 2.6. The actuator model covers the flap pneumatic system controlling the flap and the flap structure itself, providing the output flap deflection resulting from the input flap control signal. The validation consists of three phases. In the first phase, the flap actuator model is

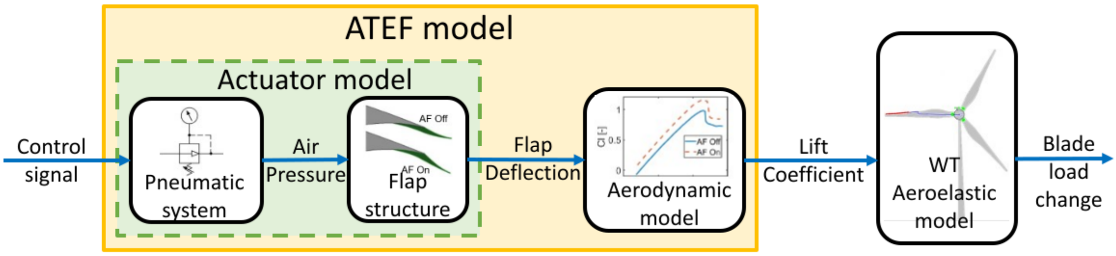

Figure 2.6: Structure of the ATEF aeroelastic model implemented in BHawC and HAWC2

tuned via video-tracking of the flap deflection acquired by a camera installed on the blade with the PT operating at low wind speed.

In the second phase, the aerodynamic flap model is tuned and validated by comparing the simulated average transient of the lift coefficient (Cl) with the transient obtained from the measurements. The Cl measurements were obtained from the one-day long measurement campaign conducted by [45] in June 2020 with an inflow and pressure measurement system temporarily mounted in the middle of the PT flap, see bottom right photo of Figure 2.1. From the measurement campaign, 53 Cl transients are obtained during flap activation and 46 during flap deactivation, all characterized by wind speeds ranging between 4 and 5 m/s. The average measured Cl transients for flap activation and deactivation are then derived. The average simulated Cl transients are obtained for the two aeroelastic codes from 12 simulations run at the constant wind speed of 5 ms^{-}1 with an equally spaced azimuthal angle at which the flap is actuated.

In the last phase, the aeroelastic ATEF models are validated through the blade root load transients measured from October to December 2020 with varying weather conditions. This measurement campaign provided 150 activation and 135 deactivation relevant measurements (almost constant wind speed, wind direction, rotor speed, pitch angle, and yaw angle during flap actuation. No effect of turbulence from nearby wind turbines) distributed between 5 and 20 m s^{-1}. To properly calculate the load transients during flap actuation, the simulation setup has to match the environmental conditions at the PT at the flap actuation time. An approach similar to the O2O is used to compute the model setup. The atmospheric conditions (mean wind direction, mean shear, mean yaw misalignment angle, mean air density) are obtained from a 20 s measurement interval centered on the flap actuation time, time corrected with a time lag due to the distance between the met mast and the PT. The wind speed is estimated from the averaged operational parameters (rotor speed, pitch angle, and generator power). The turbulence is omitted because the validation on the previous step showed that turbulence is not significantly influential on the average transients. The azimuth angle at the time of flap actuation is also matched. A novel approach is introduced to measure the impact of the flap on the blade root loads. This method is derived from the blade-to-blade approach introduced by [48] and computes the difference between azimuthal synchronized flapwise bending moments at the blade root of adjacent blades (MBrM). The transient of MBrM during flap actuation is computed for each measurement and simulation. Afterward, the averaged transient for measurements and simulation are derived and compared.

The key contributions from the presented article are as follows:

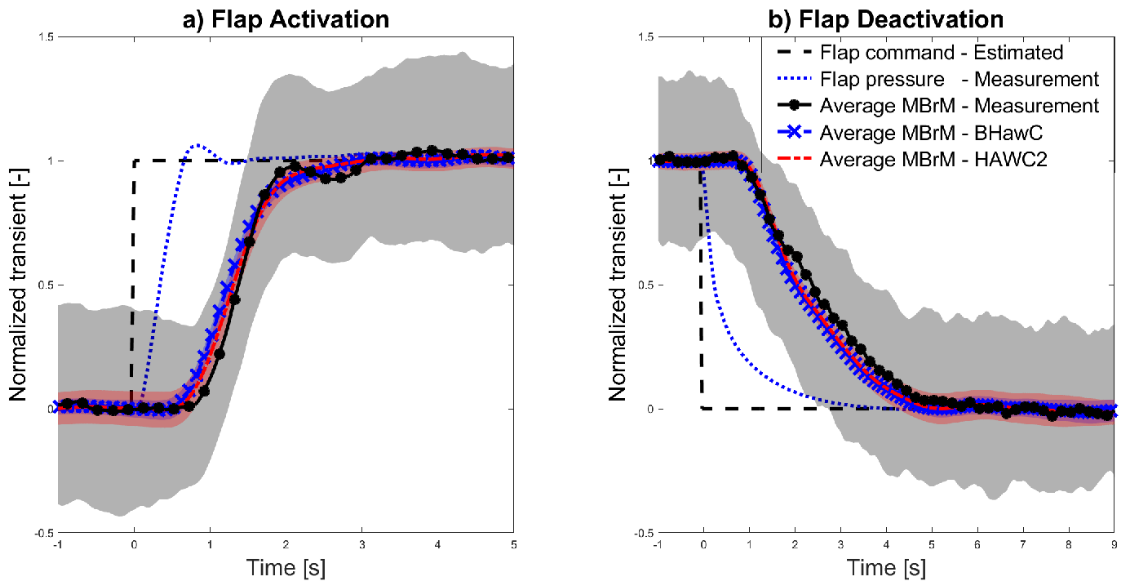

Figure 2.7: Comparison of the normalized averaged b2b blade root bending moment (MBrM) transient obtained from BHawC (blue dashed line with x marker) and HAWC2 (red dash-dotted line) simulations and measurements (black line with asterisk marker) during flap activation (a) and deactivation (b), including an error band of 1 std of the matching colors. The measured flap pressure (blue dotted line) and the estimated flap command (black dashed line) are also included.

- The flap actuator model was tuned to accurately reproduce the flap deflection transient during the 2 s activation and the 5 s deactivation, where the transient time is defined as the time to reach 99% of the steady-state response.
- Azimuthal angle at the flap actuation time highly affects the Cl and MBrM transients. Therefore representative averaged transients are achievable only if there is a balanced distribution of flap actuation azimuthal angle in the dataset.
- Azimuthally synchronized blade-to-blade approach is a reliable method to quantify the impact of flap actuation on blade loads.
- BHawC and HAWC2 aeroelastic ATEF models provide almost identical average transients during flap activation and deactivation, with the main difference caused by a relative time shift lower than 0.04 s between the Cl transients and below 0.1 s between the MBrM transients.

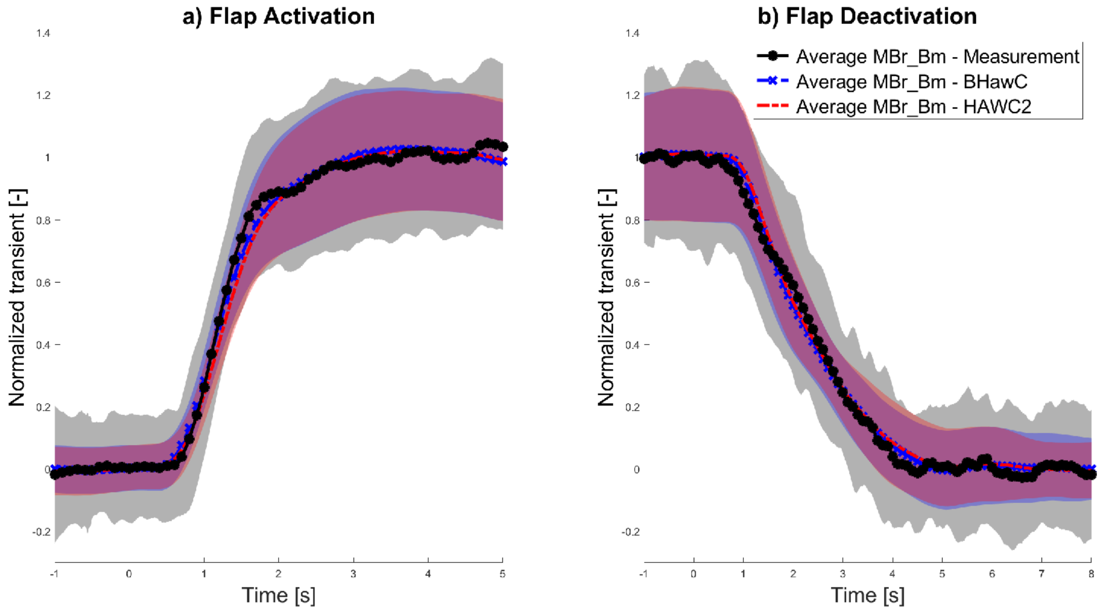

Figure 2.8: Comparison of the normalized averaged b2b blade root bending moment (MBrM) transient obtained from all BHawC (blue dashed line with x marker) and HAWC2 (red dash-dotted line) simulations and all measurements (black line with asterisk marker) during flap activation (a) and deactivation (b), including an error band of 1 std of the matching colors.

- BHawC and HAWC2 average transient of Cl and MBrM are in good agreement with the corresponding measured transients, as shown in Figure 2.7 for the Cl transients and Figure 2.8 for the MBrM transients. The comparisons confirm that the aeroelastic ATEF models provide an accurate and reliable estimation of the impact of the flap on the wind turbine during flap actuation. The maximum differences between the simulated and the measured Cl transient are below 8% of the ΔCl due to flap actuation and within 0.15 s of time shift during flap activation, below 8% ΔCl and within 0.2 s of time shift during flap deactivation. Regarding the MBrM transients, the maximum difference is below 1% of the mean blade load during flap activation and below 1.7% during flap deactivation, with a delay within 0.2 s for both flap actuation cases.
- The Near Wake model does not significantly affect the average transient of Cl and MBrM, with differences below 4% and 1%, respectively. As expected, the Near Wake model reduces the ΔMBrM due to flap activation, even if marginally (2%), improving the agreement with measurement data. This result supports the conclusion from [33] that the trailed vorticity affects marginally integral loads, like MBrM, when the flap actuation frequency is below 1P, like in the validation described in the current paper.
- Some differences between the simulation and measurements emerged, particularly in the shape of the Cl and MBrM transients during flap activation. These differences can originate from an incomplete flap deflection model, imperfect flap aerodynamic properties, or an incomplete aerodynamic model. Additional measurements can clarify the differences causes and improve the accuracy and reliability of the ATEF aeroelastic models.

The flap actuator model tuned in this study is also able to reproduce the deflection pattern of the flap under cyclic activation, as shown in Figure 2.9. The measurements of the cyclic flap deflection were obtained in the same campaign that provided the data for the single actuation model tuning.

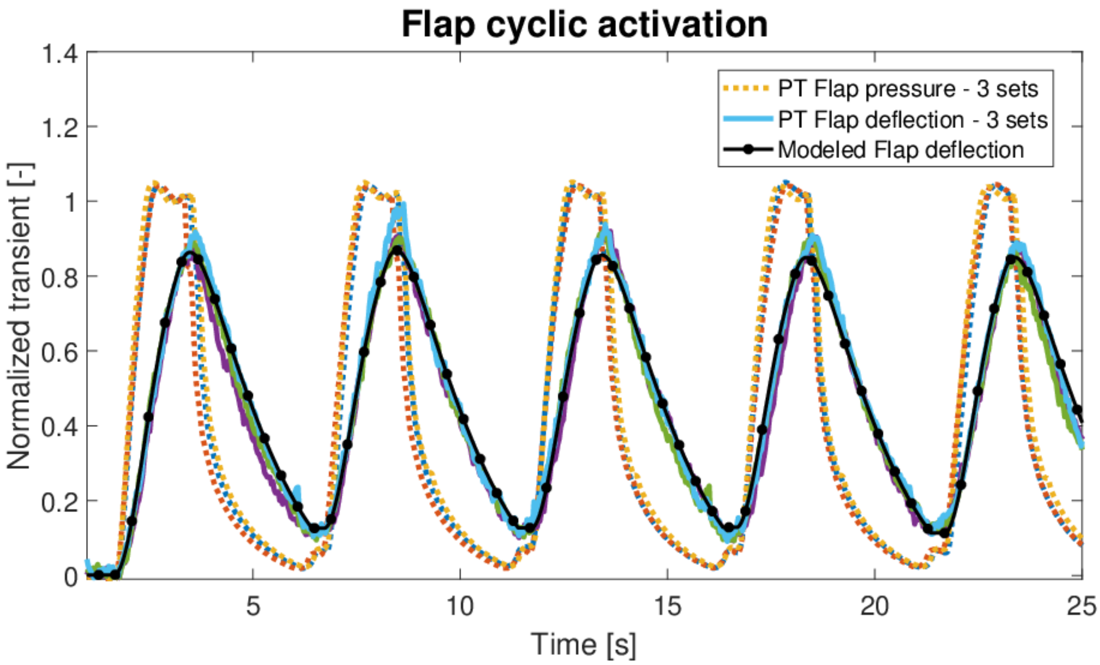

Figure 2.9: Comparison of the modeled flap deflection (black line with round marker) with three independent sets of measured deflection (solid lines) during cyclic flap activation. Corresponding flap activation pressure (dotted lines) are included as a reference of the flap state.

2.4 Impact of flap unsteady aerodynamics

This section presents the investigation of how the unsteady aerodynamics due to flap motion (detailed modeled in the ATEFlap model) evolves as the flap operative condition changes. The results from HAWC2 equipped with ATEFlap are compared with the BHawC model results under increasing cyclic flap activation frequency. The study aims to identify the activation frequency at which the unsteady aerodynamics due to flap motion significantly impacts the blade root loads.

2.4.1 ATEF unsteady aerodynamics

ATEFlap is the active flap "engineering" model implemented in HAWC2. It was developed to compute the unsteady aerodynamic forces and pitching moments for a 2D airfoil section undergoing arbitrary motion and flap deflection. Compared to the steady ATEF models, like the BHawC ATEF model, ATEFlap models the unsteady effects originated by the flap motion. The ATEF model validations described in the previous sections showed that the HAWC2 (with ATEFlap) and BHawC models provide almost equivalent results for stationary flap activation (Section 2.2) and for slow flap activation (Section 2.3). It is reasonable to assume that as the flap actuation speed increases, the unsteady effect on the aerodynamic forces due to the flap motion will become more prominent. Consequently, the difference between the results from the HAWC2 model with ATEFlap and the BHawC model might increase. This study compares the HAWC2 and BHawC models' results as the flap actuator speed increases. The speed increase is achieved by simulating a flap cyclic activation with activation frequencies ranging from 1P to 6P. The comparison between the models' results included the wind turbine operative conditions and the blade root loads. These signals are commonly available in wind turbines, reducing the complexity of future field validation measurements.

2.4.2 Method

The BHawC and HAWC2 models validated in Section 2.2 and Section 2.3 are used in this study. The flap actuator model is re-tuned to reproduce the required flap oscillation motion without delay. The flap motion follows a sinusoidal cyclic pattern, oscillating between flap inactive and fully active flap states. The oscillation frequency is constant in each simulation.
For both aeroelastic models, eight different cases are simulated: flap not active (AFOff), flap steadily active (AFOn), and six cases with flap oscillating at a specific frequency X (AFOn_XP), where X is an integer multiple of the PT rotational frequency (e.g., AFOn_3P means flap oscillating at a 3P frequency). The tested oscillating frequencies are from 1P to 6P. In each case, wind speeds from 6 to 20 m/s with 2 m/s steps are simulated. Four simulations are run per wind speed, each starting at a different equidistant azimuthal angle to remove the impact of the azimuth angle on the averaged load transient. Every simulation is 70 seconds long and is performed with constant wind speed, without turbulence, standard air density, and wind shear of 0.2. In the cases with cyclic flap motion, the flap starts from an inactive state and is activated after 5 seconds.
The PT performance comparison between the two aeroelastic models is performed by comparing the mean value of power, rotor speed, and pitch angle for each wind speed. The load comparison focuses on the MBrM, the difference between azimuthal synchronized flapwise bending moments at the blade root of adjacent blades introduced in Section 2.3. For every wind speed, the MBrM is averaged among the four different simulations and normalized to the MBrM computed in the steady flap activation case for the corresponding wind speed and aeroelastic model.

2.4.3 Results and discussion

The differences in the PT operational parameters between the HAWC2 and BHawC models are negligible. In all cases, the difference is below 0.5% for the power, below 0.1% for the rotor speed, and below 0.2 deg for the pitch angle.
In all the investigated cases, the reduced frequencies k at the blade sections covered by the flap, defined as harmonic oscillation frequency times the half-sectional chord length normalized by the sectional flow speed, are well below 0.3 (max value of 0.11). These conditions ensure the assumption of uniform upwash velocity along the chord made by the ATEFlap model provides a negligible error [49].
Regarding the normalized MBrM, the HAWC2 oscillation range of MBrM decreases compared to the BHawC MBrM range as the flap actuation frequency increases. Figure 2.10 shows the averaged MBrM time series at 10 m/s wind computed with HAWC2 (red line) and BHawC (blue dotted line) for a flap activation frequency of 1P (left column), 3P (central column) and 5P (right column). From the time plot (upper row) and the plot function of the flap actuation state (lower row), it is visible that the HAWC2 MBrM oscillates for a smaller range compared to the BHawC MBrM at 5P; meanwhile, it is equivalent at 1P. The overview of the difference between the HAWC2 and BHawC MBrM range for the analyzed wind speeds and actuation frequencies is shown in Figure 2.11a. The data for 4P are obtained from interpolation as the simulation results are unreliable due to instabilities on the flap actuator model at that activation frequency. At 1P, the two models have an MBrM range within $\pm 5\%$ of each other, except at 14 and 16 m/s where the HAWC2 MBrM range is 8% higher than the BHawC MBrM range. As the flap activation frequency increases, the HAWC2 MBrM range consistently becomes smaller than the BHawC one, reaching a difference of -25% at 6P for 10 m/s wind. To understand if these differences can be easily detected in a field measurement, the MBrM range differences are normalized to the mean blade root flapwise bending moment (MBx) for the case of the flap not active. The results, plotted in figure 2.11b, show the differences below 0.5% of MBx for activation frequency of 3P and below. From 5P, the differences are consistently higher than 1% of MBx with a max difference of -2.6% at 6P for 10 m/s wind. Differences in the load

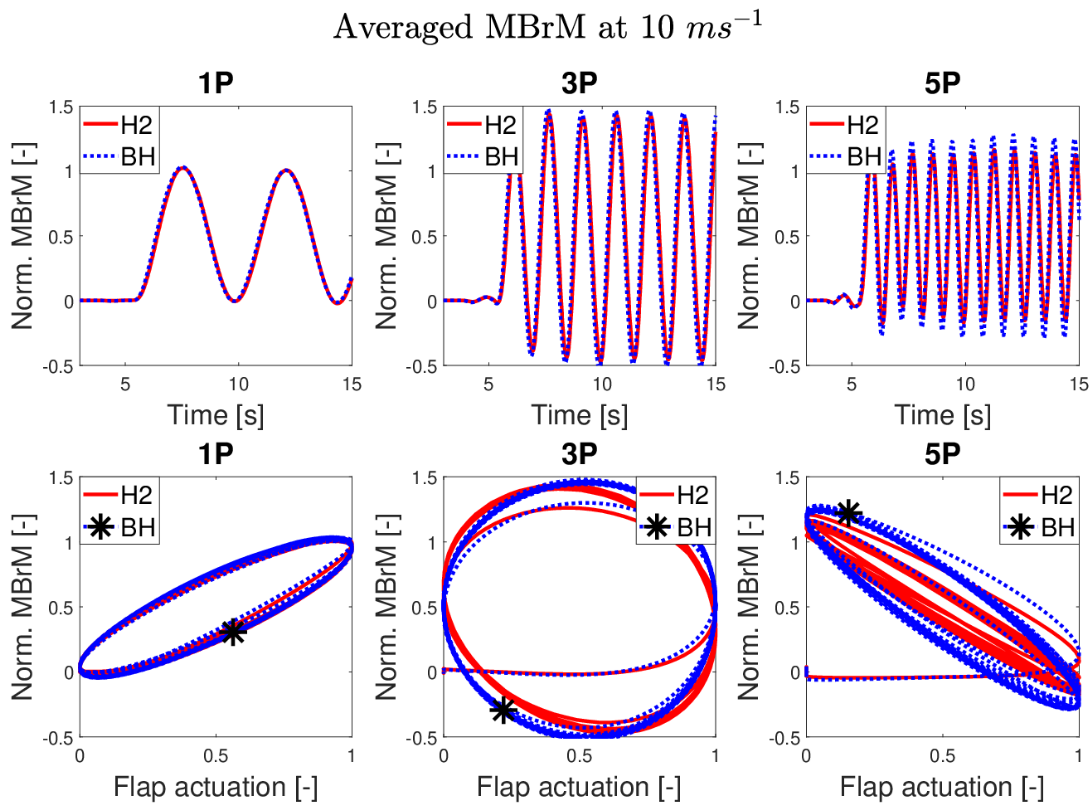

Figure 2.10: Normalized averaged b2b blade root bending moment (MBrM) time series for 10 m/s wind speed with 1P (left), 3P (center), or 5P (right) flap activation frequency. In the upper row, the time series is plotted in function of the time, for a reduced time interval of 15 s. In the lower row, MBrM is plotted as a function of the flap actuation state. MBrM is normalized to the steady state value for stationary flap actuation in all plots.

variation due to flap activation higher than 1% of the mean blade moment can be detected in a field test, making flap activation of 5P and higher good candidates for the ATEFlap model validation. On the other side, for flap activation frequency of 3P and below, the steady ATEF models are accurate as the impact of the unsteady aerodynamics due to flap motion is limited.

2.4.4 Conclusions

The study investigated the impact of the modeling of the unsteady aerodynamics due to the flap motion (included in the HAWC2 ATEFlap model) on the PT performance and blade root loads compared to the steady ATEF model (BHawC model). The study showed no difference in the PT operational parameters computed with the two models. The range of the MBrM moment significantly differs between the two models for flap activation frequency of 5P and above. If relevant for future WT design, these flap activation frequencies should be tested to confirm the validity of the ATEF models. For frequency of 3P and below, the results from the two models are instead almost equivalent.

2.5 Suggestion for future validations

The studies conducted in this PhD project provided valuable experience in the validation process of the active flap. Based on this experience, some recommendations are suggested to improve future validation campaigns of active flap:

- The accurate estimation of the flap deflection is critical in validating the aerodynamic

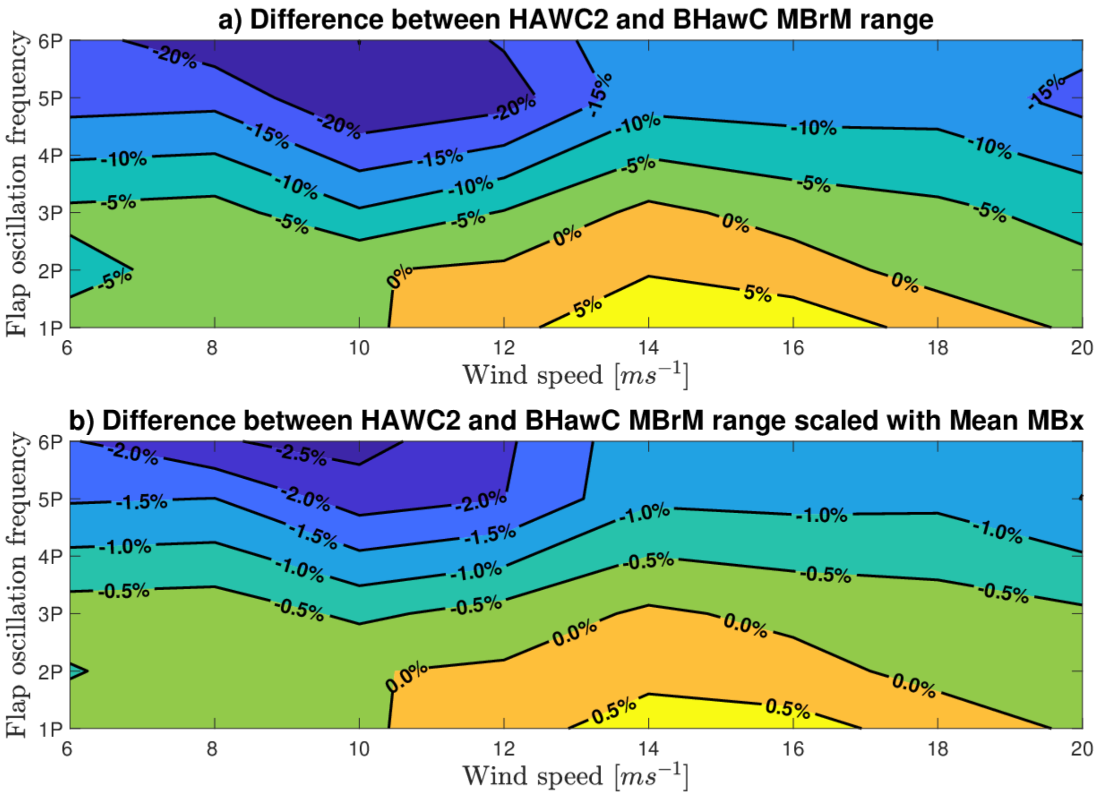

Figure 2.11: a) Difference between the HAWC2 and BHawC normalized averaged b2b blade root bending moment (MBrM) range as a function of wind speed and flap activation frequency. b) Difference between the HAWC2 and BHawC MBrM range scaled with the mean blade root bending moment MBx. 4P case is omitted due to instability in the actuator model.

model of active flaps. If a measurement system of the flap position is not available, the flap actuator model should be tuned with flap deflection data from various flap actuation patterns (e.g., step activation or cyclic activation), wind speeds, and operative conditions.

- The accuracy of the aerodynamic model validation is strongly affected by uncertainties in the aerodynamic properties of the flap profiles. The aerodynamic properties of all the relevant flap profiles should be measured. Alternatively, the impact on Cl and Cd due to the flap can be derived from similar profiles with acceptable accuracy.

- The correct time synchronization of all the different measurement systems is crucial to ensure the proper time precision in measuring and validating the transient of the Cl and Load channels. Therefore, the flap actuator control signal (or any other channel that can be used to estimate the flap actuation time) is required. To achieve proper time precision in validating Cl and load transients, all the different measurement systems must be precisely synchronized. Furthermore, the flap actuator control signal (or any other channel that can be used to estimate the flap actuation behavior timely) is required to synchronize the simulated flap motion with the measurements correctly.

- The transients of Cl and blade loads are strongly affected by the azimuthal angle at which the flap is actuated. The measurement campaign should aim to obtain measurements with a balanced distribution of these angles per wind speed.

2.6 Summary

This chapter summarizes the research on field validation of aeroelastic models of active trailing edge flaps. The focus is the first research question of the PhD project, which is: *Do the aeroelastic models of wind turbines equipped with active trailing edge flaps estimate accurately and reliably the loads and behavior of an actual commercial-scale wind turbine?*

Section 2.2 confirms that the ATEF models implemented in HAWC2 and BHawC can accurately and reliably estimate the operative condition and blade loads for a commercial-scale wind turbine when the flap is steadily active.

Section 2.3 shows the HAWC2 and BHawC ATEF models correctly represent the dynamic response of the Cl and blade loads during flap actuation. To achieve it, accurate tuning of the flap actuator model is crucial, as well as accurate measurements of the aerodynamic properties of the flap profiles. Other suggestions to improve the future validation campaigns are collected in Section 2.5.

Finally, Section 2.4.1 suggests that unsteady aerodynamics due to flap motion is critical in the wind turbine design for high activation frequencies (5P or above). However, it is negligible at low frequencies (3P and below).

Chapter 3

Performance state estimation of wind turbine active flaps

This chapter summarises the research article titled:
Active Trailing Edge Flap System fault detection via Machine Learning *[50] (See Appendix Article 4).*

In the following chapter, an investigation into the second topic of the thesis work, performance state estimation of wind turbine active flaps, is presented. The topic background is introduced, followed by the outline of the relevant thesis article. Finally, the research question is answered in the summary section.

3.1 Background

Every time a new component is included in a wind turbine's design, the safe and reliable continuous wind turbine operation must be ensured for the whole turbine's lifetime. To fulfill this requirement, additional components, systems, and controller strategies are needed to identify, quantify and resolve any potential issue deriving from the fault of the new component without compromising the WT safety.

Once the active flap reaches an adequate level of maturity, the wind turbine design will rely on the load reduction provided by the active flap. Therefore, any potential fault or performance degradation of the flap system may jeopardize the safety and performance of the wind turbine if not properly managed. Therefore, a system will be needed to identify, monitor and handle active flap faults or degradation.

To date, no comprehensive investigations have been conducted into ATEF systems' fault detection and condition monitoring. To the author's knowledge, no literature addressing this specific topic is currently available. Nevertheless, different approaches for ATEF fault detection and monitoring can be derived from the methodologies currently applied to other components in the wind energy sector.

In a first approach, monitoring and diagnosis can rely on several dedicated sensors located on the flap surfaces or in their proximity to quantify the flap deflection or impact on the blade aerodynamics. This approach leads to a complex and expensive system of several sensors affected by the harsh environment of a wind turbine rotating blade.

A second approach is the model-based method, already applied in the condition monitoring of main bearing [51], sensor and actuators [52], and generator [53]. The method relies on the difference between the real system outputs and the output from a system model created using, for example, Kalman filter, observers, or model-based machine learning techniques. Model-

based methods require a reasonably good model to guarantee the detection of faults. This is challenging for ATEF fault detection, primarily related to the high nonlinearity of the WT blade dynamic, the considerable uncertainty on the wind field estimation, and the limited number of sensors available on a commercial WT. Enhancements in wind field estimations (e.g., nacelle Lidar) or additional blade pressure or load sensors can facilitate the model generations and enhance their accuracy at the price of higher system complexity and cost.
Finally, fault detection can be achieved with data-driven methods via different types of data and signal analysis, ranging from the simple detection of changes in mean signal values to the more advanced machine learning (ML) methodologies [54]. Recent technological and computational advances have allowed an exponential increase in the application of ML methodologies to fault diagnosis and condition monitoring [55] [56]. ML methodologies require a substantial amount of data for model training. Currently, the amount of ATEF field data is limited, particularly for ATEF faults. As aeroelastic simulations are commonly used for WT design, it is reasonable to assume that a sufficiently accurate aeroelastic model of a WT equipped with ATEF can be used to train an ATEF fault detection ML model. This hypothesis is investigated in the following section, where two data-driven methods based on ML and trained with aeroelastic simulation to classify the ATEF fault states are investigated.

3.2 Study results

This study focused on developing two simple ML applications to estimate the performance state (also called the health state) of active trailing edge flaps. The detection of the health state of the AFlap presents significant challenges. The identification of the flap boundary operative states, full activation or full deactivation, is hard to achieve. The wide range of environmental conditions in which the WT operates causes a wide variability in the load signals. This variability is visible in the left image of Figure 3.1 where the error bands of the blade root bending moment with flap not active (red area) and flap fully active (Black area) widely overlap even if the averaged value lines are well separated. Furthermore, several different phenomena can impact and reduce the flap performance. From the slow degradation of the flap performance due to the wear and tear of the ATEF system to ice or lightning that instantaneously compromises the entire system's functionality.
As it is unfeasible to test all the possible fault combinations, a set of flap performance states were selected to cover a wide range of flap fault conditions. These states are: Flap not active (AF_Off); Flap active (AF_On); Flap active even if required to be not active (AF_Off_Fault); Flap not active due to fault (AF_On_Fault); Flap active with performance reduced to 25% (AF_On_25pc), 50% (AF_On_50pc), and 75% (AF_On_75pc). These states can occur only on one blade (asymmetrical faults) or on all three blades contemporaneously (symmetrical faults). The performance state detection has been investigated for normal power production and for the pre-startup WT state at which the WT is idling and waiting to startup. The latter case would allow the identification of a fault even before the WT starts to operate, preventing the startup or triggering a safe startup with faulty flaps. The performances of flaps in a static actuation state are investigated to obtain a detection system independent from any specific ATEF controller strategy, ATEF system design, or fault dynamics. This system can be integrated into a flap status check routine that regularly locks one flap activation state and verifies its performance state.
The study relied on aeroelastic simulations performed with the aeroelastic tool BHawC developed by SGRE. A realistic ATEF configuration was ensured by using the aeroelastic model of the 4.3 MW prototype tuned and validated in [47]. The flap performance degradation states were reproduced by properly scaling the aerodynamic properties of the flap, as shown in the right picture of Figure 3.1. A set of 1500 independent simulations (700 for training, 300 for

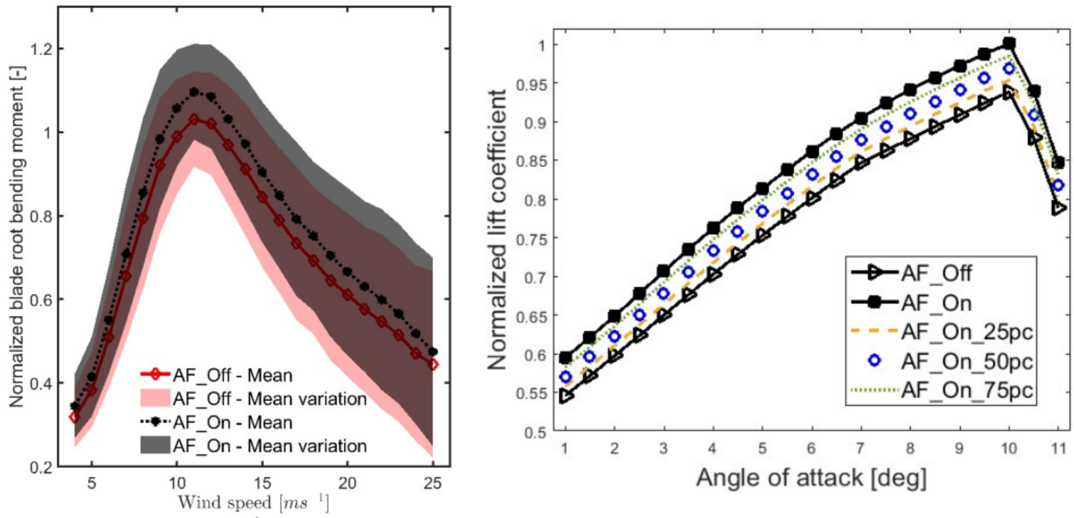

Figure 3.1: Left: Mean value of the normalized blade root bending moment when the AFlap is deactivated (AF_Off) and activated without degradation (AF_On), binned in the function of the wind speed. The colored areas covers the range of ± 1 std. Right: Example of flap normalized lift coefficient of the baseline (AF_Off, line with triangle), flap active (AF_On, line with squares), and flap active with performance reduced to 25% (AF_On_25pc, dashed line), 50% (AF_On_50pc, circles), and 75% (AF_On_75pc, dotted line).

test, and 500 for validation) were computed for each combination of flap state and fault symmetry for the WT in normal power production, covering a wind speed range between 3.5 m/s and 25 m/s. For each combination, 450 simulations (200 for training, 100 for test, and 150 for validation) were computed for the WT in pre-startup, covering a wind speed range between 1 m/s and 3.5 m/s. To account for the variability of the environmental conditions on the wind turbine's aeroelastic response, the main environmental conditions were modeled as random variables of pre-imposed statistical properties, as shown in Figure 3.2. The flap state was kept constant for the whole 600 s simulation time.

The flap performance state estimation was approached as a multivariate time-series classification problem. Since one of the requirements was to reduce the complexity level to a minimum, the simple and well-studied Random Forest classifier (RF) was selected. Also, only the signals commonly available on a modern wind turbine (rotor speed, pitch angle, power, tower top acceleration, blades root loads, and flap actuator signal) were selected to generate the input features for the ML classifier.

Two different approaches were investigated to generate the problem features: Manual Feature Selection (MFS), the features were selected based on the authors' experience with the effect of flap activation on the WT system; Automatic Feature generation (AFS), which applied the MiniRocket algorithm [57] to process the input channels through multiple random convolutional kernels generating 10000 features for a channel. This process was selected to explore potential hidden correlations between inputs, and flap states that the authors could have overlooked. The key contributions from the presented article are as follows:

- MFS method correctly classified (F1-score higher than 90%) all the different combinations of ATEF performance states and wind turbine operation states (normal power production and pre-startup) in the case of asymmetrical flap faults. This performance was achieved with less than 14 features, mainly related to the blade-to-blade differences of the mean blade root loads.

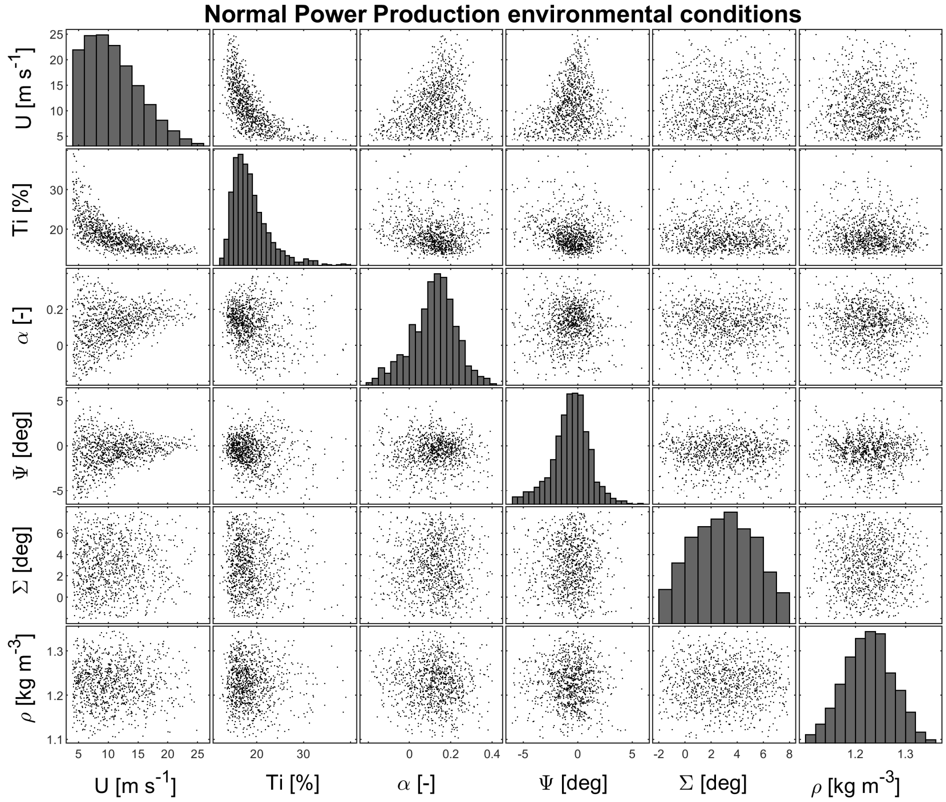

Figure 3.2: Example of environmental conditions for normal power production simulations: mean wind speed U, wind turbulence intensity TI, wind shear exponent α, horizontal inflow angle Ψ, vertical inflow angle Σ, and air density ρ.

- MFS method failed to classify the ATEF performance states in the case of symmetrical flap faults. MFS could potentially identify symmetrical flap faults if the blades are tested individually.
- AFS method failed to classify most ATEF performance states in asymmetrical and symmetrical flap faults. However, for both cases, the AFS method correctly identified Flap not active and flap not active with fault from all the other states when the wind turbine operates in normal power production.

3.3 Summary

This chapter summarizes the research on performance state estimation of wind turbine active flaps. The focus is the second research question of the PhD project, which is: *Can a machine learning model estimate the flap performance states of a wind turbine to improve the reliability of the active flap system design?*
No studies or applications exist in the literature to estimate the performance state of active trailing edge flaps.
This chapter proposes two simple approaches based on machine learning to diagnose the health state of an ATEF system. Both approaches rely only on the sensors commonly available on commercial WTs, avoiding the associated cost of additional measurement systems.
The first approach (MFS) combines manual feature engineering with a random forest classifier. The second approach (AFS) uses random convolutional kernels to create the feature vectors.

Both methods are trained and tested with aeroelastic simulations datasets based on the SGRE PT model validated in [47]. The tested flap states are: flap steadily not active, active, active with degradation of 25%, 50% 75%, active but faulty (100% degradation), not active but with fault. The flap states can occur only on one blade (asymmetrical faults) or all three blades contemporaneously (symmetrical faults).

The study shows that the MFS method is reliable in classifying all the investigated combinations of ATEF health states in the case of asymmetrical flap faults when the WT operates in normal power production and before startup. Instead, the AFS method can identify two specific ATEF health states for asymmetrical and symmetrical faults when the WT is in normal power production but not before startup. Integrating these two methodologies in a fault detection system or condition monitoring system (or both) can improve the reliability of the design of wind turbines equipped with an active flap system.

Chapter 4

Conclusions and future work

This PhD thesis presented a summary of research findings on the field validation of aeroelastic models of active trailing edge flaps for wind turbines and the estimation of the flap performance state with machine learning. This chapter provides conclusions of the present work and future research directions.

4.1 Conclusions

The goals of this industrial PhD thesis were *the validation of the aeroelastic models of active trailing edge flap with full-scale field measurements* and *the development of an application to estimate the performance state of the active flap system*. To achieve them, two research questions were investigated: 1) *Do the aeroelastic models of wind turbines equipped with active trailing edge flaps estimate accurately and reliably the loads and behavior of an actual commercial-scale wind turbine?* and 2) *Can a machine learning model estimate the flap performance states of a wind turbine to improve the reliability of the active flap system design?*
Regarding the first question, the validations have shown the flap models implemented in the aeroelastic codes BHawC and HAWC2 accurately and precisely model the impact of the flap actuation on the aerodynamic, loading, and operational parameter of a commercial scale wind turbine (4.3 MW rated power, 120 m diameter, 20 m flap length). The research has also highlighted the modeling and tuning of the flap actuator, and the flap aerodynamic properties are crucial elements for the correct modeling of active flaps in wind turbine aeroelastic codes. Finally, the research has suggested that the capability of the active flap model to estimate the unsteady effect on the aerodynamic forces due to the flap motion would become relevant at high flap actuation frequencies.
Regarding the second question, an application has been developed for the first time to estimate the flap performance states for asymmetrical faults. The application has remarkable precision, higher than 90%, and is based on a simple and well-proven machine learning technique. Furthermore, it requires only input signals commonly available on commercial wind turbines, simplifying its possible implementation in future wind turbines.
The presented research has significantly contributed to increasing the accuracy and reliability of the active flap aeroelastic tools and the capability of detecting active flap system faults. These contributions are essential milestones to enable the safe and reliable design of future wind turbines equipped with active flaps.

4.2 Future work

This thesis presented the research on field validation of aeroelastic flap models and flap performance state estimation. However, as outlined below, many further research opportunities

exist in these areas.
The validation activities described in this thesis have covered stationary flap states and single flap actuation. Additional field validations are recommended to ensure the accuracy and reliability of aeroelastic models for most of the active flap feedback control strategies for load reduction proposed in the literature. Among them, cyclic 1P flap actuation is one of the most suggested strategies. Field validation of this flap actuation strategy can verify if the aeroelastic codes adequately represent the unsteady aerodynamics due to the continuous flap motion. Furthermore, the validation for flap cyclic activation frequencies higher than 4P can confirm the need for ATEFlap-like models for these flap operational configurations. Adding load measurement locations along the blade length in future field measurements can enable the validation of the Near Wake model.
The aeroelastic flap models have been validated under normal power production conditions. During its lifetime, a wind turbine can experience wind conditions that exceed the simplification and assumption of the active flap aerodynamic models. These conditions include operation at high angles of attack (wind gusts), operation in a fully separated regime (idling), or operating with high yaw misalignment angles (more probable when wake steering control strategies are in place). These conditions can lead to instabilities (e.g., vortex-induced vibration, stall-induced vibration) and peaks in the wind turbine loads. Therefore additional studies are needed to understand, model, and validate the behavior of active flaps in these extreme conditions.
The flap performance state estimation technique developed for asymmetric faults has shown excellent performance with aeroelastic simulation data. The consequent following step is to validate this technique with measurement data. Transfer learning methods can be used to extend the trained machine learning models to similar but different wind turbines, expanding the measurements pool the flap fault performance state estimation technique can be tested with.
The detection of flap performance states for symmetric faults requires further research. Among the several machine learning methodologies potentially available, Multirocket (MiniRocket evolution) or HYDRA offer easy integration into the technique developed in this thesis, together with improved feature generation and exploration.

Bibliography

[1] J. Skea, P. Shukla, A. Reisinger, R. Slade, M. Pathak, A. Al Khourdajie, R. van Diemen, A. Abdulla, K. Akimoto, M. Babiker, Q. Bai, I. Bashmakov, C. Bataille, G. Berndes, G. Blanco, K. Blok, M. Bustamante, E. Byers, L. Cabeza, K. Calvin, C. Carraro, L. Clarke, A. Cowie, F. Creutzig, D. Dadi, D. Dasgupta, H. de Coninck, F. Denton, S. Dhakal, N. Dubash, O. Geden, M. Grubb, C. Guivarch, S. Gupta, A. Hahmann, K. Halsnæs, P. Jaramillo, K. Jiang, F. Jotzo, T. Jung, S. Kahn Ribeiro, S. Khennas, Ș. Kılkış, S. Kreibiehl, V. Krey, E. Kriegler, W. Lamb, F. Lecocq, S. Lwasa, N. Mahmoud, C. Mbow, D. McCollum, J. Minx, C. Mitchell, R. Mrabet, Y. Mulugetta, G.-J. Nabuurs, G. Nemet, P. Newman, L. Niamir, L. Nilsson, S. Nugroho, C. Okereke, S. Pachauri, A. Patt, R. Pichs-Madruga, J. Portugal-Pereira, L. Rajamani, K. Riahi, J. Roy, Y. Saheb, R. Schaeffer, K. Seto, S. Some, L. Steg, F. Toth, D. Ürge-Vorsatz, D. van Vuuren, E. Verdolini, P. Vyas, Y.-M. Wei, M. Williams, and H. Winkler". ""PCC, 2022: Summary for Policymakers"". English. In: *Climate Change 2022: Mitigation of Climate Change*. United Kingdom: Cambridge University Press, 2022. DOI: 10.1017/9781009157926.001.

[2] I. R. E. Agency. *World Energy Transitions Outlook 2022 - 1.5°C Pathway*. eng. International Renewable Energy Agency IRENA, 2022.

[3] G. W. E. Council–GWEC. *Global wind report 2023*. 2023.

[4] T. Barlas, V. Pettas, D. Gertz, and H. A. Madsen. "Extreme load alleviation using industrial implementation of active trailing edge flaps in a full design load basis". In: *Journal of Physics: Conference Series*. Vol. 753. Institute of Physics Publishing, Oct. 2016. DOI: 10.1088/1742-6596/753/4/042001.

[5] L. O. Bernhammer, G. A. van Kuik, and R. De Breuker. "Fatigue and extreme load reduction of wind turbine components using smart rotors". In: *Journal of Wind Engineering and Industrial Aerodynamics* 154 (2016), pp. 84–95. ISSN: 0167-6105. DOI: https://doi.org/10.1016/j.jweia.2016.04.001. URL: https://www.sciencedirect.com/science/article/pii/S0167610516301970.

[6] V. Pettas, T. Barlas, D. Gertz, and H. A. Madsen. "Power performance optimization and loads alleviation with active flaps using individual flap control". In: *Journal of Physics: Conference Series*. Vol. 749. Institute of Physics Publishing, Sept. 2016, p. 012010. DOI: 10.1088/1742-6596/749/1/012010. URL: https://iopscience.iop.org/article/10.1088/1742-6596/749/1/012010.

[7] N. J. Abbas, P. Bortolotti, C. Kelley, J. Paquette, L. Pao, and N. Johnson. "Aero-servo-elastic co-optimization of large wind turbine blades with distributed aerodynamic control devices". In: *Wind Energy* (2023). DOI: https://doi.org/10.1002/we.2840. URL: https://onlinelibrary.wiley.com/doi/abs/10.1002/we.2840.

[8] P. Veers, C. Bottasso, L. Manuel, J. Naughton, L. Pao, J. Paquette, A. Robertson, M. Robinson, S. Ananthan, A. Barlas, A. Bianchini, H. Bredmose, S. G. Horcas, J. Keller, H. A. Madsen, J. Manwell, P. Moriarty, S. Nolet, and J. Rinker. "Grand Challenges in the Design, Manufacture, and Operation of Future Wind Turbine Systems". In: *Wind*

Energy Science Discussions 2022 (2022), pp. 1–102. DOI: 10.5194/wes-2022-32. URL: https://wes.copernicus.org/preprints/wes-2022-32/.

[9] I. E. Commission et al. "IEC 61400-1:2019: Wind energy generation systems-Part 1: Design requirements". In: *Geneva, Switzerland* (2019).

[10] I. E. Commission et al. "IEC 61400-13:2015 Wind Turbine Generator Systems—Part 13: Measurement of Mechanical Loads". In: *International Electrotechnical Commission: Geneva, Switzerland* (2015).

[11] I. E. Commission et al. "IECRE OD-501:2018: Operational Document, Type and Component Certification Scheme". In: *Geneva, Switzerland* (2015).

[12] H. A. Madsen. *INDUFLAP2*. 2023. URL: https://www.induflap.dk/ (visited on 06/10/2023).

[13] A. Gomez Gonzalez, P. Enevoldsen, T. Barlas, and H. A. Madsen. "Test of an active flap system on a 4.3 MW wind turbine". eng. In: *Journal of Physics. Conference Series* 2265.3 (2022), p. 032016. ISSN: 17426596, 17426588. DOI: 10.1088/1742-6596/2265/3/032016.

[14] J. W. Van Wingerden, A. W. Hulskamp, T. Barlas, B. Marrant, G. A. Van Kuik, D. P. Molenaar, and M. Verhaegen. "On the proof of concept of a 'smart' wind turbine rotor blade for load alleviation". eng. In: *Wind Energy* 11.3 (2008), pp. 265–280. ISSN: 10954244, 10991824. DOI: 10.1002/we.264.

[15] V. A. Riziotis and S. G. Voutsinas. "Aero-elastic modelling of the active flap concept for load control". eng. In: *European Wind Energy Conference and Exhibition 2008* 1 (2008), pp. 140–148.

[16] P. B. Andersen. *Advanced load alleviation for wind turbines using adaptive trailing edge flaps : sensoring and control*. eng. Risø National Laboratory, 2010, Online–Ressource (unknown).

[17] M. A. Lackner and G. Van Kuik. "A comparison of smart rotor control approaches using trailing edge flaps and individual pitch control". eng. In: *Wind Energy* 13.2-3 (2010), pp. 117–134. ISSN: 10991824, 10954244. DOI: 10.1002/we.353.

[18] H. Aagaard Madsen, P. B. Andersen, T. Løgstrup Andersen, C. Bak, T. Buhl, and N. Li. "The potentials of the controllable rubber trailing edge flap (CRTEF)". eng. In: vol. 3. European Wind Energy Association (EWEA), 2010, pp. 2165–2175.

[19] D. Castaignet, T. Buhl, N. K. Poulsen, and J. J. Wedel-Heinen. "Trailing edge flaps impact on fatigue and extreme loads in power production". In: *EWEA 2011* (2011).

[20] L. Bergami and N. K. Poulsen. "A smart rotor configuration with linear quadratic control of adaptive trailing edge flaps for active load alleviation". eng. In: *Wind Energy* 18.4 (2015), pp. 625–641. ISSN: 10991824, 10954244. DOI: 10.1002/we.1716.

[21] A. Fischer and H. Aagaard Madsen. "Investigation of the theoretical load alleviation potential using trailing edge flaps controlled by inflow data". eng. In: *Wind Energy* 19.9 (2016), pp. 1567–1583. ISSN: 10991824, 10954244. DOI: 10.1002/we.1937.

[22] T. J. Larsen and A. M. Hansen. *How 2 HAWC2, the user's manual*. eng. 2023.

[23] J. M. Jonkman, M. L. Buhl, et al. *FAST user's guide*. Vol. 365. National Renewable Energy Laboratory Golden, CO, USA, 2005.

[24] E. Bossanyi. "GH Bladed–Theory Manual, Version 4.4". In: *Garrad Hassan and Partners* (2013).

[25] L. Bergami and M. Gaunaa. *ATEFlap Aerodynamic Model, a dynamic stall model including the effects of trailing edge flap deflection*. eng. Danmarks Tekniske Universitet, Risø Nationallaboratoriet for Bæredygtig Energi, 2012, 52 s.

[26] M. Gaunaa. "Unsteady two-dimensional potential-flow model for thin variable geometry airfoils". eng. In: *Wind Energy* 13.2-3 (2010), pp. 167–192. ISSN: 10991824, 10954244. DOI: 10.1002/we.377.

[27] L. Bergami, M. Gaunaa, and J. C. Heinz. "Indicial lift response function: an empirical relation for finite-thickness airfoils, and effects on aeroelastic simulations". eng. In: *Wind Energy* 16.5 (2013), pp. 681–693. ISSN: 10954244, 10991824. DOI: 10.1002/we.1516.
[28] M. Hansen, M. Gaunaa, and H. Aagaard Madsen. *A Beddoes-Leishman type dynamic stall model in state-space and indicial formulations*. eng. 2004.
[29] C. Ferreira, A. Gonzalez, D. Baldacchino, M. Aparicio, S. Gómez, X. Munduate, N. R. Garcia, J. N. Sørensen, E. Jost, S. Knecht, T. Lutz, P. Chassapogiannis, K. Diakakis, G. Papadakis, S. Voutsinas, J. Prospathopoulos, T. Gillebaart, and A. Van Zuijlen. "Results of the AVATAR project for the validation of 2D aerodynamic models with experimental data of the DU95W180 airfoil with unsteady flap". In: *Journal of Physics: Conference Series*. Vol. 753. 2. Institute of Physics Publishing, Oct. 2016. DOI: 10.1088/1742-6596/753/2/022006.
[30] L. Bergami, V. A. Riziotis, and M. Gaunaa. "Aerodynamic response of an airfoil section undergoing pitch motion and trailing edge flap deflection: A comparison of simulation methods". In: *Wind Energy* 18 (July 2015), pp. 1273–1290. ISSN: 10991824. DOI: 10.1002/we.1759.
[31] E. Jost, A. Fischer, T. Lutz, and E. Krämer. "An investigation of unsteady 3D effects on trailing edge flaps". In: *Journal of Physics: Conference Series*. Vol. 753. 2. Institute of Physics Publishing, Oct. 2016, p. 022009. DOI: 10.1088/1742-6596/753/2/022009. URL: https://iopscience.iop.org/article/10.1088/1742-6596/753/2/022009.
[32] T. Barlas, E. Jost, G. Pirrung, T. Tsiantas, V. Riziotis, S. T. Navalkar, T. Lutz, and J. W. Van Wingerden. "Benchmarking aerodynamic prediction of unsteady rotor aerodynamics of active flaps on wind turbine blades using ranging fidelity tools". In: *Journal of Physics: Conference Series*. Vol. 753. 2. Institute of Physics Publishing, Oct. 2016, p. 022027. DOI: 10.1088/1742-6596/753/2/022027. URL: https://iopscience.iop.org/article/10.1088/1742-6596/753/2/022027.
[33] J. M. Prospathopoulos et al. "Simulation of oscillating trailing edge flaps on wind turbine blades using ranging fidelity tools". In: *Wind Energy* 24.4 (2021), pp. 357–378. ISSN: 10991824. DOI: 10.1002/we.2578. URL: https://doi.org/10.1002/we.2578.
[34] G. R. Pirrung, H. A. Madsen, T. Kim, and J. Heinz. "A coupled near and far wake model for wind turbine aerodynamics". In: *Wind Energy* 19.11 (2016), pp. 2053–2069. DOI: https://doi.org/10.1002/we.1969. URL: https://onlinelibrary.wiley.com/doi/abs/10.1002/we.1969.
[35] G. R. Pirrung, H. Madsen, T. Kim, and J. Heinz. "A coupled near and far wake model for wind turbine aerodynamics". In: *Wind Energy, doi* 10 (2020).
[36] T. K. Barlas, W. van Wingerden, A. Hulskamp, G. Van Kuik, and H. Bersee. "Smart dynamic rotor control using active flaps on a small-scale wind turbine: aeroelastic modeling and comparison with wind tunnel measurements". eng. In: *Wind Energy* 16.8 (2013), pp. 1287–1301. ISSN: 10991824, 10954244. DOI: 10.1002/we.1560.
[37] A. G. Gonzalez, P. Enevoldsen, T. K. Barlas, H. A. Madsen, and A. S. Olsen. "Consolidated results of the laboratory and full scale field validation of an active flap system". In: *Journal of Physics: Conference Series* 1618.5 (2020), p. 52024. ISSN: 17426596. DOI: 10.1088/1742-6596/1618/5/052024.
[38] T. K. Barlas, A. S. Olsen, H. A. Madsen, T. L. Andersen, Q. Ai, and P. M. Weaver. "Aerodynamic and load control performance testing of a morphing trailing edge flap system on an outdoor rotating test rig". In: *Journal of Physics: Conference Series* 1037.2 (June 2018), p. 022018. DOI: 10.1088/1742-6596/1037/2/022018. URL: https://dx.doi.org/10.1088/1742-6596/1037/2/022018.

[39] S. Bartholomay, S. Krumbein, V. Deichmann, M. Gentsch, S. Perez-Becker, R. Soto-Valle, D. Holst, C. N. Nayeri, C. O. Paschereit, and K. Oberleithner. "Repetitive model predictive control for load alleviation on a research wind turbine using trailing edge flaps". eng. In: *Wind Energy* 25.7 (2022), pp. 1290–1308. ISSN: 10991824, 10954244. DOI: 10.1002/we.2730.

[40] S. Bartholomay, S. Krumbein, S. Perez-Becker, R. Soto-Valle, C. N. Nayeri, C. O. Paschereit, and K. Oberleithner. "Experimental assessment of a blended fatigue-extreme controller employing trailing edge flaps". eng. In: *Wind Energy* 26.2 (2023), pp. 201–227. ISSN: 10991824, 10954244. DOI: 10.1002/we.2795.

[41] J. C. Berg, M. F. Barone, and B. R. Resor. "Field test results from the Sandia SMART rotor". eng. In: *51st Aiaa Aerospace Sciences Meeting Including the New Horizons Forum and Aerospace Exposition 2013* (2013).

[42] D. Castaignet, T. K. Barlas, T. Buhl, N. K. Poulsen, J. Wedel-Heinen Jens, N. A. Olesen, C. Bak, and T. Kim. "Full-scale test of trailing edge flaps on a Vestas V27 wind turbine: active load reduction and system identification". eng. In: *Wind Energy* 17.4 (2014), pp. 549–564. ISSN: 10991824, 10954244. DOI: 10.1002/we.1589.

[43] A. Gomez Gonzalez, P. Enevoldsen, A. Gamberini, T. Barlas, and H. A. Madsen. "Operational experience during a four year test program of active flaps on a wind turbine blade". eng. In: *X ECCOMAS Thematic Conference on Smart Structures and Materials - SMART 2023* (2023).

[44] A. Gamberini, T. Barlas, A. Gomez Gonzalez, and H. A. Madsen. "Validation of aeroelastic dynamic model of Active Trailing Edge Flap system tested on a 4.3 MW wind turbine". In: *Wind Energy Science Discussions* 2023 (2023), pp. 1–28.

[45] H. A. Madsen, T. Barlas, A. Fischer, A. S. Olsen, and A. Gomez Gonzalez. "Inflow and pressure measurements on a full scale turbine with a pressure belt and a five hole pitot tube". In: *Journal of Physics: Conference Series* 2265 (2022). ISSN: 17426596. DOI: 10.1088/1742-6596/2265/2/022096.

[46] P. Fisker Skjoldan. *Aeroelastic modal dynamics of wind turbines including anisotropic effects*. eng. Risø National Laboratory, 2011, Online–Ressource (unknown). ISBN: 9788755038486.

[47] A. Gamberini, A. Gomez Gonzalez, and T. Barlas. "Aeroelastic model validation of an Active Trailing Edge Flap System tested on a 4.3 MW wind turbine". eng. In: *Journal of Physics. Conference Series* 2265.3 (2022), p. 032014. ISSN: 17426596, 17426588. DOI: 10.1088/1742-6596/2265/3/032014.

[48] A. Gomez Gonzalez, P. Bay Enevoldsen, A. Barlas, and H. A. Madsen. "General rights Field test of an active flap system on a full-scale wind turbine Field test of an active flap system on a full-scale wind turbine". In: *Wind Energ. Sci* 6 (2021), pp. 33–43. DOI: 10.5194/wes-6-33-2021. URL: https://doi.org/10.5194/wes-6-33-2021.

[49] T. Buhl, M. Gaunaa, and C. Bak. "Potential load reduction using airfoils with variable trailing edge geometry". eng. In: *Journal of Solar Energy Engineering* 127.4 (2005), pp. 503–516. ISSN: 15288986, 01996231. DOI: 10.1115/1.2037094.

[50] A. Gamberini and I. Abdallah. "Active Trailing Edge Flap System fault detection via Machine Learning". In: *Wind Energy Science Discussions* 2023 (2023), pp. 1–28. DOI: 10.5194/wes-2023-24. URL: https://wes.copernicus.org/preprints/wes-2023-24/.

[51] H. D. M. de Azevedo, A. M. Araújo, and N. Bouchonneau. "A review of wind turbine bearing condition monitoring: State of the art and challenges". In: *Renewable and Sustainable Energy Reviews* 56 (2016), pp. 368–379.

[52] S. Cho, Z. Gao, and T. Moan. "Model-based fault detection, fault isolation and fault-tolerant control of a blade pitch system in floating wind turbines". In: *Renewable energy* 120 (2018), pp. 306–321.

[53] M. Gálvez-Carrillo and M. Kinnaert. "Sensor fault detection and isolation in doubly-fed induction generators accounting for parameter variations". In: *Renewable Energy* 36.5 (2011), pp. 1447–1457. ISSN: 0960-1481. DOI: https://doi.org/10.1016/j.renene.2010.10.021. URL: https://www.sciencedirect.com/science/article/pii/S0960148110004921.

[54] H. Badihi, Y. Zhang, B. Jiang, P. Pillay, and S. Rakheja. "A Comprehensive Review on Signal-Based and Model-Based Condition Monitoring of Wind Turbines: Fault Diagnosis and Lifetime Prognosis". In: *Proceedings of the IEEE* 110.6 (2022), pp. 754–806. DOI: 10.1109/JPROC.2022.3171691.

[55] F. P. García Márquez and A. Peinado Gonzalo. "A Comprehensive Review of Artificial Intelligence and Wind Energy". eng. In: *Archives of Computational Methods in Engineering* 29.5 (2022), pp. 2935–2958. ISSN: 18861784, 11343060. DOI: 10.1007/s11831-021-09678-4.

[56] A. Stetco, F. Dinmohammadi, X. Zhao, V. Robu, D. Flynn, M. Barnes, J. Keane, and G. Nenadic. "Machine learning methods for wind turbine condition monitoring: A review". eng. In: *Renewable Energy* 133 (2019), pp. 620–635. ISSN: 18790682, 09601481. DOI: 10.1016/j.renene.2018.10.047.

[57] A. Dempster, D. F. Schmidt, and G. I. Webb. "Minirocket: A very fast (almost) deterministic transform for time series classification". In: *Proceedings of the 27th ACM SIGKDD conference on knowledge discovery & data mining*. 2021, pp. 248–257.

Article 1.

Aeroelastic model validation of an Active Trailing Edge Flap System tested on a 4.3 MW wind turbine.

Pubblished in contribution to the TORQUE 2022 conference in Delft, The Netherlands.

Aeroelastic model validation of an Active Trailing Edge Flap System tested on a 4.3 MW wind turbine

A Gamberini[1 2], A Gomez Gonzalez[1], T Barlas[2]
[1]Siemens Gamesa Renewable Energy A/S, Brande, Denmark
[2]DTU, Dept. of Wind Energy, Roskilde, Denmark
E-mail: andgam@dtu.dk

Abstract. Active Trailing Edge Flap Systems (ATEFS) have shown promising results on reducing Wind Turbine fatigue and ultimate loads and increasing the Annual Energy Production. However, the current lack of field validation creates uncertainty in the fidelity level and accuracy of the engineering models used for the aeroelastic modeling of active flaps, and these systems actual load reduction capabilities are in question. This article describes the validation based on field data of the aeroelastic engineering models of the ATEFS developed for the BEM-based solvers HAWC2 and BHawC for the case of stationary activation of the flap. The validation is based on the field test data from a 4.3 MW Wind Turbine with one blade equipped with an ATEFS and operating in normal power production. With simulation results differing from the measurement of a max of $\pm 3\%$ on mean power, ± 0.2 deg on mean pitch angle, ± 0.1 rpm on rotor speed, and $\pm 2\%$ on flapwise blade loads, the study showed the HAWC2 and BHAWC aeroelastic ATEFS models provide a reliable and precise estimation of the impact of the ATEFS on the Wind Turbine for the case of stationary activation of the flap.

1. Introduction

To decrease the Levelized Cost of Energy, the size of utility-scale Wind Turbines (WT) has been steadily increasing over the past years, leading to a significant increase in the loads carried by the WT components. Among the different technologies studied to reduce the WT loading, actively controlled flaps located at the blade trailing edge, so-called Active Trailing Edge Flap Systems (ATEFS), have shown promising results on reducing fatigue and ultimate loads and increasing Annual Energy Production, see most recent studies [1] and [2].

The majority of the studies on active flap agree on the great potential of reducing loads by this technology, however the full-scale validation of ATEFS aeroelastic engineering models and their load reduction applications is limited. Furthermore, validation is not an easy task. An extensive code-to-code comparison of several existing modeling options for the simulation of active flap on rotating blades has been performed in [3], comparing the state-of-the-art BEM models with models of higher fidelity, including free-wake lifting line and fully resolved CFD models. Subsystem validations have been performed with wind tunnel tests, and on an outdoor rotating rig [4]. As for field tests on a full-scale WT, only three are known: Sandia field test on a Micon 65/13 turbine (115kW) [5]; DTU and Vestas test on a V27 (225kW) turbine [6], Siemens Gamesa Renewable Energy (SGRE) and DTU tests on an SWT-4.0-130 (4.0 MW) [4] as part of the INDUFLAP2 project. These field tests confirmed the potential of active flaps in controlling the aerodynamic loads but also showed the need for further development and validation of the

numerical ATEFS models. From 2019, SGRE and DTU have started the Validation of Industrial Aerodynamic Active Add-ons (VIAs) project, described by [7], where a 4.3 MW rated power and 120m diameter wind turbine prototype (PT) has been equipped with an ATEFS on a single blade. The active flap has been tested with different actuation strategies and actuation pressure levels between May 2021 and February 2022, providing the measurement data necessary for the ATEFS aeroelastic model validation described in this article. This validation, the first (to the author's knowledge) based on field measurements on a commercial scale WT prototype, focuses on the aeroelastic ATEFS model of BHawC and HAWC2 tools for the case of stationary activation of the flap. The validation investigates if the flap models estimate with sufficient accuracy ($\pm 5\%$) the WT mean operational parameters such as power, rotor speed and pitch angle, and the mean and max blade loads when the flap is operated in a stationary actuation level. This achievement is the first step in fully validating the ATEFS aeroelastic model that can enable the aeroelastic design of the future WT equipped with a reliable flap system.
In this article, the field test campaign setup is briefly described in chapter 2, followed by the descriptions of the aeroelastic models and the validation procedure in chapter 3. Afterward, the results are shown in chapter 4 and discussed in chapter 5.

2. Field test

2.1. Field Test setup

In the VIAs project, an ATEFS has been equipped on a single blade of the PT owned by SGRE and located in the test site of Høvsøre (DK). The active flap, detailed described in [7], is placed on the trailing edge of the outer 20 meters of the blade and activated via a pressure supply system placed in the hub of the wind turbine. The pressure supply system can operate the flap at different pressure levels yielding different flap deflections. The PT Supervisory Control and Data Acquisition (SCADA) system continuously logged the operational parameters, such as power, pitch, and rotor speed, with a 25Hz sampling. In addition, all three blades had strain gauges instrumented, allowing to measure flapwise and edgewise bending moments with the same sampling of the SCADA. Strain gauges were located at a distance of 3 m from the root. Furthermore, a met mast located approximately 2.5 diameters in front of the WT provided the wind speed and direction, atmospheric pressure, temperature, and humidity.

2.2. Field Campaign

The VIAs project tested the ATEFS with different actuation strategies and actuation pressure levels between May 2021 and February 2022. For the aeroelastic model validation of the active flap in a stationary state, the 10 minutes flap stationary state cycle data are selected. This cycle consisted of 10 minutes of stationary flap activation (AFOn) followed by 10 minutes of stationary flap deactivation (AFOff) while the WT was in normal power production, acquiring two independent standard 10 min time statistics of load and power for every cycle. This cycle was performed for four different activation pressure levels, labeled level 1 through 4, where level 1 corresponds to an angular flap deflection of approximately 13 deg and level 4 to an angular flap deflection of approximately 23 deg. The measurements are filtered so that only normal operation measurements are included. Moreover, filtering based on wind direction and wind direction change is applied to the available database to ensure the wind data measurements are not affected by nearby wind turbine wake or wide wind direction changes. Furthermore, periods with malfunctioning of the ATEFS, the met mast wind sensor, or load sensors are removed. Among the remaining measurements, only the activation pressure level 3 case has sufficient measurements for the aeroelastic model validation, and therefore it is the test case used in the validation described in the following chapters. The available number of measurements AFOn at pressure level 3 and AFOff are shown in table 1, binned by their mean wind speed. The AFOff

Table 1. Number of measurements binned per mean wind speed for AFOff and AFOn at pressure level 3.

Wind speed [m/s]	6	7	8	9	10	11	12	13	14	15	16	17	18	19	20	Total
# AFOff measurements	28	100	79	56	67	76	77	50	65	36	19	20	10	7	5	695
# AFOn measurements	4	15	14	17	19	11	15	25	13	16	15	7	5	0	0	176

state is common to other tests performed on the flap and therefore it has more measurements than the AFOn.

3. Aeroelastic models validation

3.1. BHawC model

BHawC is the aeroelastic engineering tool based on the Blade Element Momentum (BEM) [8] developed internally by SGRE. It includes a Flap Module modeling the aerodynamic and the actuator system of the flap.
SGRE provided the initial BHawC model of the SGRE WT prototype. The Flap Module aerodynamic is updated with the aerodynamic characteristics of the ATEFS prototype operated at different pressure levels obtained by wind tunnel measurement in the VIAs project [9]. Figure 1 shows an example of the impact on the normalized lift coefficient and gliding ratio of a section of the active flap. The curve labeled as baseline represents the airfoil without flap. Instead, the tuning of the Flap Module actuator model is not relevant for the aeroelastic model validation of the flap in a stationary state, and it is omitted in this study.

3.2. HAWC2 model

HAWC2 is the aeroelastic engineering tool based on BEM developed by DTU Wind Energy [10] and [11]. It includes the Beddoes-Leishman type ATEFlap dynamic stall model [12] to account for the unsteady aerodynamics associated with the active flaps. The HAWC2 model of the SGRE WT prototype is derived from the BHawC model. The structural models of the rotor, nacelle, and tower are tuned to match the HAWC2 model with a difference in masses below 1 kg, in the CoG positions below 10 cm, and for the principal moments of inertia below 1%. The frequencies of the first 20 WT modes are within 1.6% and the dampings are mainly below 6%. The HAWC2 blade aerodynamic model directly utilizes the BHawC blade profile coefficient file. The Preproc_ATEFlap tool is utilized to convert the ATEFS profiles aerodynamic coefficient files in the ATEFlap format where aerodynamic coefficients are given as a function of angle of attack and flap. In detail, coefficients of fully activated flap are assigned at 10 deg flap, of fully deactivated flap at 0 deg flap, and of the blade without flap for -20 deg flap. The last assignment is needed to properly model the two blades without flap inside the ATEFlap model. As the controller, the HAWC2 model implements an external dll file provided by SGRE, replicating the WT prototype controller implemented in the BHawC model.

3.3. Wind model

To minimize the source of uncertainties in the model comparison, the same wind input is applied to both BHawC and HAWC2 models. For a constant wind, this is achieved by defining the same wind box size and node locations in both models and applying the same wind shear model based on power law. For turbulence winds, the turbulence box is computed by an external code, written in MATLAB language [13], reproducing the BHawC internal turbulence generation and scaling process. The turbulence boxes are computed for every Turbulence Intensity (TI) and wind speed combination and then loaded in the models without further scalings. Figure 2 shows the same time series of 12.5 m/s mean, 5% TI and 3.9 deg yaw misalignment of wind speed at hub height in both aeroelastic codes. The small time shift, always within two time steps, is present in case of yaw misalignment due to the different definitions of the origin of the wind reference system. A compensation for this difference is currently under development.

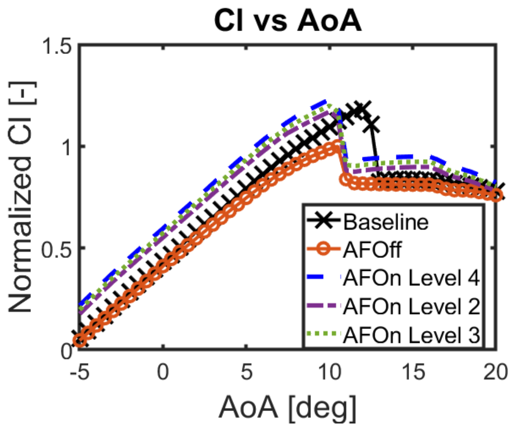

Figure 1. Example of normalized aerodynamic coefficient of ATEFS.

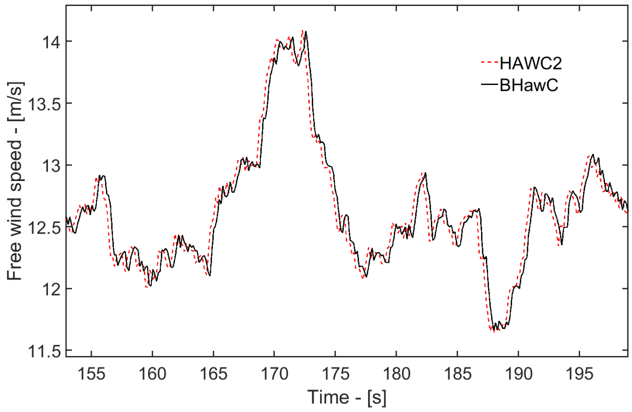

Figure 2. Example of the same time series of 12.5 m/s mean, 5% TI and 3.9 deg yaw misalignment of wind speed at hub height in BHawC and HAWC2.

3.4. Steady state validation
The steady state comparison of the HAWC2 and BHawC ATEFS models investigates the differences between the two models on computing the active flap impact on WT operational parameters (power, rotor speed, and pitch angle) and blade root bending moments (both flapwise and edgewise loads) when the flap is activated in a stationary condition. The steady state comparison has been divided into three phases: comparison without ATEFS model (No ATEFS), to define the baseline of the differences between the two aeroelastic tools; comparison with flap model included and flap deactivated (AFOff), and with flap stationary activated (AFOn). All the aeroelastic simulations were computed with constant wind speed with intensity from 3 to 10 m/s with step of 1 m/s.

3.5. Field data validation
The validation of the ATEFS with field data is inspired by the IEC61400-13 guideline. It is performed by comparing the measurements from the PT to BHawC and HAWC2 simulation results, where environmental wind condition (mean wind speed, mean wind direction, TI, mean wind shear, mean air density) measured on the site is mirrored into the simulation setup. Every 10 minutes measurement is matched with a 10 minutes simulation (so called O2O simulation) with equivalent environmental conditions. The 10 minutes statistics (mean, std, max) of WT operational parameters and blade loads are then binned in function of the wind speed. ATEFS model validation is then achieved by comparing the binned value of simulations with the measurements. The binning value of the std is not obtained by averaging but by computing the variance of the set of variances. As motivated in chapter 2.2, only the measurements with flap pressure activation level 3 are included and only the wind speeds with more than 10 AFOn measurements, reducing the wind range between 7 to 16 m/s. Initially, for the ATEF model, the flap aerodynamic polars corresponding to activation level 3 were initially selected but due to high blade load overestimation the pressure level 2 polars have been preferred for the validation.

Table 2. Comparison of HAWC2 and BHawC Blade Root Moments for steady state simulations.

Case	HAWC2 vs BHawC Blade Root Flapwise Bending Moment		HAWC2 vs BHawC Blade Root Edgewise Bending Moment	ATEFS impact Blade Root Flapwise Bending Moment	
	Max	Mean	Max	Max	Mean
No ATEFS	0% to 3%	0.5% to 2%	-2% to 1%	-	-
AFOff	-1% to 3%	0.5% to 3%	-2% to 1%	-1% BwF	-2% BwF
AFOn	-1% to 4%	0.5% to 4%	-2% to 1%	up to +10% BwF up to -5% BNF	

4. Results

4.1. Steady state validation

The steady state comparison of the PT HAWC2 and BHawC models without active flap shows a difference within ±1% in the mean power, ±0.1 rpm in the mean rotor speed, and ±0.2 deg in the mean pitch angle. The ATEFS model, activated or not, does not change the relative differences of the WT operational parameters. Table 2 summarizes the differences in the blade root bending moments. In the case without flap, HAWC2 provides up to +2% mean and up to +3% max flapwise moment. When the ATEFS models are included in both codes, differences in the mean flapwise moment of the blade with flap increases by 1% for AFOff and by 2% for AFOn. Max flap moment difference increases to +4% only for AFOn. The difference in the blade root edgewise moment is within ±2% and is not affected by the ATEFS models.

4.2. Field data validation

This section describes the results from comparing the PT measured data with the so-called O2O simulations, defined in chapter 3.5, obtained for both BHawC and HAWC2 aeroelastic codes. The comparison is based on the binned 10 minutes statistics of WT operational parameters (power, rotor speed, and pitch angle) and blade root bending moments. Due to space limitations, in this paper, the comparison is not generally shown for every binned wind speed, but the general trends over the wind speed range are summarized. When relevant, the comparison is detailed to the wind speed window before or after the rated wind speed (RWS). The mean and Coefficient of Variation (CV) are used to compare the WT operational parameters and blade loads. The absolute maximum value is also included in the blade loads comparison, as it is a critical parameter in the blade design. For clarity, it is reminded to the reader the CV is defined as the ratio of the standard deviation to the mean, expressed in percentage, and its variations in this paper are meant as absolute differences.

The upper part of Table 3 summarizes the comparison for the WT operational parameters. The computed mean power is within ±2% of the measured value for AFOff and within ±3% for AFOff. The computed power CV is 6% lower for wind speed below RWS and increases up to +1% above RWS. The computed mean rotor speed is within ±0.1 rpm with a reduction of CV within -2%, mainly below RWS. The BHawC mean pitch angle is within ±0.2 deg, and the HAWC2 one is within ±0.3 deg. For both calculated values, the standard deviation is reduced up to 0.5 deg above RWS (Std is used instead of CV because the pitch angle mean approaches zero around RWS and CV will tend to infinite).

The lower part of Table 3 summarizes the impact of the ATEFS activation on both measured and computed WT operational parameters. ATEFS activation impacts the mean powers less than 1.5% on the mean value, mainly below RWS, and increases the CV of up 8% for the measurements and up to 25% for the computed values. The mean rotor speeds are impacted less than 1% and the CV below 2% (0.7% in the simulations). The mean pitch angle above RWS increases up to 0.9 deg and its std up to ±0.2 deg.

Table 3. WT operational parameters. Top: Models to measurement comparison. Bottom: ATEF impact.

	BHawC (BH) and HAWC2 (H2) vs Measurements		
	Mean		**CV or Std**
Power	±2% AFOff / ±3% AFOn	CV:	-6% below RWS to 1% above RWS
Pitch	±0.2 deg BH / ±0.3deg H2	Std:	0 deg below RWS to -0.5 deg above RWS
Speed	±0.1 rpm below RWS	CV:	-2% to 0 below RWS

	ATEFS impact on Measurements (PT), BHawC (BH) and HAWC2 (H2)		
	Mean		**CV or Std**
Power	Max ±1.5% below RWS	CV:	PT: +8% to 0 below RWS BH and H2: +2% to 0
Pitch	Up to +1 deg above RWS	Std:	0 deg below RWS to ±0.2 deg above RWS
Rotor speed	Within ±1% below RWS	CV:	PT: Up to +2% below RWS BH and H2: +0.7%

Table 4. Mean Blade root flapwise bending moment: models to measurement comparison.

BHawC (BH) and HAWC2 (H2) vs Measurements Mean Blade root flapwise bending moment						
Blade	**ATEFS**	**Mean BH**	**Mean H2**	**CV (BH and H2)**		
				Below RWS	**At RWS**	**Above RWS**
B (ATEFS)	AFOff	-1% to +2%	+1% to +4%	+2.5%	+1%	+2.5%
	AFOn	-1% to +2%	+2% to +5%	+1%	+1%	+2.5%
A	AFOff	-1% to +2%	0 to +3.5%	+2.5%	+0.5%	+2.5%
	AFOn	-1% to +2%	+1% to +4%	+1%	+1%	+4%
C	AFOff	-0.5% to +1.5%	+1% to +3.5%	+0.5%	+0.5%	+2.5%
	AFOn	-1% to +1.5%	0 to +3%	+0.5%	+0.5%	+1.5%

Table 4 summarizes the model to measurement comparison results for the mean blade root flapwise bending moment. The results are shown for the three blades where Blade B is equipped with flap. The BHawC computed mean blade load is within -1% to +2% the measured value, independently by the ATEFS presence or status. HAWC2 model is between 0 to +4% the measured value in the blades without flap and in Blade B when AFOff. With AFOn, the difference increases by 1%. The difference of the blade load CV is similar between the two tools and independent of the ATEFS presence or status. CV difference is minimum around RWS, with a max 1% difference, and increases above RWS to 4%. Below RWS, it fluctuates between 1% to 2.5%. The differences for the max blade load are summarized in Table 5: for BHAWC simulations, max blade load are up to 1.5% higher than measurements when flap is not active and up to to 2% when flap is activated; for HAWC2 simulations, the flap activation increases the difference from 2.5% to 4% in blade with flap and 1.6% to 3% in blades without flap.

The impact of ATEFS on the blade root flapwise bending moment is shown in Table 6. In the blade equipped with flap, the measurements show an increase of the mean of 4.5% to 7.5%. The increase in the BHawC simulations (+5% to +8%) and HAWC2 simulations (+6% to + 9%) is slightly higher. The max blade loads increase by 3%, 4%, and 5% in the measurement and BHawC and HAWC2 simulations, respectively. The CV is similar for the three cases, increasing up to 2%. In the two blades without flap, measurements and simulations show a reduction of the mean load up to -5%; meanwhile, the max load also reduces up to -1.9% in the measurement and around 1% in the simulations. Finally, the load CV decreases up to -3% in the measurements

Table 5. Max Blade root flapwise bending moment: models to measurement comparison.

BHawC (BH) and HAWC2 (H2) vs Measurements Max Blade root flapwise bending moment			
Blade	**ATEFS**	**Max BH**	**Max H2**
B (ATEFS)	AFOff	+1.5%	+2.5%
	AFOn	+2%	+4%
A	AFOff	+1.3%	+1.6%
	AFOn	+2%	+3%
C	AFOff	+0.1%	+0.1%
	AFOn	+0.1%	+0.1%

Table 6. Blade root flapwise bending moment: ATEFS impact.

ATEFS impact on Measurements (PT), BHawC (BH) and HAWC2 (H2) Blade root flapwise bending moment			
Blade	**Mean**	**CV**	**Max**
B (ATEFS)	+7.5% to 4.5% PT +8% to 5% BH +9% to 6% H2	+0% to 2%	+3% PT +4% BH +5% H2
A	0 to -5%	-2% to +1% PT +0 to -1% BH, H2	-1.9% PT -1.3% BH -0.5% H2
C	0 to -5%	-3% to 0 PT -1.5% to 0.5% BH, H2	-1.1% PT -1% BH -1% H2

and up to -1.5% in the simulations.

5. Discussion

The steady state comparison shows that the BHawC and HAWC2 simulations of the PT are in good agreement, with negligible differences in WT operational parameters, ±2% in the max blade root edgewise bending moment and +2% mean (+3% max) in the blade root flapwise bending moment. When introduced, the ATEFS model does not significantly affect the relative difference between the two models except for the mean and max flapwise bending moment that increases by 1% when the flap is deactivated and another 1% when the flap is activated. It can be concluded that the BHawC and HAWC2 ATEFS models are equivalent when simulating flaps at a constant activation state. When the flap is included, the load reduction measured on the blade with flap (BwF) can be understood looking at figure 1 where the normalized lift coefficient of the profile with flap deactivated (red line with circle markers) is lower than the baseline (black line with x markers). When the flap is activated, the aerodynamic properties of the BwF shift to higher values (blue dash line), increasing the blade flap loads. The load reduction in the BNF is also an indirect consequence of the higher lift on the BWF. When the WT is in a pitch-controlled regime, if the flap is activated, the lift (and consequently the torque) generated by the BwF increases. The controller, to keep the rotor speed at the rated value, reacts increasing the pitch angle. The increase in pitch effects all the blades: on the BNF it reduces the blade loads, as observed; on the BwF it reduces the load increase due to the flap activation. The impact of the flap on the pitch angle is visible in figure 3b where the difference

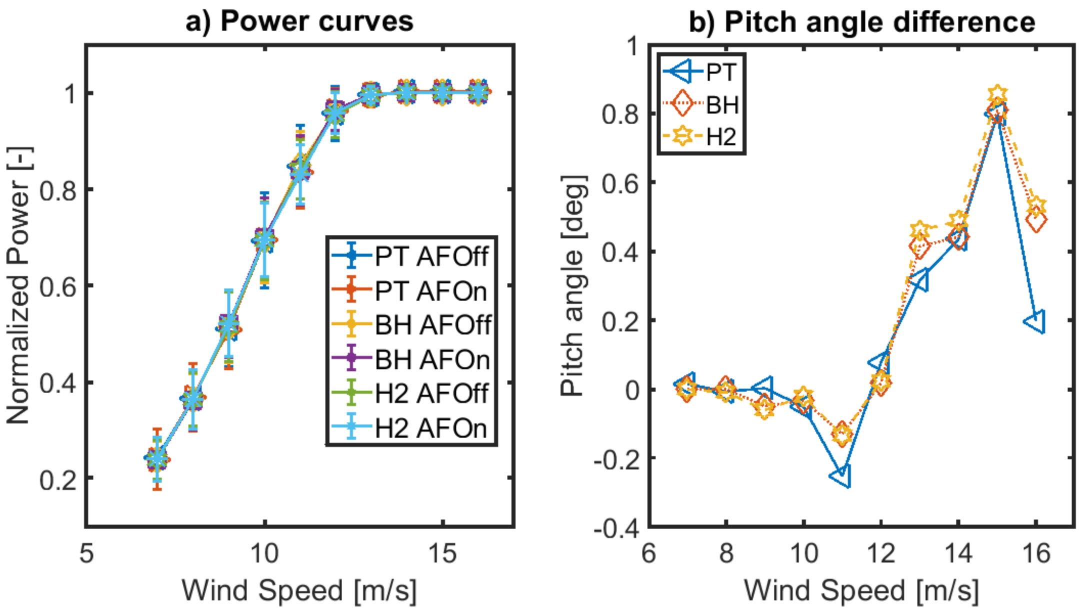

Figure 3. a) Power curves comparisons. b) Pitch angle differences due to ATEFS activation.

between PT pitch angle in AFOn and AFOnff are shown.
The validation based on the field data measurements shows that both BHawC and HAWC2 O2O simulations are in good agreement with the measured data from the PT. Differences between computed and measured WT operational parameters, summarized in the upper part of Table 3, are acceptable and are not affected by the flap activation state. The power curve comparison is shown in figure 3a, where the estimated mean power curves (with std included in the error bar) overlap the corresponding measured curves for AFOff and AFOff. Plots of comparison of computed rotor speed and pitch angle versus measurements (not included in the paper due to space limitation) show similar correlations. The ATEFS models of the two aeroelastic codes therefore correctly simulate the impact of the flap in stationary actuation state on power, pitch and rotor speed as summarized in the lower part of the table 3. Figure 3b shows the variation of the mean pitch due to the flap activation. The difference of the measured pitch on the WT prototype (blue line with triangle markers) is matched within 0.2 deg by the difference of the computed pitch estimated by both aeroelastic codes.
The comparison of the blade loads, summarized in Table 4 and Table 5, shows that the BHawC model consistently overestimates the mean blade loads of max 2%, independently from the flap model presence and state, meaning the BHawC ATEFS model does not impact the simulation accuracy. The HAWC2 ATEFS model instead slightly increases the load difference (+0.5% AFOff, +1% AFOn) for the blade with flap, as seen in the steady state validation. The Max blade loads follow a similar pattern, with an increase of +1% due to the flap model of HAWC2. Both codes also slightly overestimate the blade load CV, mainly above RWS, but it does not seem affected by the flap state. In conclusion, the computed loads by BHawC and HAWC2 ATEFS models consistently match the measured loads within a constant and acceptable error when the flap is activated on a stationary state.
The mean load increase on the blade with flap due to flap activation is slightly overestimated (+1% from BHawC, +1.5% by HAWC2) as well as the max load (+1% BHawC and +2% HAWC2), but it is not observed in the corresponding load reduction on the blades without flaps (reduction explained earlier in this chapter). The flap load overestimation is visible in figure 4a

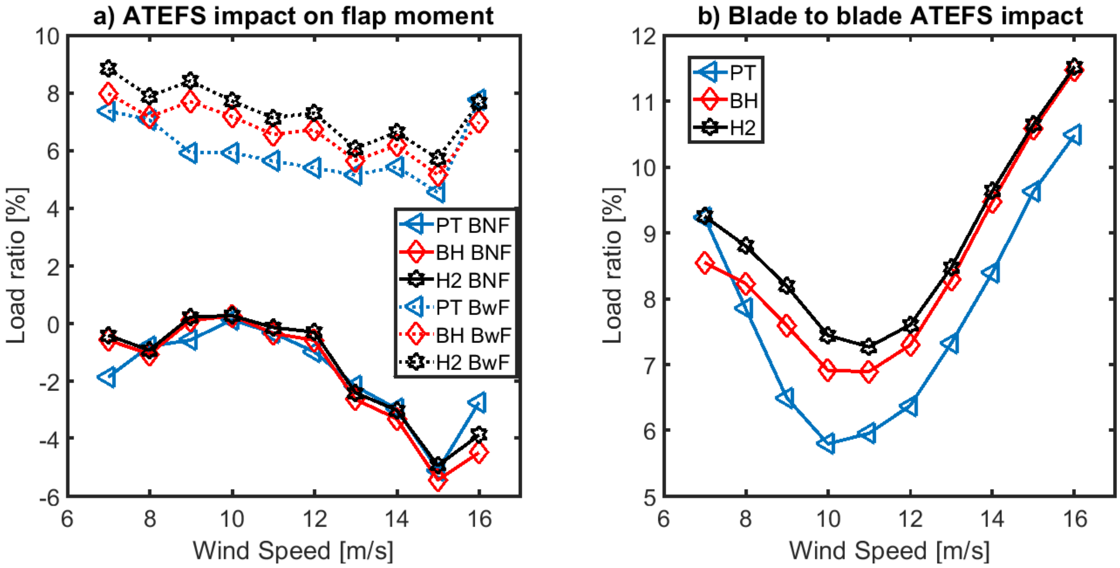

Figure 4. a) Variation of flap bending moment on BNF and BWF due to ATEFS activation. b) Blade to Blade load variation due to ATEFS activation.

where the measured (blue line with triangular markers) and computed (BHawC: red line with diamonds markers, HAWC2: black line with hexagonal markers)) impact of flap activation on both BwF (dotted lines) and BNF (solid lines) are shown. The flap load overestimation only on the BwF can be explained by flap polars coefficients overestimating the actual flap aerodynamic performance. From the WT load design perspective, the small overestimation of the blade loads can be seen as a safe condition, providing conservative extreme (max load) and fatigue (mean and CV) loads. However, if the flap load variation is used as a handler to mitigate the load level of the blade of other components, the overestimation of the load mitigation handle can lead to underestimating the WT loading with a severe consequence of the turbine integrity and lifetime. The flap polars used in the current study were based on a delta-approach utilizing wind tunnel measurements performed on a similar airfoil model (see [9]) for the active flap at different activation levels. The underlying assumption is that the difference in lift, drag, and moment coefficient is equivalent for the airfoil sections of the blade in question and that these relative differences are scalable with respect to the relative size of the active flap device and the local chord of the blade. In future studies, a more detailed CFD (or experimental) analysis of the active flap device located in different positions along the blade will be performed to increase the accuracy of the polar coefficients.

In the VIAs project [7] the characterization of the steady state response of the PT active flap has been performed via a blade-2-blade (b2b) method. In summary, this method estimates the flap impact by comparing the loads on the flap-equipped blade to a neighbor blade without a flap. A similar b2b method is applied to the measurements and aeroelastic simulations analyzed in this paper, obtaining the flap load impacts shown in Figure 4b. The b2b flap load impact based on measurements (blue line with triangular markers) has a similar shape and values of the corresponding one (level 3 magenta lines) shown in Figure 5 of [7]. Even if the validation via aeroelastic simulations of the b2b approach is out of the scope of this study, the preliminary and almost qualitative comparison between the ATEFS load impacts obtained via the b2b approach supports this methodology.

6. Conclusion

Within the framework of the VIAs project, an Active Trailing Edge Flap System has been installed on a fully instrumented 4.3 MW test wind turbine and has undergone field testing for over 1.5 years. The measurement data obtained in the field test have been the foundation for the validation of the ATEFS model of the aeroelastic engineering tools BHawC and HAWC2. The model validation has been focused the flap stationary activation state. At first, the ATEFS models of the two aeroelastic tools showed to be in good agreement (max difference of+2% for max blade loads) for steady state simulations. Furthermore, with an accuracy of ±3% on mean power, ±0.2 deg on mean pitch angle, ±0.1 rpm on rotor speed, ±2% on flapwise blade loads (±5% for HAWC2), the measurement to simulation comparison showed both HAWC2 and BHawC aeroelastic ATEFS models provide a reliable and precise estimation of the impact of the flap on the wind turbine. To the authors' knowledge, this is the most extensive (in terms of wind condition time and flap size) validation of the aeroelastic ATEFS models and a fundamental milestone for the safe and reliable aeroelastic design of commercial WT equipped with active flaps.

References

[1] Barlas T, Pettas V, Gertz D and Madsen H A 2016 Extreme load alleviation using industrial implementation of active trailing edge flaps in a full design load basis *Journal of Physics: Conference Series* vol 753 (Institute of Physics Publishing) ISSN 17426596

[2] Pettas V, Barlas T, Gertz D and Madsen H A 2016 Power performance optimization and loads alleviation with active flaps using individual flap control *Journal of Physics: Conference Series* vol 749 (Institute of Physics Publishing) p 012010 ISSN 17426596 URL `https://iopscience.iop.org/article/10.1088/1742-6596/749/1/012010` `https://iopscience.iop.org/article/10.1088/1742-6596/749/1/012010/meta`

[3] Prospathopoulos J M *et al.* 2021 *Wind Energy* **24** 357–378 ISSN 10991824 URL `https://doi.org/10.1002/we.2578`

[4] Gonzalez A G, Enevoldsen P, Barlas T K, Madsen H A and Olsen A S 2020 **1618** 52024 ISSN 17426596

[5] Berg J C, Barone M F and Resor B R 2013 *51st Aiaa Aerospace Sciences Meeting Including the New Horizons Forum and Aerospace Exposition 2013*

[6] Castaignet D, Barlas T K, Buhl T, Poulsen N K, Wedel-Heinen Jens J, Olesen N A, Bak C and Kim T 2014 *Wind Energy* **17** 549–564 ISSN 10991824, 10954244

[7] Gomez Gonzalez A, Enevoldsen P B, Madsen H A and Barlas A 2022 *TORQUE 2022*

[8] Fisker Skjoldan P 2011 *Aeroelastic modal dynamics of wind turbines including anisotropic effects* (Risø National Laboratory) ISBN 9788755038486

[9] Gomez Gonzalez A, Enevoldsen P, Akay B, Barlas T, Fischer A and Madsen H A 2018 *J. Phys.: Conf. Ser.*

[10] Larsen T and Hansen A 2007 *How 2 HAWC2, the user's manual* (*Denmark. Forskningscenter Risoe. Risoe-R* no 1597(ver. 3-1)(EN)) (Risø National Laboratory) ISBN 978-87-550-3583-6

[11] Aagaard Madsen H, Juul Larsen T, Raimund Pirrung G, Li A and Zahle F 2020 *Wind Energy Science* **5** 1–27 ISSN 23667451 URL `https://doi.org/10.5194/wes-2019-53`

[12] Bergami L, Gaunaa M and Technical Univ of Denmark R N L f S E W E D 2012 *ATEFlap aerodynamic model, a dynamic stall model including the effects of trailing edge flap deflection* ISBN 9788755039346

[13] MATLAB 2018 *9.7.0.1190202 (R2019b)* (Natick, Massachusetts: The MathWorks Inc.)

Acknowledgments
We thank Jose Fernandez Bolanos Maya for the assistance with the wind models comparison and Mathias Stolpe, Helge Aagaard Madsen and one anonymous reviewer whose comments and suggestions helped improve and clarify this manuscript.
This research was partially funded by Danmarks Innovationsfond, Case no. 9065-00243B, PhD Title: "Advanced model development and validation of Wind Turbine Active Flap system".
The Validation of Industrial Aerodynamic Active Add-ons (VIAs) project is a collaboration between Siemens Gamesa Renewable Energy, DTU Wind Energy and Rehau AS, partially funded by EUDP under journal nr. 64019-0061.

Article 2.

Validation of aeroelastic dynamic model of Active Trailing Edge Flap system tested on a 4.3 MW wind turbine.

Under review at the Wind Energy Science journal.

Validation of aeroelastic dynamic model of Active Trailing Edge Flap system tested on a 4.3 MW wind turbine

Andrea Gamberini[1,2], Thanasis Barlas[2], Alejandro Gomez Gonzalez[1], and Helge Aagaard Madsen[2]

[1]Siemens Gamesa Renewable Energy A/S, Brande, Denmark

[2]DTU, Dept. of Wind and Energy Systems, Roskilde, Denmark

Correspondence: Andrea Gamberini (andgam@dtu.dk)

Abstract. Active Trailing Edge Flap (ATEF) is a promising technology for Wind Turbine load reduction and AEP improvement. However, this technology still needs extensive field validations to prove the reliability of the ATEF aeroelastic modeling codes. This article describes the validation of the dynamic response of the ATEF aeroelastic models developed for the BEM-based solvers HAWC2 and BHawC. The validation relied on field data from a 4.3 MW Wind Turbine (WT) equipped with an ATEFS on one blade and operating in normal power production. The validation consisted of three phases. At first, video recording of the ATEF deflection during WT operation allowed the tuning of the flap actuator model. In the second phase, the aerodynamic flap model was tuned and validated through the lift coefficient (Cl) transients measured with an innovative autonomous add-on measurement system placed on the blade in the middle of the spanwise extension of the ATEF. Finally, the aeroelastic ATEF model was validated based on the blade root moment (BMrM) transients over three months, from October to December 2020, with varying weather conditions. The validations showed that the simulations transient of Cl and MBrM are in good agreement with the corresponding measured transients, with a maximum difference for the blade-to-blade MBrM transients below 1% of the mean blade load during flap activation and below 1.7% during flap deactivation. An analysis of the possible root causes of these differences suggested additional measurements to improve the ATEF model tuning. The validation confirmed that the aeroelastic ATEF models provide a reliable and precise estimation of the impact of the flap on the wind turbine during flap actuation.

1 Introduction

In recent years, the steady growth in the size of utility-scale Wind Turbines (WT) led by the pursuit of lower levelized cost of energy resulted in a significant increase in the load carried by the WT components. One of the most promising technologies to mitigate the load increase consists of actively controlled flaps located at the blade trailing edge, the so-called Active Trailing Edge Flap (ATEF). From the pioneering works of Van Wingerden et al. (2008), Andersen (2010), Lackner and Van Kuik (2010),Aagaard Madsen et al. (2010) and Castaignet et al. (2011), to some of the more recent research by Bergami and Poulsen (2015), Barlas et al. (2016), Fischer and Aagaard Madsen (2016) and Bernhammer et al. (2016), several studies support that the integration of the ATEF in the WT design has the potential to reduce extreme and fatigue loads. These load reductions can be exploited to lower the components' cost or to increase the AEP, as shown by Pettas et al. (2016) and Abbas et al. (2023).

Despite the consensus on the potential benefits of active flaps in load reduction, the full-scale validation of ATEF aeroelastic engineering models and their potential load reduction is limited. Validating these models is challenging. An extensive code-to-code comparison of various existing models for simulating active flaps on rotating blades was performed in Prospathopoulos et al. (2021), where state-of-the-art Blade Element Momentum (BEM) models (hGAST, HAWC2, and FAST) were compared with higher fidelity models, including free-wake lifting line (GENUVP) and fully resolved Computational Fluid Dynamics (CFD) models (MaPFlow and FLOWer). The comparison concluded that the BEM models cannot reproduce the correct distribution of the local thrust forces in the proximity of the flap edges because they neglect the 3D effects originated by the vorticity trailed from the edges and along the span of the flap section. However, these BEM models reasonably estimate the impact of an oscillating flap on the integrated overall thrust when the oscillating frequency is 1P. This result is explained by the over-prediction of the flap impact in the flap region being overall compensated by the flap impact under-prediction in the blade regions near the flap edges. With the increase of the flap activation frequency, BEM model accuracy decreases. Finally, the study showed that modifying the BEM models to account for 3D effects due to the vorticity trailed from the flap edges (HAWC2 with Near Wake model and modified FAST) improved their prediction of both the local and the global impact of the flap on the thrust force.

ATEF subsystem validations have also been conducted through wind tunnel tests (e.g. Barlas et al. (2013)) and outdoor rotating rig experiments Gonzalez et al. (2020). Recently, 3-dimensional lab-scale tests were performed within the large wind tunnel of the TU Berlin on BeRT, a $3\,\mathrm{m}$ diameter research turbine equipped with ATEF on each blade. The ability of different controllers employing trailing edge flaps to reduce fatigue (Bartholomay et al. (2022)) and extreme (Bartholomay et al. (2023)) flapwise blade root bending moments were assessed meanwhile providing datasets for future validation of numerical models. Regarding full-scale validation, only three field tests have been reported so far. These tests include the Sandia field test on a Micon 65/13 turbine ($115\,\mathrm{kW}$) Berg et al. (2013), the DTU and Vestas test on a V27 ($225\,\mathrm{kW}$) turbine Castaignet et al. (2014), and the Siemens Gamesa Renewable Energy (SGRE) and DTU tests on an SWT-4.0-130 ($4.0\,\mathrm{MW}$) turbine as part of the INDUFLAP2 project Gonzalez et al. (2020). Although these field tests confirmed the potential of active flaps in controlling aerodynamic loads, they also highlighted the need for further development and validation of numerical models for ATEF.

To address this gap, the Validation of Industrial Aerodynamic Active Add-ons (VIAs) project was carried out between 2019 and 2022 by SGRE and DTU, as described in Gomez Gonzalez et al. (2022). As part of this project, a prototype wind turbine with a rated power of $4.3\,\mathrm{MW}$ and a diameter of 120m (PT) was equipped with an pneumatically activated ATEF on a single blade. From May 2020 to February 2021, extensive testing of the active flap was conducted with different actuation strategies and flap deflection angles. The data collected in VIAs field tests allowed Gamberini et al. (2022) to validate for flap stationary activation state the ATEF model of the aeroelastic engineering tools BHawC (Fisker Skjoldan (2011)) and HAWC2 (Larsen and Hansen (2023) and Aagaard Madsen et al. (2020)). The study relied on the measurements of the 10 minutes mean and maximum blade bending moments at the root of the three blades of the PT collected with the flap locked in a fully activated or deactivated position. A one-to-one validation approach was followed, where the aeroelastic simulations were performed under the wind conditions measured during the test campaign. The validation showed that the BHawC and HAWC2 tools equipped with ATEF agree with each other (difference within 2% for max and mean blade loads) and can estimate the blade loads with accuracy within $\pm5\%$ for ATEF stationary activation state.

The subsequent step in the ATEF model validation is the comparison of the aeroelastic response to the step actuation of the flap. In this article, the transient response of the BHawC and HAWC2 ATEF models during flap activation and deactivation is investigated and compared to the field data gathered in the VIAs project. The purpose of this validation is to enable reliable aeroelastic modeling of the load reduction strategies based on the actuation of trailing edge flaps, a fundamental milestone in the design of future WT equipped with ATEF.

In this article, section 2 resumes the active flap system installed on the PT, and section 3 describes the PT aeroelastic model developed in BHawC and HAWC2 together with the structure of the ATEF model. The validation of the aeroelastic model is conducted in steps. The first step is tuning the actuator model, described in section 4. This step covers both the pneumatic system and flap sub-system response. Then the aerodynamic model is initially validated with a 3 hours field campaign where the lift coefficient (Cl) was measured on a specific section of the PT, described in section 5. Finally, section 6 describes how the model is validated with a three months field campaign, covering a broad range of wind conditions but relying only on blade root loads. The overall results are then discussed in section 8.

2 Flap system and measurement setup

The VIAs project implemented an ATEF system on a single blade of the SGRE PT located at the Høvsøre test site in the northwest of Denmark. Gomez Gonzalez et al. (2022) provides a detailed description of the active flap system, which consisted of a pneumatic supply system located in the hub connected with a hose to the active flap. The flap, shown on the left of Figure 1, was placed on the trailing edge of the outer 20 meters of the blade, between 64% and 98% of the blade radius. The pneumatic supply system had a remotely programmable control that regulated the pressure in the hose via a pressure valve. The air pressure in the hose controlled the flap movement; the higher the pressure, the higher the flap deflection amplitude. Throughout the field campaign, the PT was equipped with a Data Acquisition System (DAS) system that continuously logged operational parameters, such as power, pitch, and rotor speed, with a 25 Hz sampling rate. The same sampling rate was used to measure the flapwise and edgewise bending moments of all three blades by strain gauges located in the blades at $3\,\mathrm{m}$ from the root. Also, the pressure at the pressure valve in the hub was recorded and integrated into the DAS. Furthermore, a met mast located approximately 2.5 D ($300\,\mathrm{m}$) in front of the WT provided the wind speed and direction at three different heights, the atmospheric pressure, the temperature, and the humidity.

In June 2020, an inflow and pressure measurement system was temporarily added to the PT to measure the aerodynamic properties at a specific ATEF section, as described in Madsen et al. (2022) and showed in the central photo of Figure 1. The system, developed by DTU, consisted of an inflow 5-hole Pitot tube sensor, a belt with 15 pressure taps, and an autonomous data acquisition and transmission system (flyboard). Both Pitot tube and flyboard were installed on the blade leading edge at $50\,\mathrm{m}$ from the hub flange, in the middle of the spanwise extension of the ATEF. The pressure belt was wrapped around the blade at a spanwise position of $49\,\mathrm{m}$. The inflow and pressure measurement system provided data with a 100 Hz sampling rate that was synchronized with the PT measurement data by the recorded GPS time. A close view of the pressure belt and flyboard

Figure 1. Left photo: Active flap placed on the trailing edge of the blade of the SWT-DD-120 turbine at the Høvsøre test field. Central photo: installation of the flyboard and pressure belt in June 2020. Bottom right photo: close look at the flyboard and the pressure belt. Top right photo: Camera and fins installed to measure the flap deflection. Photos curtesy of SGRE and DTU

is shown in the bottom right photo of Figure 1.

Additionally, two couples of small plastic fins were installed near the pressure belt location to analyze the ATEF deflection visually. The fins of each couple lay aligned on the same blade section, with the two couples spaced around $0.5\,\mathrm{m}$ apart spanwise. For each couple, one fin was attached to the moving ATEF and the other to the blade structure. A GoPro camera was installed closely to record the flap deflection using the fins as reference points, as shown in the top right picture of Figure 1.

3 Aeroelastic setup

3.1 BHawC model

SGRE has internally developed and validated the aeroelastic engineering tool BHawC, based on the Blade Element Momentum (BEM). SGRE has furthermore developed a ATEF Module to model the flap aerodynamic and actuator system.

The BHawC model adopted in this paper was provided by SGRE and fine-tuned by the authors in Gamberini et al. (2022) where they showed the aeroelastic simulations were able to estimate the PT operational parameters with an accuracy of $\pm 3\%$ and blade loads within $\pm 2\%$ for the condition of stationary flap state. The current paper covers the tuning and validation of the ATEF Module actuator and the part of the aerodynamic model responsible for the aeroelastic response to the flap actuation.

3.2 HAWC2 model

HAWC2 is the aeroelastic engineering tool developed by DTU Wind. It is based on BEM and models the unsteady aerodynamics associated with the active flaps with the Beddoes-Leishman type ATEFlap dynamic stall model Bergami and Gaunaa

(2012). The authors tuned the HAWC2 model of the SGRE WT prototype in Gamberini et al. (2022), based on the BHawC model, obtaining negligible code-to-code differences (max difference below 1%) for mass properties and WT operational parameters and a max difference within 4% for the blade loads. For the ATEFlap model, the suggested values of the coefficients for the indicial response exponential function and the exponential potential flow step response were used. These parameters were tuned to describe the step response of the NACA 64-418 profile (18% thickness) that can be considered an acceptable approximation for the modeled ATEF.

3.3 Modeling of the Flap system

The ATEF system installed on the PT was simplified as a controlled pneumatic system that regulated the pressure inside a hose connected to the flap located on the trailing edge of one blade. Increasing the air pressure inflated the hose that deflected the flap. The flap deflection changed the blade profile shape, consequently modifying the local aerodynamic forces and affecting the loading of the whole PT.

In the ATEF aeroelastic model, depicted in Figure 3, the pneumatic system and the flap structure were merged in the actuator model. This model linked the controller signal directly to the flap deflection, disregarding the air pressure signal. This simplification was possible because the pneumatic system did control only the final pressure value but did not control the pressure transient. This transient depended only on the pneumatic system layout. Therefore the air pressure and the consequent flap deflection were expected to have a constant transient for every defined activation pressure value.

The actuator model provided the flap deflection to the aerodynamic model that computed the dynamic aerodynamic properties of the flap section, needed by the aeroelastic code to compute the PT loads. In both codes, the ATEF aerodynamic model relied on the stationary lift and drag coefficient (Cl and Cd) curves of the flap profiles for both active and not active flap states. SGRE provided the aerodynamic characteristics of the 21% thickness flap profile. Similarly to the method described in Gomez Gonzalez et al. (2018), SGRE measured the aerodynamic characteristics in a wind tunnel campaign performed at the Low-Speed Low-Turbulence wind tunnel facilities of the faculty of aerospace of TU Delft. The measurements, run at a Reynolds number of mainly 4 million, focused on the 21% thickness profile where three different shapes of the deflected flap were modeled with a corresponding fixed add-on. The measurements provided the aerodynamic characteristics for the flap that was not active, which was activated with low pressure and activated with high pressure. The data for middle activation pressure were instead obtained by interpolation, as previous tests in the VIAs project showed a linear relation between flap deflection and pressure for the studied ATEF system. To fully simulate the flap on the PT, the aerodynamic characteristics of the 24% and 18% thickness flap profiles were needed. They were computed assuming that the same flap deflection leads to the same lift and drag variation across the family of flap profiles. Under this assumption, from the 21% thickness profile, the lift and drag increases due to a specific flap deflection were calculated as a function of the angle of attack. These ΔCl and ΔCd were added to the 24% and 18% thickness profile properties after being linearly scaled to adjust to the actual chord length of the new profiles. Figure 2 shows an example of the normalized Cl curves for flap not active (black line) and flap active at low pressure (red line) of the 21% (left), 18% (top right) and 24% (bottom right) thickness profiles. It also shows the ΔCl obtained from the 21% thickness profile (center). The ATEFlap model of HAWC2 required the aerodynamic properties to be in a specific format, where aero-

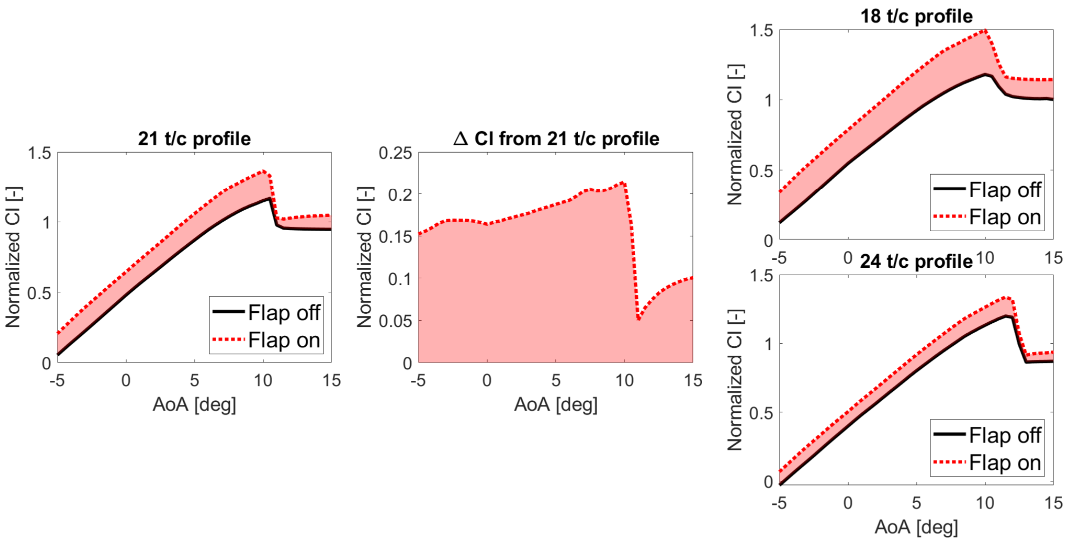

Figure 2. Left: Normalized Cl curve of 21% thickness profile with flap not active (black) and flap active at low pressure (red dotted line). Center: ΔCl from 21% thickness profile due to flap activation. Right: Normalized Cl curve of 18% (Top) and 24% (Bottom) thickness profile with flap active at low pressure (red dotted line) obtained by adding the scaled ΔCl from 21% thickness to the curves with flap not active (black lines).

dynamic coefficients were given as a function of the angle of attack and the angle of flap deflection. This format was obtained utilizing the Preproc ATEFlap tool. BHawC and HAWC2 aerodynamic models assume a linear proportional relationship between the flap deflection and the variation of the static Cl and Cd. Both codes derive the dynamic properties with a partially different approach, mainly due to different dynamic stall models, properties that are then passed to the global WT aeroelastic model.

The tuning and validation of the ATEF model was performed in three steps. At first, the actuator model was tuned to match the actual flap deflections obtained on the PT for the required activation flap pressure. The second step consisted of an initial validation based on the Cl measurements obtained from the flyboard installed at the PT flap location in a three hours long field campaign. Finally, the ATEF aerodynamic model was validated based on blade root load transients measured in a three months long field test.

4 Actuator model tuning

To validate the aerodynamic model, a reliable flap actuator model was needed to compute the flap position and its transient. In this paper, the development and tuning of the flap actuator model were obtained by the analyses of video recordings of the PT flap actuation.

In June 2020, a GoPro camera and two sets of plastic fins were temporarily installed on the PT blade. The camera captured

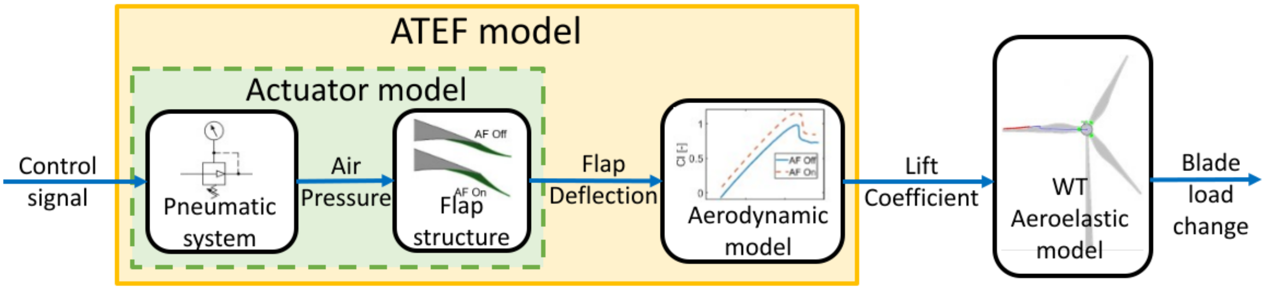

Figure 3. Structure of the ATEF aeroelastic model implemented in BHawC and HAWC2

the movements of the flap during its activation and deactivation under three distinct activation pressure levels (low, middle, and high) and two operational states of the wind turbine: idling mode and normal operation at 6 rpm. Each combination was repeated four times to ensure data reliability. The video analysis and modeling tool Tracker (Brown et al. (2023)) was utilized to extract the flap deflection in each video by tracking the relative position of the two fins during the flap activation and deactivation. For each combination, the four recorded cases consistently yielded a similar flap deflection transient during flap activation; their binning and normalization resulted in the characteristic flap activation deflection transient (activation deflection curve) that ranged between 0 (flap not active) and 1 (flap fully deployed). The characteristic flap deflection transient for deactivation (deactivation deflection curve) was obtained with a similar process.

The comparison of the flap deflection transients showed a substantial overlap of the curves obtained for middle and high activation pressure, with the low-pressure case being slightly faster. Although increasing the activation pressure resulted in higher flap deflection, the normalized flap deflection transient remained independent of pressure from middle activation pressure and above. Furthermore, the flap displayed a slower activation and a faster deactivation when the WT was in normal operation compared to the idling state. The latter behavior can be attributed to the effect of the aerodynamic pressure distribution on the blade section, which generates an aerodynamic force that opposes the flap deflection during activation and supports it during deactivation. The magnitude of this aerodynamic force, higher in the normal operation state compared to the idling state, directly affects the time required for full activation and deactivation, with higher forces resulting in slower activation and quicker deactivation.

In modeling the flap actuator, we assumed the activation and deactivation curves were independent of the actual activation pressure. This assumption was valid for high and middle activation pressure scenarios which are most of the available PT field data. The actuator model should also include the impact of the aerodynamic loads on the flap dynamic, which varies in function of the wind speed and WT operational state. Therefore, we selected the middle and high-pressure deflection transients for normal production, assuming a negligible impact of the aerodynamic load change around the measured operative condition. The impact of the aerodynamic loads on the total flap deflection was also neglected based on the results from Gamberini et al. (2022), where the stationary flap properties were validated for a wide range of wind speeds.

On the PT pneumatic system, the signal of the flap controller was not recorded. Therefore the pressure channel was used to

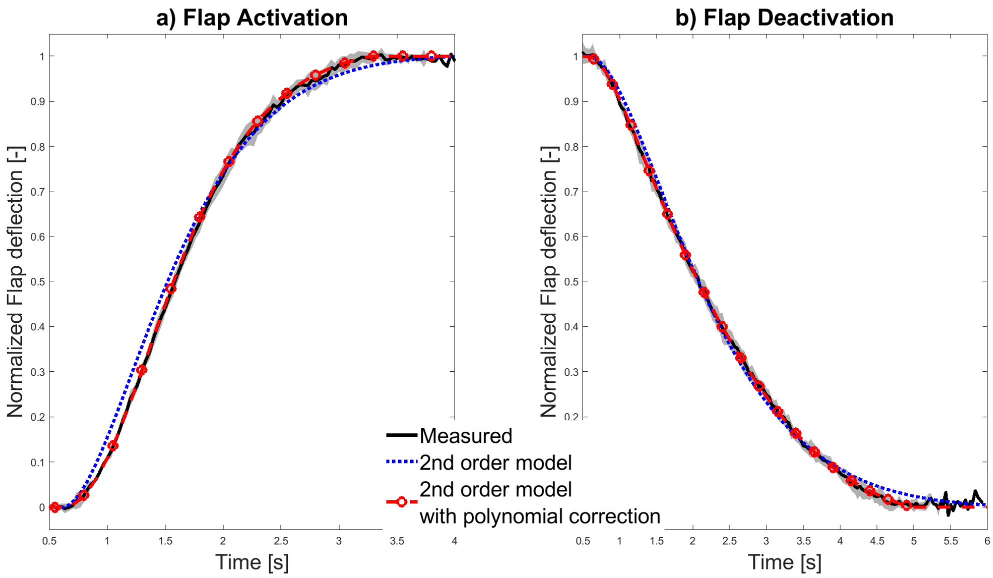

Figure 4. Normalized flap deflection transients measured with the video tracking (black line) from the second-order transfer function model (blue dotted line), and the second-order transfer function model fine-tuned with a fourth-order polynomial function (red dashed line with circles) for flap activation (figure a) and deactivation (figure b). The measured lines are shown with the mean value line enveloped by the grey 1 std error band

initially identify the controller activation time, assuming no delay between the controller activation and the opening of the pressure valve. The flap actuator was finally modeled as a simple second-order transfer function without poles. A fourth-order polynomial function was added to improve the similarity with the deflection curve data. In Figure 4a, the activation deflection curve for middle and high pressure (black line) with the error band of 1 standard deviation (std) is compared with the modeled second-order transfer function (blue dotted line), and the improved model with the fourth-order polynomial function (red dashed line with circles). Similarly, Figure 4b compares the experimental and modeled flap deactivation transients.

5 ATEF Aerodynamic model validation on a WT blade section

The aerodynamic model of the ATEF aeroelastic module was initially validated for a single PT blade section equipped with the active flap. This validation relied on a three hours measurement data set focused on one wind speed. It compared the transient of the lift coefficient measured on the PT blade with the Cl transient calculated via aeroelastic simulations during the flap activation and deactivation. The validation furthermore included the comparison of the measured and simulated transient of the blade-to-blade flapwise bending moment at the root of the blades.

5.1 Measurements

In June 2020, an inflow and pressure measurement system was temporarily mounted on the PT in the middle of the blade span equipped with the active flap for around one day (Madsen et al. (2022)). The measurement system comprised a pressure belt with 15 taps, a 'flyboard' with the data acquisition system, and a five-hole Pitot tube measuring the local inflow to the blade section. The data acquisition system in the flyboard sampled the data from the pressure scanners and the five-hole Pitot tube with a sampling rate of 100 Hz. The captured raw data from the flyboard and pressure belt were processed and converted into quantities of interest. This process includes the calibration of the Pitot tube pressure data and conversion into two flow angles (inflow angle and sideslip angle) and a velocity. The inflow measurement quantities were further corrected to transform the Pitot tube inflow angle into the airfoil angle of attack AoA and relative velocity. This transformation was based on 2D CFD simulations performed by SGRE on the airfoil section for zero and full flap states, where the flow velocity and angle at the point of measurement of the Pitot tube were extracted as a function of the geometric angle of attack (AoA), see Madsen et al. (2022). The pressure belt data was integrated into 2D aerodynamic forces by chordwise trapezoidal integration of the pressures, where a trailing edge pressure was added as an average of the two nearest points. The local pressure and lift coefficients (Cl) were calculated using the corrected dynamic pressure and angle of attack from the Pitot tube. Due to uncertainties in the conversion process based on 2D CFD, the absolute value of AoA, and the consequent absolute Cl, could not be used for the validation. Therefore, the lift coefficient validation focused on comparing the Cl transients unaffected by the conversion uncertainties. During most of the measurement period, the wind speed was relatively low, between 4 and $6\,\mathrm{m\,s^{-1}}$, keeping the wind turbine close to the minimum operational rotor speed. For the validation, a three-hour time interval characterized by a relatively constant wind (between 4 and $5\,\mathrm{m\,s^{-1}}$ 10 minutes mean wind speed) with low turbulence intensity (below 10%) was selected from the measurement period. The low variation of mean wind speed and low turbulence intensity were beneficial in reducing the variability range of the lift coefficient, facilitating the calculation of the average Cl transient curve during flap actuation. In this selected time interval, the flap was performing on-off actuation cycles, switching between $60\,\mathrm{s}$ at full middle-pressure activation and $60\,\mathrm{s}$ at complete deactivation, for a total of $90\,\mathrm{s}$ full activation and deactivation cycles.

5.2 Aeroelastic simulations

The same set of aeroelastic simulations was performed with BHawC and HAWC codes to compute the average Cl transient curve during flap activation and deactivation. The Cl was affected by the variation of the wind field along the rotor plane (due to wind shear or wind veer, for example) and by the rotor tilt and cone angles. The average Cl transient curve was obtained by averaging simulations with flap actuation occurring at different azimuth angles (FA angle), reducing the Cl azimuthal fluctuation's impact on the transient estimation. Precisely, the set consisted of 12 simulations with FA angles evenly spaced. All simulations were 2 minutes long and were run at a constant wind speed of $5\,\mathrm{m\,s^{-1}}$, without turbulence, at the standard air pressure, and with a wind shear of 0.2. The flap started in the deactivated position, was activated at t=30 s, and deactivated after $60\,\mathrm{s}$, at t=90 s, reproducing the activation and deactivation cycles performed on the PT. The flap actuator model of both BHawC and HAWC PT aeroelastic models were updated to match the tuning described in Chapter 4. The Cl was calculated at the blade section where the pressure measurement system was installed. To minimize the difference between the two aeroelastic models, the aerodynamic setup of the models was configured as similarly as possible. Both models had the BEM implemented on a polar grid, as described in Aagaard Madsen et al. (2020), to better account for the rotor induction imbalance due to the flap equipped on only one blade. Furthermore, they implemented a potential flow tower shadow model linked to the tower top movements.

5.3 Average lift coefficient transient

The rotor cone and tilt angles of the wind turbine, along with the variations in wind speed resulting from wind shear, veer and large turbulence structures, contribute to periodic fluctuations in the lift coefficient. These fluctuations challenged the detection and characterization of the transient Cl caused by flap actuation. The averaging of cases with flap actuation occurring at different azimuthal positions substantially reduced the azimuth-dependant variation of Cl, with the average Cl transient quality improved as the flap actuation azimuthal positions were evenly and balanced spread.

In the case of the aeroelastic simulations, the average Cl transient was derived through the binning based on the simulation time of the 12 simulations with evenly spaced FA angles. This procedure was performed for both BHawC and HAWC2 simulations. Figure 5a shows the Cl time series (dotted lines), normalized to the average Cl increase, from the BHawC simulations around the flap activation time (t=0 s). The azimuth-dependant oscillations of Cl amount to around 40% of the Cl variation due to flap activation (ΔCl_F) and affect the slope and shape of Cl transient during the flap activation. Instead, the average Cl transient (black line) is constant before the activation and rises at an almost constant rate until it settles to a constant value after approximately 2.5 s. A similar pattern, but with a longer settling time of around 5 s, is exhibited by the averaged Cl transient during flap deactivation, as shown in Figure 5b. The results from the HAWC2 simulations were almost identical to the BHawC results and are not included in this paper for brevity.

Regarding the measurement data, the times of flap actuation (both activation and deactivation) were determined by identifying the instant at which the gradient of the flap actuation pressure started to change, as the flap valve was located directly at the output of the supply valve. Subsequently, the Cl time series were segmented into temporal windows centered around the flap actuation time and synchronized accordingly. The average Cl transient was finally obtained by binning the Cl signals based on the time window. Different filtering techniques were tested to reduce the oscillation of the averaged Cl transient caused by turbulence and measurement noise. The best results were achieved with a low-pass, zero-phase digital filter set to attenuate frequencies above 9P (9 times the rotor rotational frequency) without affecting the slope of the Cl transient. For accurate validation, synchronizing the Cl measurement with the PT measurements was crucial in ensuring the precise timing of the Cl variation relative to flap actuation pressure. Initially, the synchronization relied on the GPS time recorded by the flyboard, which was further refined by aligning the time of maximum acceleration along the blade length measured on the flyboard with the time the blade was oriented toward the ground. During the average Cl calculation, some measurements were discarded due to insufficient data quality, leading to 46 measured transients being used for activation and 63 for deactivation. The measurements had an acceptable distribution of the flap actuation azimuthal angle, as shown in Table 1, with three cases or more for all sectors. Figure 5c shows the normalized measured Cl transient during flap activation (dotted lines). These transients exhibit

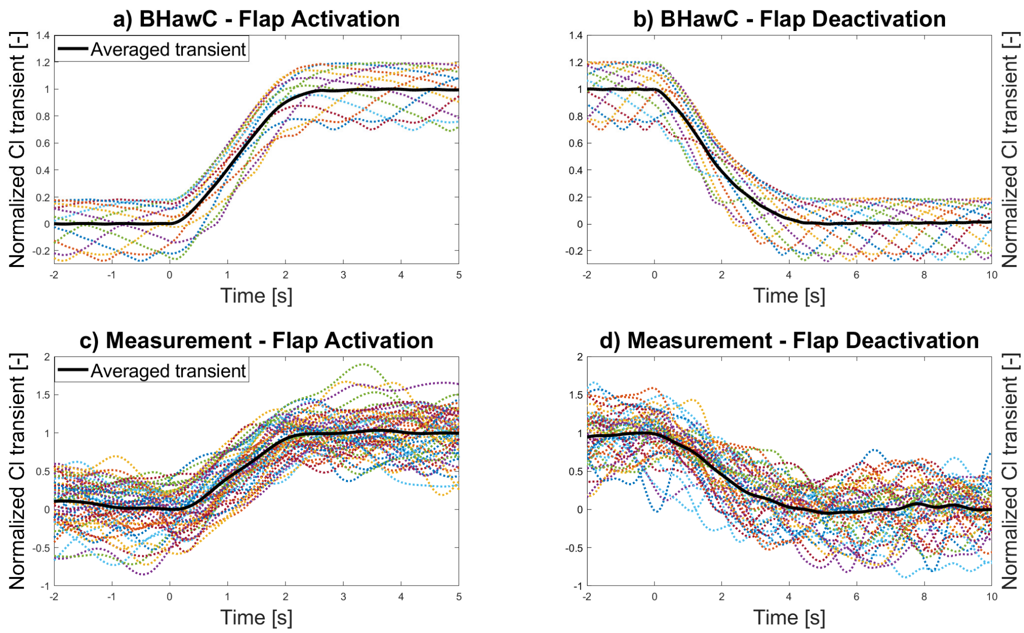

Figure 5. Figures a and b show the normalized averaged Cl transient (black line) for flap activation and flap deactivation, respectively, obtained from the averaging of the Cl transient of 12 BHawC simulations (dotted lines). Similarly, Figures c and d show the normalized averaged Cl transient (black line), respectively, for flap activation and deactivation, obtained from averaging the measured Cl transient (dotted lines).

a higher variability than the aeroelastic simulations, with a range of the same order of amplitude of the increase in Cl due to flap activation, variability mainly caused by the wind turbulence (omitted in the simulations due to the difficulties in estimating the correct value of turbulence for very short simulations). Nevertheless, the averaged Cl transient (black line) exhibits a clear and almost linear variation from a slightly decreasing value before the activation to an almost constant value after the activation. The averaged Cl transient during flap deactivation (black line in Figure 5d) shows a higher fluctuation behavior than the activation transient but is still considerably smoother than the measurements.

5.3.1 Blade-to-blade azimuth based blade root moment

Another crucial aspect for validating the aeroelastic model of the ATEF was the analysis of the blade root moment transient resulting from flap actuation. However, measuring this load transient proved challenging due to its high-frequency response, often hidden within the complex dynamics of the blades responding to factors such as turbulence, shear, vibrations, and rotation. Gomez Gonzalez et al. (2021) introduced a blade-to-blade (b2b) analysis method to compute the load transient caused by the ATEF actuation. This approach involved calculating the difference between the loads acting on the blade with the flap and the load acting on another blade without the flap, but delayed by a time corresponding to a third of one rotor rotation. This artificial

	Number of measured transients per flap actuation azimuth angle												
	Total	***0***	***30***	***60***	***90***	***120***	***150***	***180***	***210***	***240***	***270***	***300***	***330***
Cl activation	53	4	7	3	3	3	2	5	5	5	2	9	5
Cl deactivation	46	3	3	3	3	4	3	4	6	4	5	4	4
MBr activation	69	6	8	4	4	4	9	5	5	6	3	9	6
MBr deactivation	69	7	5	3	9	5	5	4	5	6	8	6	6

Table 1. Number and azimuth distribution of measured cases used for the calculation of the average Cl transient and average blade to blade moment difference (MBr) during flap activation and deactivation.

time shift aimed to synchronize the load time series of blades in the same azimuthal position, thereby mitigating the influence of periodic signal dynamics resulting from rotation, forced vibrations, and wind shear.

This paper proposes a novel azimuth-based b2b method (az-b2b) calculating the load difference by interpolating the loads based on the cumulative azimuth position instead of relying on time shifting. The method comprises three steps. Firstly, the Cumulative Sum of the azimuthal Angle (CSA) is calculated for each blade. Secondly, the load of the blades without the flap is interpolated as a function of the CSA of the blade with the flap. Lastly, the difference between the load of the blade with the flap and the interpolated load of the blade without the flap is calculated.

Notably, the az-b2b method eliminates the need to initially segment the time series around the relevant event, as the previous b2b method requires. It can be applied directly to the entire time series in a single run. Additionally, the az-b2b method is not dependent on the calculated mean rotor speed, which is influenced by the time extension of the segments. This characteristic makes it less sensitive to minor variations in rotor speed. By ensuring that the load difference is between two blades positioned at the same azimuthal location, the az-b2b method effectively reduces azimuthal-dependent load fluctuations. However, precise measurement of the azimuthal angle is essential to avoid errors during the interpolation phase. Like the original b2b method, the az-b2b method is still sensitive to high rotor speed variation that can result in a significant variation of data density for azimuthal angle, potentially affecting the quality of the interpolation result.

The az-b2b method was utilized to calculate the differences in flapwise bending moments at the blade root (MBr1 and MBr2) between the blade with flap (BF) and the remaining blades (B1 and B2) in the aeroelastic simulation sets of BHawC and HAWC2. As shown later in this paper, the two blade-to-blade differences did not differ significantly in both simulations and measurements; therefore, the mean MBr (MBrM) of the two b2b differences was used as reference transient. Finally, the binning of the twelve simulations as a function of the simulation time computed the average MBrM transient. Figure 6a shows the MBrM transients (dotted lines) obtained from the BHawC simulations, together with the average MBrM (black line). All the signals were normalized in order to make the increase of the b2b moment due to flap actuation unitary. The azimuthal variability of the MBrM transients is present but significantly lower than the Cl transients, being less than 10% of the average transient. The average MBrM transient is almost constant before the flap actuation, and it rises smoothly from around $0.5\,\mathrm{s}$ until it converges to an almost constant value after $2\,\mathrm{s}$. The average transients of the individual b2b differences (MBr1 and

MBr1 represented by a dotted blue line and a dotted red line, respectively) exhibit only a small difference between themselves. Similar considerations are valid for the MBrM transients during flap deactivation shown in Figure 6b. The MBrM transients from the HAWC2 simulations were almost identical to the BHawC results and are not included in this paper for brevity.

Regarding the measurement data, the same methodology employed for the Cl transient was applied to compute the blade load difference. The measurement signals were segmented into temporal windows centered around the actuation time and synchronized accordingly. Subsequently, the consistency of the azimuthal angle signal was verified, and the rotor speed was leveraged to compute the missing or erroneous values. Afterward, the MBrM transients were computed, and the average MBrM was obtained using the binning approach. In the average MBrM calculation, the same number of measured time series (69) were used for flap activation and flap deactivation. The distribution among the rotor sector of the flap actuation azimuthal angle was also acceptable, with most sectors having at least five cases. Similarly to the results from the Cl transients, the MBrM measured transients (dotted lines in Figure 6c) show a high oscillation, mainly caused by the wind turbulence, with a range comparable with the load increase due to the flap activation. Nevertheless, the averaged MBrM transient (black line) is almost constant before the activation and smoothly increases and converges to the flap actuation value with minor oscillations. The average MBr1 and MBr2 are also close to each other, with a max difference of 0.1. Similar considerations can be done for the flap deactivation case, shown in 6d.

5.4 Validation results and discussion

In comparing the simulation results with the measurements, the actuation pressure signal was used to synchronize the transients. In detail, the time the flap pressure gradient undergoes a quick change was aligned with the flap activation time in the simulations. For the deactivation case, an additional delay of $0.3\,\mathrm{s}$ was added to the simulation flap deactivation time to properly align the Cl and blade-to-blade loads with the measurements. We believe this delay is related to the structure of the pneumatic actuator system, and it would have been identified during the actuator system tuning if the controller signal had been available. For the activation phase, a time delay was not clearly needed.

The simulated and measured Cl transients are compared in Figures 7a for flap activation and 7b for flap deactivation. In the figures, the synchronized flap actuation time is indicated by the estimated flap command (black dashed line), used in the simulation to actuate the flap, and the measured flap pressure signal (blue dotted line). The transients from BHawC (blue dashed line with x marker) and HAWC2 (red dashed-dotted line) simulations closely match each other, with a maximum difference below 6% of the ΔCl generated by the flap actuation in both flap activation and deactivation cases, mainly caused by an offset of a single time step ($0.04\,\mathrm{s}$) between the two transients. The simulated Cl has transients significantly similar to the measurements (black line with round markers). In the activation case, the maximum difference is below 40% of the measurements std, below 8% of the ΔCl, with the simulated Cl starting to increase $0.1\,\mathrm{s}$ (5% of the time for full flap activation) before the measurement Cl but at a lower slope, and it converges to full activation with a delay of $0.15\,\mathrm{s}$ (7.5% of the full flap activation time). In the deactivation, the maximum difference is below 6% of the measurements std, below 8% of the ΔCl, and the simulated Cl starts to decrease with a delay of $0.2\,\mathrm{s}$ (4% of the full flap deactivation time) that quickly recovers, and afterward it precedes the measurement slope of less than $0.1\,\mathrm{s}$ (2% of the full flap deactivation time) until full deactivation. The std of the simulated

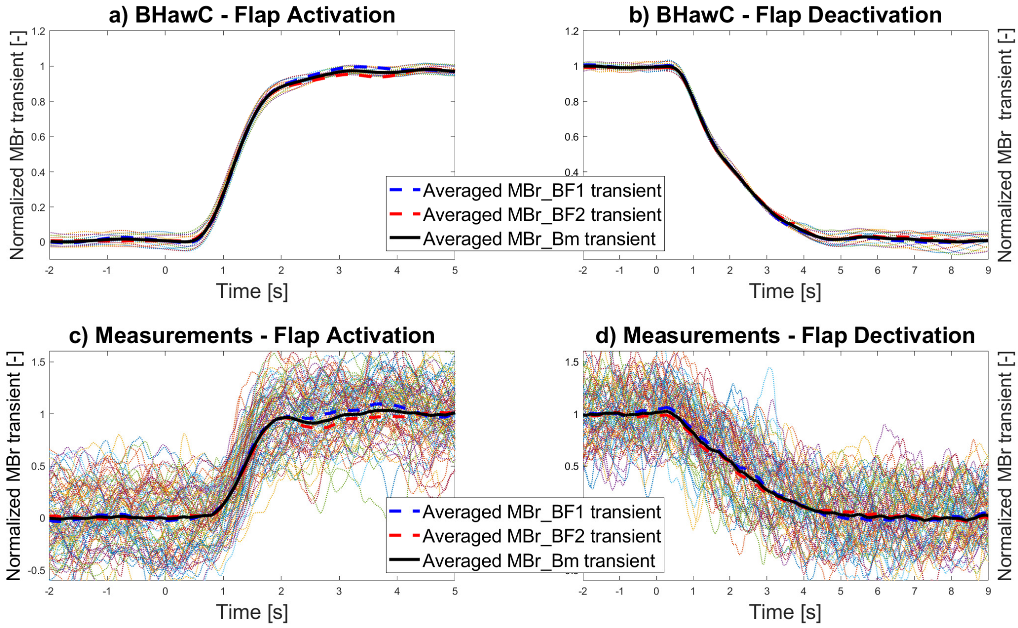

Figure 6. Figure a and b show the normalized averaged b2b bending moment difference at blade root (MBrM) transient (black line) for flap activation and flap deactivation respectively, obtained from the averaging of the MBrM transient of 12 BHawC simulations (dotted lines). Similarly Figure c and d show the averaged normalized MBrM transient (black line) for flap activation and deactivation respectively, obtained from the averaging of the measured MBrM transient. All the plots also include the b2b bending moment difference between the blade with flap and the blades without (MBr1: dashed blue line, MBr2: dashed red line)

transients are often equivalent, and nearly half of the measurement std. This difference is mainly due to the omission of turbulence in the aeroelastic simulations.

The b2b moment transients are compared in Figures 8a for flap activation and 8b for flap deactivation. Similarly to the Cl comparison, the MBrM transients from BHawC (blue dashed line with x marker) and HAWC2 (red dashed-dotted line) simulations closely match each other, with a maximum difference below 7% of the ΔMBrM due to the flap actuation in both flap activation and deactivation cases, mainly caused by an offset of $0.06\,\mathrm{s}$ between the two transients. Both transients have a std significantly smaller compared to the Cl transients, showing the benefit of the az-b2b method in removing the impact of the azimuthal load oscillations. HAWC2 transient having a std almost twice the std of the BHawC simulations is mainly related to higher rotor speed oscillations caused by a not perfect implementation of the SGRE controller in the HAWC2 code. The simulated MBrM has transients similar to the measurements (black line with round markers). In the activation case, the maximum difference is below 55% of the measured std and 17% of the ΔMBrM due to the flap activation. Mirroring the Cl transients, the simulated MBrM begins to increase $0.2\,\mathrm{s}$ (10% of the full flap activation time) before the measured MBrM but at a lower slope, and it converges to full activation within the measurement fluctuation transient. In the deactivation, the maximum difference is below

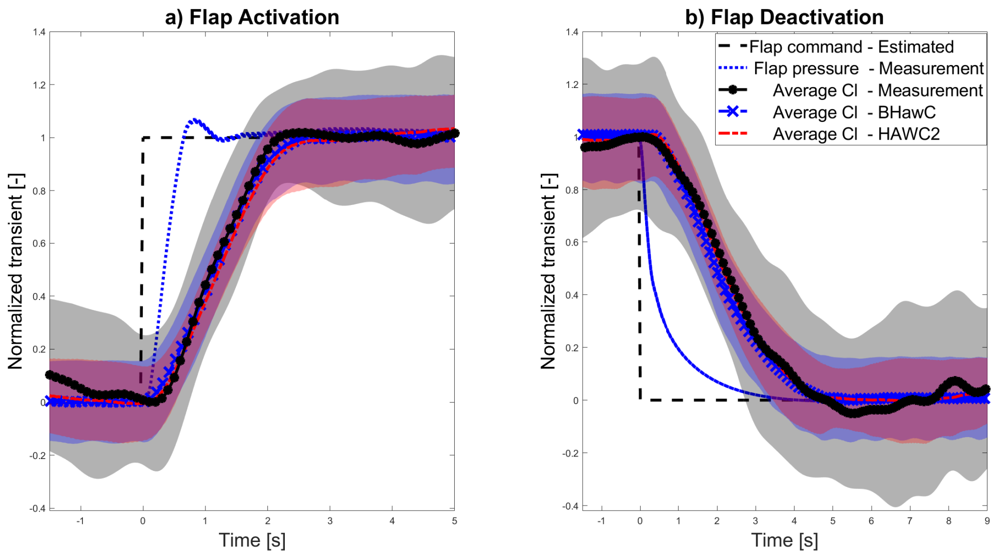

Figure 7. Comparison of the normalized averaged Cl transient obtained from BHawC (blue dashed line with x marker) and HAWC2 (red dash-dotted line) simulations and measurements (black line with asterisk marker) during flap activation (a) and deactivation (b), including an error band of 1 std of the matching colors. The measured flap pressure (blue dotted line) and the estimated flap command (black dashed line) are also included.

60% of the measured std, below 20% of the ΔMBrM, and the simulated Cl starts to decrease with a delay of $0.2\,\mathrm{s}$ (5% of the full flap deactivation time) that quickly recovers and afterward precedes the measurement slope of less than $0.1\,\mathrm{s}$ until full deactivation.

Another purpose of the initial validation was tuning the ATEF model to ensure the proper synchronization between the simulated and measured Cl and MBrM transients. Figure 9a shows all the ATEF aeroelastic model signals relevant for the model tuning during flap activation. The measured controller signal was not recorded in the measurement campaign. Therefore, the measured flap pressure (blue dotted line) synchronizes the simulated flap control signal (black dotted line). This control signal commands the flap deflection (red dashed line with circular markers), deflection obtained from the post-processing of the flap deflection videos (green squared markers). The Cl transient follows the flap deflection by a few milliseconds in the simulations (blue line with squares and orange line) and by $0.1\,\mathrm{s}$ in the measurements (grey line with arrow marker). The slight difference between the simulated and measured Cl transients (especially if compared to the measurements std) confirms the current model(with the linear relation between flap deflection and Cl variation) provides reliable results. After the Cl increase, the MBrM transient starts $0.5\,\mathrm{s}$ later, with the simulations anticipating the measurements of $0.2\,\mathrm{s}$. Figure 9b shows the signals relevant for the ATEF model tuning during flap deactivation. To properly align the simulations Cl and MBrM transients with the measurements, a delay of $0.3\,\mathrm{s}$ was introduced in the actuator model between the flap controller and the flap deflection during deactivation only.

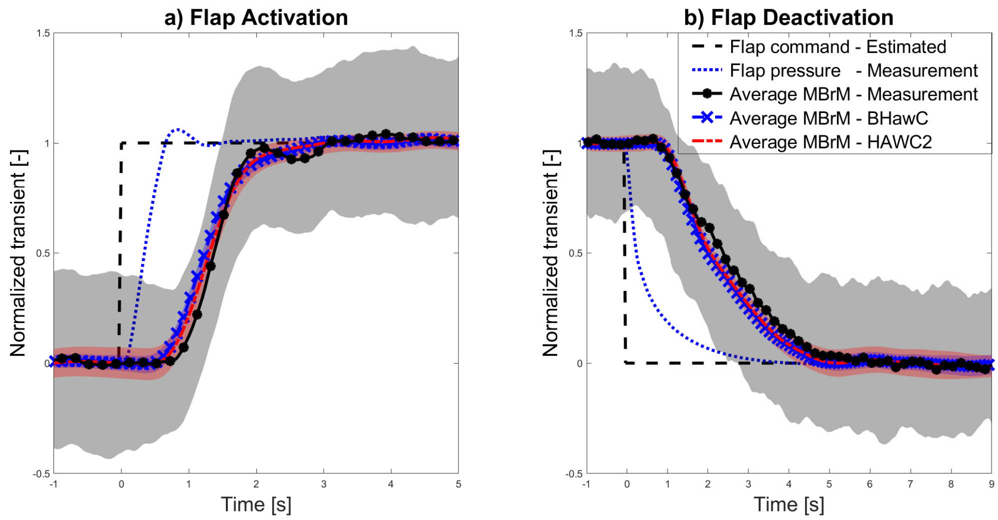

Figure 8. Comparison of the normalized averaged b2b blade root bending moment (MBrM) transient obtained from BHawC (blue dashed line with x marker) and HAWC2 (red dash-dotted line) simulations and measurements (black line with asterisk marker) during flap activation (a) and deactivation (b), including an error band of 1 std of the matching colors. The measured flap pressure (blue dotted line) and the estimated flap command (black dashed line) are also included.)

In conclusion, the initial validation showed a good agreement between the simulated and measured Cl and MBrM transients. However, small differences in the transients motivated the broader validation described in the following section.

6 Extended ATEF Aerodynamic model validation

The validation of the aerodynamic model of ATEF aeroelastic was extended to a wider range of environmental conditions with the measurements obtained with the PT field campaign between October and December 2020, when the ATEF system was tested for different pressure activation and activation patterns. In this test campaign, the flyboard was not present, and the validation did not rely on the Cl measurements but only upon comparing the transient of the blade-to-blade moment at the blade root (MBrM) during flap activation and deactivation. The validation followed the so-called one-to-one (o2o) approach, where the measurements are compared with a set of simulations reproducing the WT operating under the same environmental conditions measured at the time of the flap actuation. As the validation focused on the short transient happening within 10 s after the flap activation and deactivation, the simulations did not rely on the 10 minutes averaged environmental condition but on the actual condition measured at the flap actuation time.

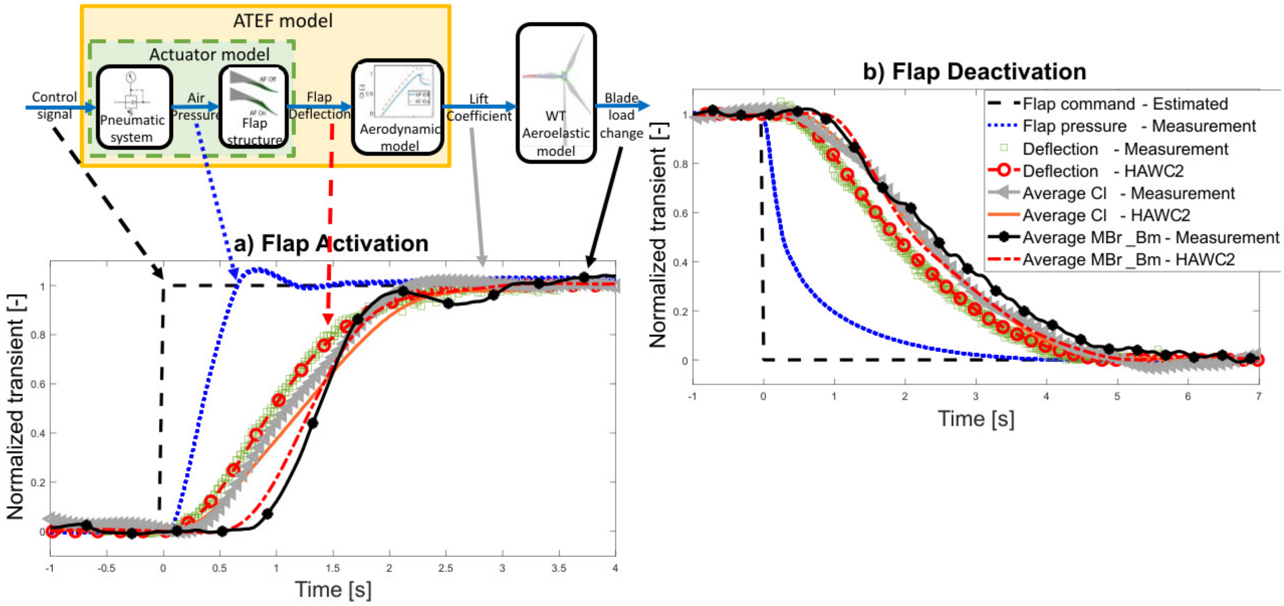

Figure 9. a) Signals relevant for the modeling and validation of the flap model during flap activation, linked to the ATEF model scheme. Transients of Flap controller command (black dashed line), flap pressure (blue dotted line), measured and estimated flap deflection (green squares and red dashed line with circles), measured and estimated Cl (gray line with triangle and red line) and measured and estimated MBrM (black line with asterisks and reddash-dotted line) are plotted to verify the time tuning of the aeroelastic model. b) Signals relevant for the modeling and validation of the flap model during flap deactivation

6.1 Field campaign

Between October and December 2020, the ATEF system on the PT was tested for several actuation pressure and activation pattern. The measurements of full activation and deactivation cycles at middle activation pressure with the WT operating in normal production were selected for validation. Additional filtering removed the measurements at which the wake of the PT or the nearby WTs affected the met mast measurements. As a change in the WT operative condition could result in an MBrM variation interfering with the load transient due to flap actuation, only flap actuation cases occurring when the WT was in almost stationary condition were selected. This selection was achieved by removing the cases where, within $10\,\mathrm{s}$ before and after the flap actuation, the pitch angle varied more than 1 deg, the rotor speed more than $0.5\ \mathrm{rpm}$, and the yaw direction more than $1\ \mathrm{rpm}$. Finally, a total of 150 measurements for flap activation and 135 for flap deactivation were obtained, distributed between 5 and 20 ms^{-1} as shown in Figure 10a.

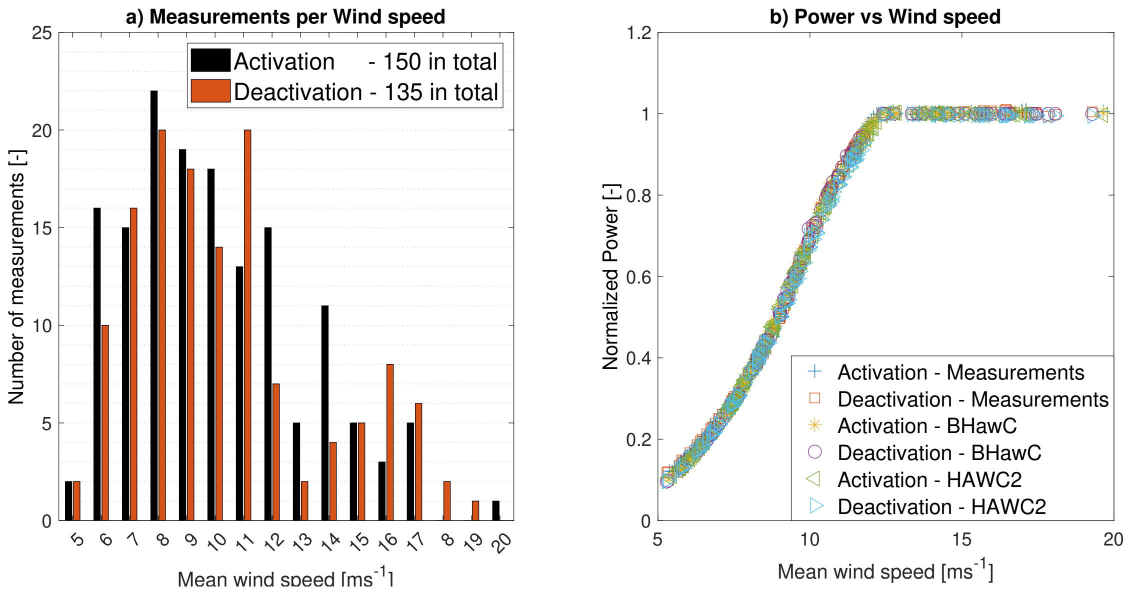

Figure 10. a) Number of selected measurements per wind speed for flap activation (black) and deactivation (red). b) Normalized power curve of the selected measurements and simulation (both BHawC and HAWC2) for flap activation and deactivation.

6.2 Models and simulations setup

The BHawC and HAWC2 models from the initial validation described in section 5 were used for this validation, including the additional $0.3\,\mathrm{s}$ deactivation delay in the flap actuator model.

To properly calculate the b2b load transient during flap actuation, the simulation setup had to match the environmental conditions at the WT at the specific time of the flap actuation. The environmental conditions were measured at the met mast, located $300\,\mathrm{m}$ in front of the PT. This distance introduced a time delay Td corresponding to the time the wind needs to cover the distance Dm between the met mast, where it was measured, and the WT rotor. This delay is inversely proportional to the wind speed (Td=$60\,\mathrm{s}$ for a low $5\,\mathrm{m\,s^{-1}}$ wind speed and Td=$15\,\mathrm{s}$ for $20\,\mathrm{m\,s^{-1}}$ wind) and for a discrete and constant sampling time ΔT was calculated as

$$Td = k * \Delta T$$

where k is the first time step, previous of the flap actuation time t_0, for which the sum of the distances traveled by the sampled wind speeds $w_{(-i)}$ covers the distance Dm.

$$k = \min(i \in Z^{+} | \sum_{i=0}^{k} w_{(-i)} * \Delta T \geq Dm)$$

The flap actuation time t_0 was identified by using the flap actuation pressure gradient, as described in section 5. A $20\,\mathrm{s}$ time interval centered on the actuation time, corrected by the corresponding Td, was selected for each flap actuation. For each time

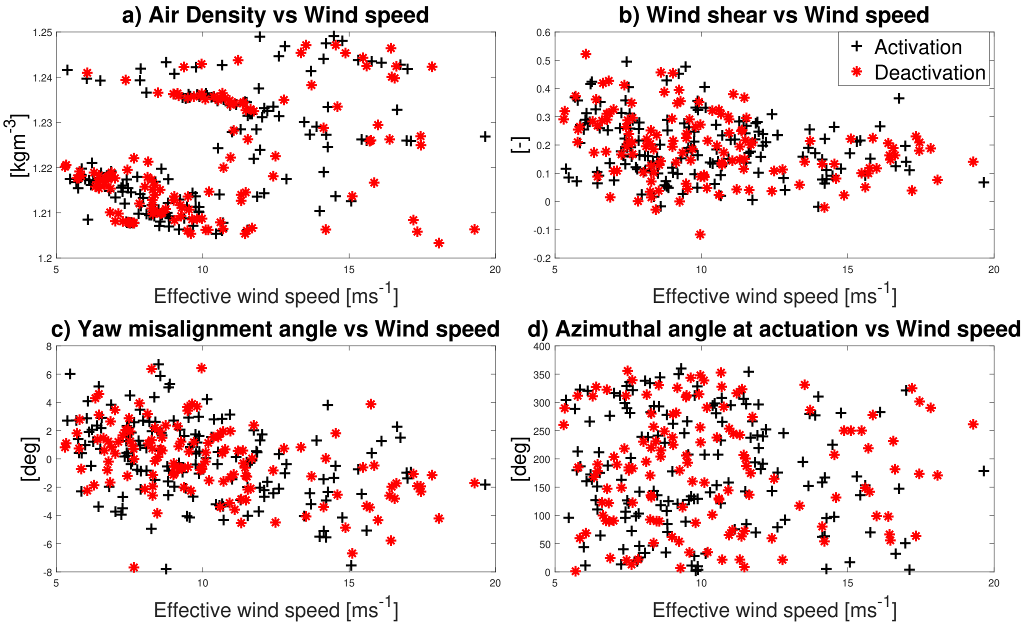

Figure 11. Distribution of Air density (a), Wind shear (b), Yaw misalignment angle (c) and azimuthal angle at flap actuation (d) in function of the effective wind speed used for the flap activation (black cross) and deactivation (red asterisk marker) aeroelastic simulations.

interval, the mean values of air density, wind shear, and the misalignment angle between the wind direction and the WT yaw angle were input to the aeroelastic simulations. As for the simulated wind speed, the effective wind speed value was preferred to the measured wind speed. The effective wind speed is the wind speed that makes the WT operate at the measured rotor speed, generator power, and pitch angle. This wind speed was obtained by interpolating the measured characteristic power, pitch, and rotor speed curves at the corresponding mean values measured in the selected time interval. The MBrM transient comparison in section 5 shows the turbulence has a small impact on the average load transient due to flap actuation. This average is instead affected by the distribution of the azimuthal angle at which the flap actuation happens. These conclusions supported the decision to omit the turbulence in the current validation, avoiding the additional complexity of measuring and modeling the equivalent turbulence. At the same time, in the simulations, the flap was actuated at the corresponding measured FA angle. Figure 11 shows the distribution of Air density (a), Wind shear (b), Yaw misalignment angle (c), and FA angle (d) in the function of the effective wind speed used in the simulations. Figure 10b shows the mean power obtained in the simulations matches the measured one for all the flap actuation cases.

6.3 Extended Validation results

The extended validation of the ATEF aerodynamic model relied on the comparison of the average MBrM transients. The MBrM signal was calculated and synchronized for measurements and simulations as described in section 5.

Figure 12a shows the comparison of the average MBrM transient during flap activation of the measurements (black line with asterisk marker), BHAwC simulations (blue dashed line) and HAWC2 simulations (red dash-dotted line) based on all the available data. The simulation transients are almost equivalent, with a time shift within $0.1\,\mathrm{s}$ (less than 3 time steps), bringing the load difference within 5%. The transient pattern also differs from the transient obtained in the initial validation. The load keeps increasing and fluctuates after the flap's full activation, a behavior also shown by the measurement transient. This behavior is probably caused by the averaging of the load difference obtained from all the different wind conditions. The simulation transients are well within the error band of measurement transient, with a maximum difference below 50% of the measured std, and below 10% of the ΔMBrM due to the flap activation. Similarly to the initial validation, the simulation transients start to increase earlier (around $0.1\,\mathrm{s}$, 5% of the actuation time of $2\,\mathrm{s}$) but with a lower slope, under-predicting the load increase in the second half of the flap activation and accumulating a delay of $0.2\,\mathrm{s}$, 10% of the actuation time) and then converging within the measured oscillating transient. As observed in the initial validation, the simulations cannot reproduce the s-shaped behavior the measurements manifest.

Figure 12b compares the average MBrM transients during flap deactivation. The simulations transients differ less than 3%, with a time shift within $0.08\,\mathrm{s}$ (2 time steps). The simulation transients are well within the measured error band, with a maximum difference below 60% of the measured std, and below 15% of the ΔMBrM. The simulation transient decreases $0.2\,\mathrm{s}$ (4% of the $4.5\,\mathrm{s}$ deactivation time) later than the measured transient, but they quickly converge within the measurement oscillation transient.

During the actuator model tuning, the flap displays a slower activation and a faster deactivation when the WT is in normal operation compared to the idling state. This behavior suggests that the aerodynamic loading on the blade section may influence the deflection of the flap. To investigate this hypothesis, the averaged MBrM transients were computed for wind speed ranges of $2\,\mathrm{m\,s^{-1}}$, a wind range with similar aerodynamic load values. The averaged transients are shown in Figure 13 for flap activation and Figure 13 for flap deactivation. For wind speed ranges up to $13\,\mathrm{m\,s^{-1}}$, the simulated transients closely resembled the corresponding measured transients, exhibiting differences similar to those observed in the global transients. For the range above $13\,\mathrm{m\,s^{-1}}$, insufficient data results in irregular and oscillating transients. From the comparison of the measured averaged trends shown in figure 15a for flap activation and 15b for flap deactivation, a correlation between the wind speed and the transient shape does not emerge clearly. The measured transients all lie within a range of $0.2\,\mathrm{s}$ in both the activation and deactivation phases without a clear relation to the aerodynamic load.

7 Near Wake model study

In the ATEF model validations described in the previous sections, as well as in the stationary validation of the same ATEF models described in Gamberini et al. (2022), the aeroelastic codes did not model the 3D effects originated by the vorticity trailed from the edges and along the span of the flap section. HAWC2 code can account for these 3D effects via the optional Near-Wake induction model. This model, introduced by Pirrung et al. (2017), is a simplified version of the lifting line model specifically designed to examine the wake near each blade. The Near-Wake model, being fully dynamic, accounts for the

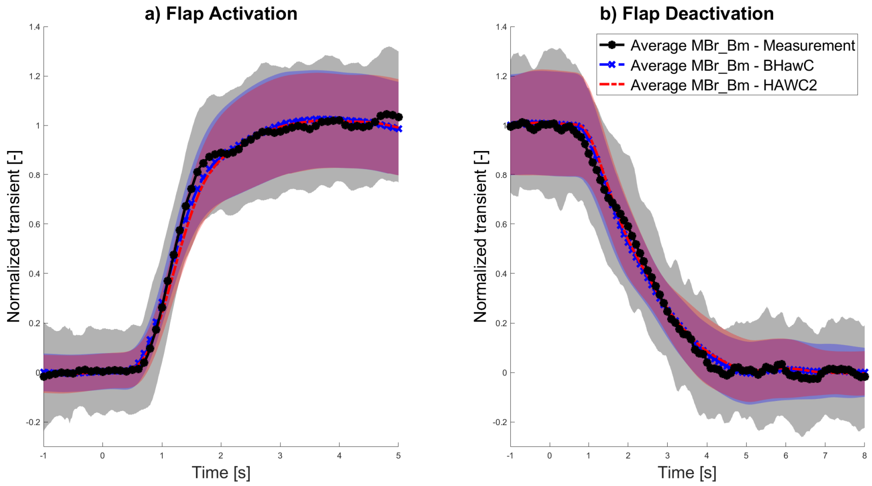

Figure 12. Comparison of the normalized averaged b2b blade root bending moment (MBrM) transient obtained from all BHawC (blue dashed line with x marker) and HAWC2 (red dash-dotted line) simulations and all measurements (black line with asterisk marker) during flap activation (a) and deactivation (b), including an error band of 1 std of the matching colors.

temporal evolution of the trailed vorticity. The vorticity is traced between all the aerodynamic sections on the blade, allowing the model to capture various vortices such as tip and root vortices. Furthermore, the model takes into consideration vorticity trailed at the edges of flaps and vorticity resulting from radial load fluctuations in turbulent inflow. The strength of the trailed vortex at each trailing point is determined by computing the disparity in bound vorticity between adjacent aerodynamic blade sections. This calculation incorporates an approximation of the buildup of unsteady circulation. The validation of the WT section properties and the extended validation were performed with the Near-Wake model active in the HAWC2 simulations (H2-NW). The Near Wake model impacts the ΔCl at the analyzed flap location, reducing the increase of Cl during flap actuation of 7% compared to the HAWC2 results without the Near Wake model (H2). The averaged Cl transients differ less than 3% of the ΔCl during flap activation, mainly due to a time shift of almost 2 time steps, and less than 4% ΔCl (time shift around 3 time step) during flap deactivation. The impact on the Regarding the MBrM, the H2-NW transient is almost equivalent to the H2 transient, with a difference below 1% during flap activation and below 0.6% during flap deactivation. Additionaly, the Near-Wake model impacts the ΔMBrM of the flap actuation between 2 to 2.5%.

8 General discussion

The validations described in sections 5 and 6 show the HAWC2 and BHawC aeroelastic models of the ATEF implemented on the PT provide almost equivalent results during the flap activation and deactivation. In the initial validation based on the blade section measurements, the respective HAWC2 and BHawC Cl transients have a time shift below $0.04\,\mathrm{s}$, leading to a maximum difference lower than 6% of the ΔCl occurring during flap actuation. In the extended validation, the simulated b2b

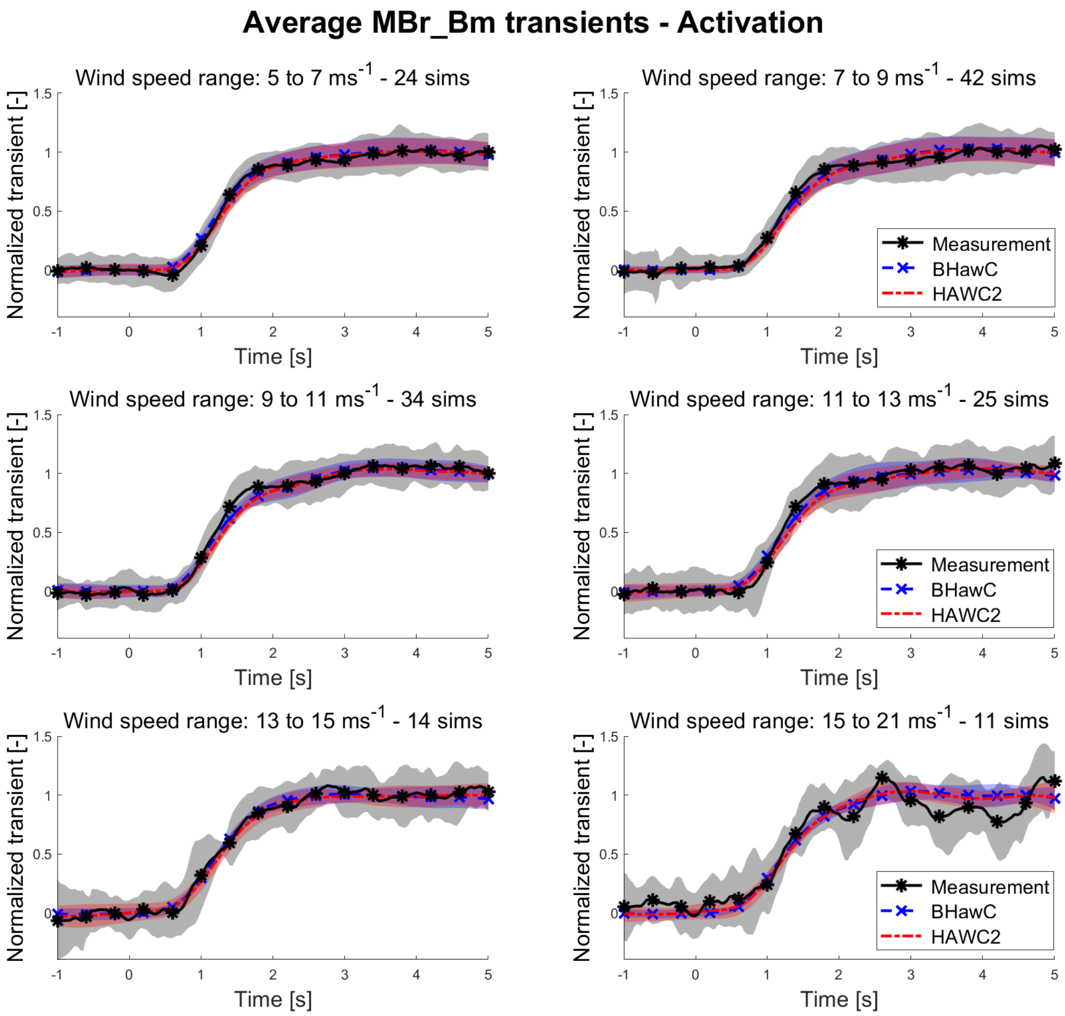

Figure 13. BHawC (blue dashed line with x marker), HAWC2 (red dash-dotted line), and measurements (black line with asterisk marker) averaged MBrM transients obtained for wind speed intervals of $2\,\mathrm{m\,s^{-1}}$ during flap activation. The number of data-point (sims) per wind interval is also specified

load transients differ less than 5% of the ΔMBrM caused by the flap actuation, with the difference mainly originating by a maximum time shift of $0.1\,\mathrm{s}$.

The validations proved that the simulations are in good agreement with the measurements. The simulated average Cl transients are well within the error band of the measured transient, with a max difference below 8% of the ΔCl during flap activation and deactivation. The differences between the simulated and the measured average MBrM transients are below 10% of the

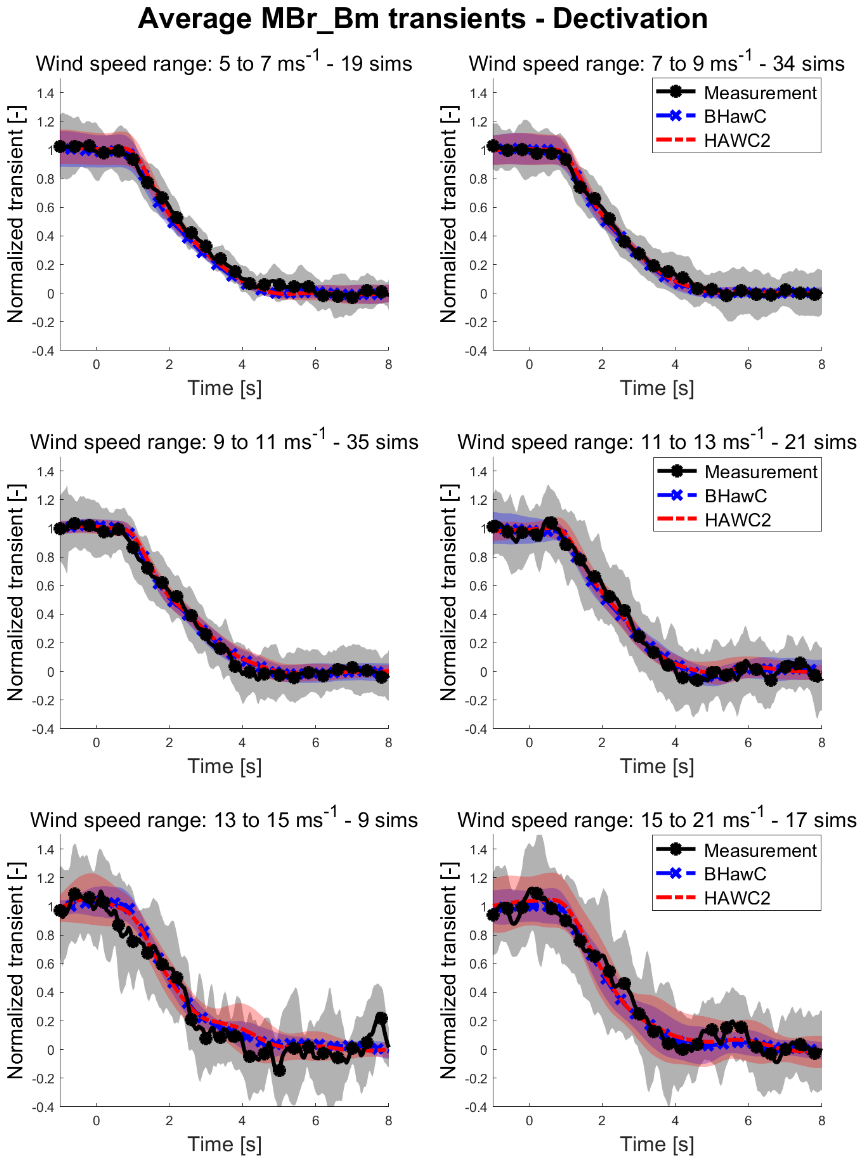

Figure 14. BHawC (blue dashed line with x marker), HAWC2 (red dash-dotted line), and measurements (black line with asterisk marker) averaged MBrM transients obtained for wind speed intervals of $2\,\mathrm{m\,s^{-1}}$ during flap deactivation. The number of data-point (sims) per wind interval is also specified

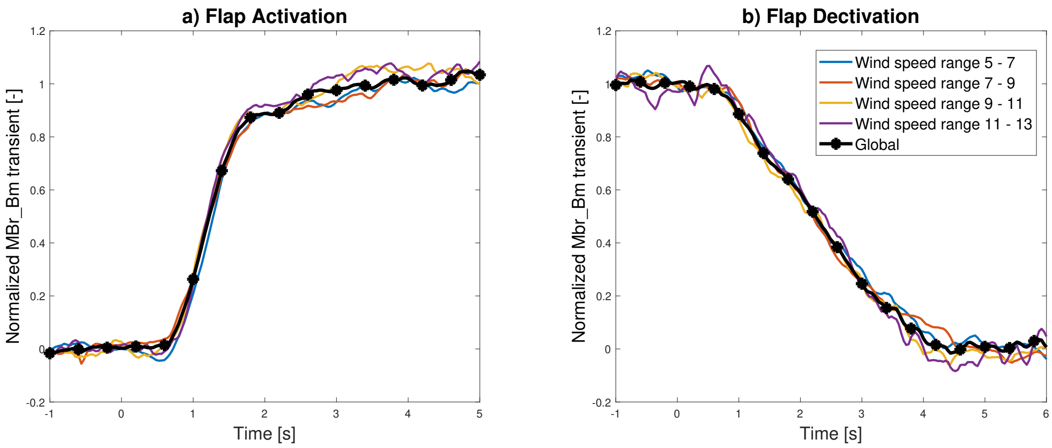

Figure 15. Comparison of the measured MBrM transients obtained for different wind speed intervals for flap activation (a) and flap deactivation (b)

ΔMBrM during flap activation and below 15% during flap deactivation. The ΔMBrM due to flap activation ranges between 6% (at rated wind speed) to 11% (at high or low wind speed) of the mean blade loads (as showed in Figure 4b of Gamberini et al. (2022)). Consequently, the maximum simulation transient error is below 1% of the mean blade load during activation and below 1.7% during flap deactivation. Within this error margin, the simulations cannot completely reproduce the average transients' shape, especially during the flap actuation, where the measurements rise later but steeply, reaching full activation value earlier. The main proposed causes of this difference in the transient shape are:

- Incomplete flap deflection model. The actuator model was tuned with the flap deflections measured only at one wind speed. The flap deflection transients may vary as the external conditions, like the aerodynamic forces or the rotational speed, change. As shown in Figure 15, comparing MBrM transients at different wind speed intervals does not correlate clearly with the WT operative condition. However, it still has a range of uncertainty comparable to the differences between simulations and measurements. Furthermore, the tuning flap deflections were measured only at one blade section, not ensuring the flap has a constant deflection characteristic along its whole $20\,\mathrm{m}$ length. A spanwise variation of the flap deflection could justify the steeper shape of the MBrM transient. Additional measurements of the flap deflection at different blade locations, wind speeds, and WT operative conditions can improve the deflection model, reducing the transient shape difference.

- Imperfect aerodynamic properties of the flap profiles. The Cl and Cd curves used in the aeroelastic simulations were all derived from the wind tunnel measurement of the 21% thickness profile. New wind tunnel measurements for the 18% and 24% profiles and for different relative sizes of flap and chord can verify if the flap profiles' aerodynamic properties are correct or responsible for the observed difference in the transients' shape.

- Uneven distribution of the angle at flap actuation time in the measurements. The Cl and MBrM transient are strongly affected by the azimuthal angle at which the flap actuation is initiated, as shown in section 5. In the available measurements, the FA angle of the measured flap activation and deactivation was not evenly distributed on the whole rotor, leading to a distorted averaged transient. In the o2o process, this was partly compensated by simulating the flap activation at the measured FA. Additional measurements aiming to improve the FA angle distribution at different wind speeds can potentially improve the quality of the measured transients and reduce the difference between measurement and simulation.

- Incomplete flap aerodynamic model. The transient shape difference can suggest a delay of the change in aerodynamic flow compared to the flap actuation, a delay dependent on the flap position (as it is not present during flap deactivation) that is quickly recovered during the activation. CFD simulations modeling the exact geometry of the flap deflection transient can verify this hypothesis.

Based on the experience gained in the validations presented in this paper, some recommendations are suggested to improve future validation campaigns of ATEF:

- The correct estimation of the flap deflection is crucial in the validation of the aerodynamic model of the ATEF. If continuous measurements of the flap position are not available, the flap deflection transient should be measured for several wind and operative conditions to ensure the correct tuning of the actuator model.

- Uncertainties on the aerodynamic properties of the flap profiles reduce the accuracy at which the aerodynamic model can be validated. Proper measurements of all the relevant flap profiles should be conducted. If that is not possible, the Cl and Cd impact of the flap can be derived from similar profiles with acceptable accuracy.

- The correct time synchronization of all the different measurement systems is crucial to ensure the proper time precision in measuring and validating the transient of the Cl and Load channels. Therefore, the flap actuator control (or any other channel that can be used to estimate the flap actuation time) is required.

- The azimuthal angle at which the flap is actuated strongly affects the transient of Cl and loads. The measurement campaign should aim to obtain a set of measurements with a balanced distribution of FA angles.

In section 7, the HAWC2 Near-Wake induction model (model accounting for the 3D effects due to the vorticity trailed from the edges and along the span of the flap section) does not effect the average transient of ΔCl and ΔMBrM as their differ respectively less than 4% and 1% compared to the HAWC2 model without Near-Wake. The Near-Wake model impact marginally the value of ΔMBrM, reducing it between 2 to 2.5%. This reduction, even if small, improve the accuracy of the model to estimate the ΔMBrM as the HAWC2 model overestimate it, as shown in Gamberini et al. (2022). This result confirms the conclusions of Prospathopoulos et al. (2021), that a BEM model without 3D trailed vorticity effects overestimates the flap contribution at the flap location as well as at the blade root, but the difference of the integral loads is rather small when the flap actuation frequency is below 1P, like in the validation described in the current paper.
Finally, the azimuth-based b2b method proved to be a reliable methodology to estimate the asymmetrical loading caused by the

ATEF equipped on a single blade of the PT. This methodology can be applied in other asymmetrical rotor loading conditions, for example, in case of individual pitch, pitch error, or blade degradation.

9 Conclusions

Within the framework of the VIAs project, an Active Trailing Edge Flap System was installed on a $4.3\,\mathrm{MW}$ test wind turbine and underwent a field test campaign for over 1.5 years. The campaign provided the measurement data to validate the aerodynamic ATEF models of the aeroelastic engineering tools BHawC and HAWC2. The validation focused on the dynamic response of the ATEF models during flap actuation and consisted of three phases. At first, the flap actuator model was tuned to accurately reproduce the flap deflection transient during the $2\,\mathrm{s}$ activation and the $5\,\mathrm{s}$ deactivation. In the second phase, the aerodynamic flap model was tuned and validated through the lift coefficient transients measured at a blade section equipped with the flap. Finally, the aeroelastic ATEF model was validated based on the blade load transients over a three month period, from October to December 2020, with varying weather conditions. A novel approach to computing the blade load impact of the flap was introduced. This method is an azimuth-based variation of the blade-to-blade approach, and it computes the difference between azimuthal synchronized loads of adjacent blades.

The validation showed that for the tested actuator model, the two aeroelastic ATEF models provide almost identical transients during flap activation and deactivation, with the main difference caused by a relative time shift lower than $0.04\,\mathrm{s}$ (one time step) between the Cl transients and below $0.1\,\mathrm{s}$ between the load transients. The validation showed that the simulations transient of Cl and MBrM are in good agreement with the corresponding measured transients, confirming that the aeroelastic ATEF models provide a reliable and precise estimation of the impact of the flap on the wind turbine during flap actuation. In comparison with the field data, the maximum differences between the simulated and the measured Cl transient are below 8% of the ΔCl and within $0.15\,\mathrm{s}$ of time shift during flap activation, below 8% ΔCl and within $0.2\,\mathrm{s}$ of time shift during flap deactivation. Regarding the MBrM transients, the maximum difference is below 1% of the mean blade load during flap activation and below 1.7% during flap deactivation, with a delay within $0.2\,\mathrm{s}$ for both flap actuation cases. Additional measurements of the flap deflection at different blade locations, under wide WT operational conditions and the direct measurement of the aerodynamic properties of all flap profiles are suggested solutions to fine tune the ATEF model.

To the authors' knowledge, this is the most extensive published validation of the aeroelastic ATEF model transients in terms of wind conditions, time, and flap size. This was enabled by measuring the aerodynamic response at a blade section during flap activation/deactivation with a unique inflow and pressure belt system. Combined with the complementary validation of the static properties of the aeroelastic ATEF model, this validation increases the safety and reliability of the aeroelastic design environment for the WT equipped with active flaps and provides the basis for further exploration of the ATEF technology. Future research should aim to identify the limits of application of the ATEF models in terms, for example, of actuator performance (e.g., maximum speed or deflection) or external conditions (e.g., wind misalignment, extreme wind speed, or direction change).

Author contributions. A.Go conceived and planned the measurements with the support of A.Ga, T.Ba, and H.Ma. A.Go, and H.Ma performed the flyboard measurements. A.Go performed the extended validation measurements and the video recording of the flap deflection. A.Ga. performed the model tuning, the calculations, and the postprocessing, supported by T.Ba for the Cl extraction. A.Ga developed the az-b2b method from the initial b2b method developed by A.Go. A.Go and T.Ba supervised the project. All authors discussed the results. A.Ga. wrote the manuscript with input from all authors.

Competing interests. A.Ga. and A.Go. are hired by Siemens Gamesa Renewable Energy, company that is developing the flap technology used as reference in the paper.

Acknowledgements. This research was partially funded by Danmarks Innovationsfond, Case no. 9065-00243B, PhD Title: "Advanced model development and validation of Wind Turbine Active Flap system".
The Validation of Industrial Aerodynamic Active Add-ons (VIAs) project is a collaboration between Siemens Gamesa Renewable Energy, DTU Wind Energy and Rehau AS, partially funded by EUDP under journal nr. 64019-0061.
The authors thank the anonymous reviewers whose comments and suggestions helped improve and clarify this manuscript.

References

Aagaard Madsen, H., Andersen, P. B., Løgstrup Andersen, T., Bak, C., Buhl, T., and Li, N.: The potentials of the controllable rubber trailing edge flap (CRTEF), vol. 3, pp. 2165–2175, European Wind Energy Association (EWEA), 2010.

Aagaard Madsen, H., Juul Larsen, T., Raimund Pirrung, G., Li, A., and Zahle, F.: Implementation of the blade element momentum model on a polar grid and its aeroelastic load impact, Wind Energy Science, 5, 1–27, https://doi.org/10.5194/wes-5-1-2020, 2020.

Abbas, N. J., Bortolotti, P., Kelley, C., Paquette, J., Pao, L., and Johnson, N.: Aero-servo-elastic co-optimization of large wind turbine blades with distributed aerodynamic control devices, Wind Energy, https://doi.org/https://doi.org/10.1002/we.2840, 2023.

Andersen, P. B.: Advanced load alleviation for wind turbines using adaptive trailing edge flaps : sensoring and control, Risø National Laboratory, 2010.

Barlas, T., Pettas, V., Gertz, D., and Madsen, H. A.: Extreme load alleviation using industrial implementation of active trailing edge flaps in a full design load basis, in: Journal of Physics: Conference Series, vol. 753, Institute of Physics Publishing, https://doi.org/10.1088/1742-6596/753/4/042001, 2016.

Barlas, T. K., van Wingerden, W., Hulskamp, A., Van Kuik, G., and Bersee, H.: Smart dynamic rotor control using active flaps on a small-scale wind turbine: aeroelastic modeling and comparison with wind tunnel measurements, Wind Energy, 16, 1287–1301, https://doi.org/10.1002/we.1560, 2013.

Bartholomay, S., Krumbein, S., Deichmann, V., Gentsch, M., Perez-Becker, S., Soto-Valle, R., Holst, D., Nayeri, C. N., Paschereit, C. O., and Oberleithner, K.: Repetitive model predictive control for load alleviation on a research wind turbine using trailing edge flaps, Wind Energy, 25, 1290–1308, https://doi.org/10.1002/we.2730, 2022.

Bartholomay, S., Krumbein, S., Perez-Becker, S., Soto-Valle, R., Nayeri, C. N., Paschereit, C. O., and Oberleithner, K.: Experimental assessment of a blended fatigue-extreme controller employing trailing edge flaps, Wind Energy, 26, 201–227, https://doi.org/10.1002/we.2795, 2023.

Berg, J. C., Barone, M. F., and Resor, B. R.: Field test results from the Sandia SMART rotor, 51st Aiaa Aerospace Sciences Meeting Including the New Horizons Forum and Aerospace Exposition 2013, 2013.

Bergami, L. and Gaunaa, M.: ATEFlap Aerodynamic Model, a dynamic stall model including the effects of trailing edge flap deflection, Danmarks Tekniske Universitet, Risø Nationallaboratoriet for Bæredygtig Energi, 2012.

Bergami, L. and Poulsen, N. K.: A smart rotor configuration with linear quadratic control of adaptive trailing edge flaps for active load alleviation, Wind Energy, 18, 625–641, https://doi.org/10.1002/we.1716, 2015.

Bernhammer, L. O., van Kuik, G. A., and De Breuker, R.: Fatigue and extreme load reduction of wind turbine components using smart rotors, Journal of Wind Engineering and Industrial Aerodynamics, 154, 84–95, https://doi.org/https://doi.org/10.1016/j.jweia.2016.04.001, 2016.

Brown, D., Christian, W., and Hanson, R. M.: Tracker, video analyses and modelling tool, https://physlets.org/tracker/, 2023.

Castaignet, D., Buhl, T., Poulsen, N. K., and Wedel-Heinen, J. J.: Trailing edge flaps impact on fatigue and extreme loads in power production, EWEA 2011, 2011.

Castaignet, D., Barlas, T. K., Buhl, T., Poulsen, N. K., Wedel-Heinen, Jens, J., Olesen, N. A., Bak, C., and Kim, T.: Full-scale test of trailing edge flaps on a Vestas V27 wind turbine: active load reduction and system identification, Wind Energy, 17, 549–564, https://doi.org/10.1002/we.1589, 2014.

Fischer, A. and Aagaard Madsen, H.: Investigation of the theoretical load alleviation potential using trailing edge flaps controlled by inflow data, Wind Energy, 19, 1567–1583, https://doi.org/10.1002/we.1937, 2016.

Fisker Skjoldan, P.: Aeroelastic modal dynamics of wind turbines including anisotropic effects, Risø National Laboratory, 2011.

Gamberini, A., Gomez Gonzalez, A., and Barlas, T.: Aeroelastic model validation of an Active Trailing Edge Flap System tested on a 4.3 MW wind turbine, Journal of Physics. Conference Series, 2265, 032 014, https://doi.org/10.1088/1742-6596/2265/3/032014, 2022.

Gomez Gonzalez, A., Enevoldsen, P. B., Akay, B., Barlas, T. K., Fischer, A., and Aa Madsen, H.: Experimental and numerical validation of active flaps for wind turbine blades, in: Journal of Physics: Conference Series, vol. 1037, Institute of Physics Publishing, https://doi.org/10.1088/1742-6596/1037/2/022039, 2018.

Gomez Gonzalez, A., Bay Enevoldsen, P., Barlas, A., and Madsen, H. A.: General rights Field test of an active flap system on a full-scale wind turbine Field test of an active flap system on a full-scale wind turbine, Wind Energ. Sci, 6, 33–43, https://doi.org/10.5194/wes-6-33-2021, 2021.

Gomez Gonzalez, A., Enevoldsen, P., Barlas, T., and Madsen, H. A.: Test of an active flap system on a 4.3 MW wind turbine, Journal of Physics. Conference Series, 2265, 032 016, https://doi.org/10.1088/1742-6596/2265/3/032016, 2022.

Gonzalez, A. G., Enevoldsen, P., Barlas, T. K., Madsen, H. A., and Olsen, A. S.: Consolidated results of the laboratory and full scale field validation of an active flap system, Journal of Physics: Conference Series, 1618, 52 024, https://doi.org/10.1088/1742-6596/1618/5/052024, 2020.

Lackner, M. A. and Van Kuik, G.: A comparison of smart rotor control approaches using trailing edge flaps and individual pitch control, Wind Energy, 13, 117–134, https://doi.org/10.1002/we.353, 2010.

Larsen, T. J. and Hansen, A. M.: How 2 HAWC2, the user's manual, 2023.

Madsen, H. A., Barlas, T., Fischer, A., Olsen, A. S., and Gomez Gonzalez, A.: Inflow and pressure measurements on a full scale turbine with a pressure belt and a five hole pitot tube, Journal of Physics: Conference Series, 2265, https://doi.org/10.1088/1742-6596/2265/2/022096, 2022.

Pettas, V., Barlas, T., Gertz, D., and Madsen, H. A.: Power performance optimization and loads alleviation with active flaps using individual flap control, in: Journal of Physics: Conference Series, vol. 749, p. 012010, Institute of Physics Publishing, https://doi.org/10.1088/1742-6596/749/1/012010, 2016.

Pirrung, G., Riziotis, V., Madsen, H., Hansen, M., and Kim, T.: Comparison of a coupled near- And far-wake model with a free-wake vortex code, Wind Energy Science, 2, 15–33, https://doi.org/10.5194/wes-2-15-2017, 2017.

Prospathopoulos, J. M. et al.: Simulation of oscillating trailing edge flaps on wind turbine blades using ranging fidelity tools, Wind Energy, 24, 357–378, https://doi.org/10.1002/we.2578, 2021.

Van Wingerden, J. W., Hulskamp, A. W., Barlas, T., Marrant, B., Van Kuik, G. A., Molenaar, D. P., and Verhaegen, M.: On the proof of concept of a 'smart' wind turbine rotor blade for load alleviation, Wind Energy, 11, 265–280, https://doi.org/10.1002/we.264, 2008.

Article 3.

Operational experience during a four year test program of active flaps on a wind turbine blade.

Accepted to the 10th ECCOMAS Thematic Conference on Smart Structures and Materials in Patras, Greece.

X ECCOMAS Thematic Conference on Smart Structures and Materials
SMART 2023
D.A. Saravanos, A. Benjeddou, N. Chrysochoidis and T. Theodosiou (Eds)

OPERATIONAL EXPERIENCE DURING A FOUR YEAR TEST PROGRAM OF ACTIVE FLAPS ON A WIND TURBINE BLADE

ALEJANDRO GOMEZ GONZALEZ*, PEDER B. ENEVOLDSEN*, ANDREA GAMBERINI*†, ATHANASIOS BARLAS† AND HELGE AA. MADSEN†

*Siemens Gamesa Renewable Energy A/S (SGRE)
Technology Development
Borupvej 16, 7330 Brande, Denmark
e-mail: alejandro.gonzalez@siemensgamesa.com, web page: http://www.siemensgamesa.com/

† DTU Wind and Energy Systems (DTU Wind)
DTU Risø Campus
Frederiksborgvej 399, 4000 Roskilde, Denmark
Web page: http://wind.dtu.dk

Abstract. A prototype of a pneumatically controlled active flap system (AFS) for wind turbine blades was designed and manufactured as a part of the collaboration projects Induflap2 and VIAs between the partners Siemens Gamesa Renewable Energy, DTU Wind, and Rehau. The AFS was validated in full-scale during a four year test program consisting of four individual test phases between 2018 and 2022 on two different test turbines with rated powers of 4.0 and 4.3 MW, respectively. The objective of the field validation was to collect operational experience with the complete system, to perform a detailed experimental aerodynamic and aeroelastic characterization of the wind turbine equipped with an AFS, and to validate the numerical models used for the simulation of such a system. Besides the validation activities, different experimental techniques were developed in order to enable the accurate measurement of aerodynamic quantities within a highly dynamic and turbulent wind environment. The load control authority of the AFS was measured to be in the range of 3-20% for the flapwise bending moment. Very good agreement was found when compared to aeroelastic simulations. Furthermore, a direct measurement of fatigue reduction on the blades was performed employing a cyclic approach for the flap control leading to load reductions in the range of 10-13%. This paper discusses the main results of the complete four-year test program based on the load measurements and operational experience collected.

Key words: Wind Turbines, Smart Blades, Active Flow Control, Active Flaps, Field Tests

1 INTRODUCTION

The development of new wind turbines is continuously pushing the limits of current technology fronts within the fields of aeroelasticity, structural mechanics, material science, and advanced control, among others. With time, the design drivers of wind turbine blades have changed significantly with the demand for longer flexible blades. Blade design drivers can be related for example to extreme material strains, maximum allowable tip deflection, blade-hub interface loading, or stability limits of blades. The ability to tailor the aerodynamic performance of blades has continuously evolved, beginning with fixed pitch passive stall controlled in the late 1970's, active stall fixed-speed controlled turbines during the 1980's and 1990's, and a transition to pitch-to-feather variable-speed controlled turbines in the early 1990's and going forward. Additional degrees of aerodynamic and aeroelastic tailoring were introduced at industrial level towards the end of the 2000's and beginning of 2010's with the increased use of passive aerodynamic add-ons such as vortex generators and trailing edge serrations, as well as aeroelastic tailoring by means of bend twist coupling of the blades. An even higher degree of control authority on the aerodynamic loads introduced to the turbine and the foundation can be achieved by implementing active flow control techniques such as trailing edge flaps.

The two research projects Induflap2 (2015-2018) and VIAs (2019-2022) carried out by the partners SGRE, DTU Wind, and Rehau, aimed at developing a system of active trailing edge flaps suitable for industrial application and to demonstrate the technology in full-scale on modern wind turbines. During these two projects, a series of design iterations of the active flap were carried out, each tested at different levels of fidelity (wind tunnel, lab scale, rotating test rig, or full-scale as shown schematically in figure 1). The full-scale testing of the active flap system (AFS) was performed in four phases during which some upgrades were performed to the system based both on the operational experience collected as well as on results from laboratory and wind tunnel testing performed in parallel to the field test. This article collects some selected findings and learnings during the four-year test program and guides the reader to further references wherever applicable.

Figure 1: Schematic representation of validation steps of the active flap system, starting from detailed design activities such as CFD, proceeding with sub-system tests at wind tunnel and rotating test rig level, and concluding with full-scale verification

The article is structured as follows. The first section describes briefly the objectives of the two aforementioned publicly funded projects Induflap2 and VIAs. The next section gives a brief description of the state of the art in the field of flow control, with focus on the field validation activities. The following two sections discuss the test setup, the methodology, and results of the field validation of the AFS. These sections focus mainly on three specific validation exercises carried out: the validation of the load control authority of the active flap by means of the so-called blade-2-blade method, detailed aerodynamic measurements based on advanced inflow and pressure sensors, and detailed aeroelastic characterization by means of so-called one-2-one aeroelastic simulations. The last section summarizes the work in the form of conclusions and lessons learned.

2 OBJECTIVE

The main objective of the Induflap2 and VIAs[1] projects was to design, manufacture, and validate an AFS for rotor blades of wind turbines at different fidelity scales, as well as to develop the necessary experimental and numerical methods. The validation of the active flow control systems is not only complex, but also costly. Therefore, for these two projects to be successful, a good collaboration between industry and academic partners has proven essential. Secondary objectives of the project include

- the structural, aerodynamic, and aeroelastic characterization of the isolated AFS at laboratory level (i.e. structural static and fatigue testing, wind tunnel testing, and testing in atmospheric conditions on a rotating test rig)
- the numerical description of the isolated AFS (i.e. FEM, CFD, and FSI simulations), as well as the numerical evaluation of the full wind turbine and AFS assembly by means of aeroelastic simulations
- the development of necessary measurement devices and methods to carry out the aforementioned numerical and experimental tasks
- the demonstration of AFS manufacturing at industrial level
- to identify all the system boundaries of the AFS and mature the required peripheral systems and preliminary control strategies
- to identify technical risks and tackle them in a systematic manner by means of DFMEA's (Design Failure Mode and Effect Analysis)
- to demonstrate the functionality of the system in a long term full-scale test on a modern wind turbine and carry out the required detailed testing and simulation activities relevant to this.

[1]Induflap2 and VIAs were partially funded by EUDP under Journal Nrs. 64015-0069 and 64019-0061, respectively

This article focuses on the last bullet point. To the author's knowledge, the tests carried out during this test program represent the largest (both in terms of rotor diameter as well as rated power of the turbine) and longest (in terms of actual test time at full-scale) in the world up to date.

3 STATE OF THE ART

Reducing the levelized cost of energy (LCOE) of wind turbines can be achieved by increasing the swept area of the rotor while minimizing the loads imposed on the main components such as the hub, nacelle, tower structure, and foundation. An effective way to achieve this is through active flow control. Several active flow control concepts, including active gurney flaps, mini-tabs, plasma actuators, and boundary layer suction and blowing have been studied, but many of these are not suitable for industrial deployment due to technical feasibility and implementation challenges. An overview of some of the main flow control approaches can be found e.g. in [1, 2, 3, 4]. Some of these strategies aim directly at improving the aerodynamic efficiency of a rotor e.g. by suppressing local flow separation. Such concepts are closely related to the field of boundary layer control and include e.g. plasma actuators [5, 6] or boundary layer suction and blowing (also including synthetic jets) [7, 8, 9, 10, 11]. Other concepts focus on circulation control, including e.g. active gurney flaps and mini-tabs [12, 13]. One concept for circulation control is the rigid or morphing trailing edge flap. Such flaps have been the subject of numerous studies in the past, covering both the aerodynamic, structural, and aeroelastic modelling of the turbine-flap system, as well as the development of control strategies for load reduction (see e.g. [14, 15, 16, 17, 18].

Full-scale experimental validation of active flow control strategies is complex and costly. As a consequence, the amount of literature available for full-scale tests (on MW-sized turbines) is scarce. Among the few efforts to do this type of validation, some of the most representative are mentioned here. One representative tests was performed on a Vestas wind turbine type V27-225 kW (13m long blade) equipped with a 70cm long trailing edge flap [19, 20, 17, 18]. In these tests, the AFS was mainly operated in intervals of two minutes with and without flap control focusing mainly on alleviating blade fatigue loads. A further active flap test was carried out by Sandia Laboratories [15, 16] where a mechanically actuated hinged flap covering the aft 20% of the chord of the outer 20% span of a 9m long blade was tested. Previous work on morphing flaps carried out within the framework of the Induflap1 project [21] includes testing under atmospheric conditions in the rotating test rig as well [22, 23]. During these tests, measurements of the flapwise bending moment of the boom of the rotating rig show that a 5 deg flap actuation (15% chordwise coverage) has a similar response as 1 deg blade section pitch actuation. Similar tests were performed on a morphing trailing edge flap [14, 24, 25] developed within the framework of the EU INNWind project and was tested under atmospheric conditions on a rotating test rig at the Risoe Campus of DTU. These tests included flap actuation steps, cyclic control based on azimuth position and feed-forward control based on inflow angle. For different blade pitch positions, the AFS was actuated in cycles of 10s over a test period of 5 minutes. Azimuth and inflow based feed forward control showed an average reduction of the standard deviation of the bending moment at the base of the rotating rig boom of 12% and 11%, respectively. Besides circulation control tests (flaps), a full-scale test of a boundary layer control system with leading edge plasma actuators was performed on a 1.75 MW wind turbine [6]. Swap intervals of 10 minutes (plasma actuators on or off) were performed focusing on the turbine's power production.

The work presented in this article contributes to the state of the art by extending previously reported results of laboratory and full-scale validation of the AFS described in [26, 27, 28] to include test phase 4, and by collecting important lessons learned of complete field validation program. The test setup, instrumentation, methodology, and results are discussed in what follows.

4 TEST SETUP AND TURBINE INSTRUMENTATION

The AFS was tested on two turbines of types SWT-4.0-130 (4.0MW rated power, 130m rotor diameter) and SG-4.3-120 DD (4.3MW rated power, 120m rotor diameter) for a total of four years. The full-scale validation campaign served as basis for the three validation exercises presented in this article: full scale aeroelastic validation via load measurements on the turbine, detailed aerodynamic measurements with help of advanced inflow and pressure blade instrumentation, and validation of aeroelastic models of the turbine including AFS in the codes HAWC2 [29] and BHawC [30, 31].

The field validation of the AFS was carried out in four phases as summarized in table 1. The test program was carried out in the test site Høvsøre in northwest Denmark. The test site layout is shown in figure 2. In all phases of testing, the test turbines were equipped with numerous sensors including strain gauges at the root of the blades (installed at 1.2m from the root for test phase 1 and 2, and 3.0m from the root for test phase 3 and 4) to measure flapwise and edgewise bending moments, acceleration measurements in the nacelle, as well as all operation parameters of the wind turbines including nacelle wind speed, rotor speed, pitch position, electrical power, yaw position, and azimuth position, among others. Furthermore, the wind field was measured employing the combination of a meteorological mast[2] (met-mast) and a Lidar. The met-masts were located at a distance of 2.5 rotor diameters upstream in the westerly sector for each turbine and were used to acquire hub-height wind speed, turbulence level, pressure, temperature, and humidity. The Lidar measured wind speed and direction at ten independent heights spanning the full swept area of the rotor[3]. A complete description of the test setup is given in [26, 27] and shown schematically in figure 3.

Each testing phase was carried out aiming at collecting test data for a wide range of operational conditions of the turbine. As an example, the frequency distribution of wind speed and turbulence intensity at hub-height for test phase 3 is shown in figure 4 covering the full operational range of the wind turbine up to wind speeds beyond 25 m/s.

[2]For phase 3, the met-mast was only available until February 2021

[3]The Lidar is next to the met-mast used during phase 1 and 2 - see figure 2 and was only used to collect wind shear data

	Phase 1	Phase 2
Date	Oct 2017 - June 2018	Dec 2018 - June 2019
Turbine	SWT-4.0-130	SWT-4.0-130
AFS revision	FT008rev9	FT008rev10
AFS actuation	discretely adjustable	continuously adjustable
Validation type	on-off cycles	on-off cycles
Location on blade	47.5 - 62.5 m	42.5 - 62.5 m
Other tests	Flow visualization	None
	Phase 3	**Phase 4**
Date	June 2020 - June 2021	July 2021 - Aug 2022
Turbine	SG-4.3-120 DD	SG-4.3-120 DD
AFS revision	FT008rev10	FT008rev10
AFS actuation	continuously adjustable	continuously adjustable (faster)
Validation type	on-off cycles, cyclic 1P	on-off cycles, cyclic 1P
Location on blade	38.0 - 58.0 m	38.0 - 58.0 m
Other tests	Inflow sensor and pressure belt	Inflow sensor, pressure belt, and wake-rake

Table 1: Campaign information

5 METHODOLOGY AND RESULTS

The following sections give a short description of three main types of validation methods used for assessing the aerodynamic and aeroelastic performance of the wind turbine including the AFS: full scale validation by means of the so-called blade-2-blade method, detailed aerodynamic measurements based on inflow and airfoil pressure measurements, and aeroelastic validation by means of so-called one-2-one simulations.

5.1 Blade-2-blade method

The blade-2-blade (b2b) analysis method aims at isolating the impact of a flow control device (in this case an AFS) on the loading of a rotor blade. A description of part of the method is given in [26]. The method is particularly useful in atmospheric environments where the levels of variation of the operational point of the turbine vary continuously due to atmospheric turbulence. The method mainly consists of three types of analysis: steady state impact, transient response, and impact of damage equivalent loading (fatigue) of the AFS. The b2b method can be used to measure the characteristics of an AFS, in particular its steady-state and transient step response, as well as its response to 1P (once per revolution) cyclic activation. Details of the method for steady-state and transient analysis can be found in [26], and a short extension of the method to include 1P cyclic activation for characterization of damage equivalent (fatigue) loads is given in [28].

The steady state analysis requires a rotor equipped with strain gauges for measuring strains (and indirectly bending moments). One blade of the rotor is equipped with the AFS and is

Figure 2: Test site layout - map data taken from Google Maps (c)

referenced to a neighbour blade without the active system. A typical measurement of flapwise root bending moment as a function of wind speed (in the westerly sector where the met-mast is undisturbed and in front of the turbine) is shown in figure 5 for the reference blade A and the blade equipped with the AFS blade B. Each point in this graph represents the average values of a 10-minute measurement interval. The level of scatter shown is typical for such a load measurement as a function of wind speed. The amount of scatter is partly due to atmospheric turbulence and partly to the coherence level between the undisturbed wind measured at the met-mast and the turbine response (the further away the met-mast is located, the lesser it will be influenced by the presence of the turbine, but the level of coherence between met-mast wind signals and turbine load and power signals becomes worse). It can also be seen that blade B (with the AFS), shows different levels of bending moment, even though it is difficult to discern clearly different loading bands. A clear advantage of the b2b method is seen when plotting the bending moment values of each blade against each other as shown exemplary in figure 6, giving a much better correlation and lower scatter. The reason for this is the high correlation of loads seen by two neighbour blades (because they both experience the same level of azimuthal load variation).

The details of the transient analysis and damage equivalent blade-2-blade analysis are not discussed in this paper and the reader is referred to [27, 28].

Some of the main results of the field validation are described below for phase 3 and 4 of the test campaign. During parts of the test campaing, the AFS was activated in an on-off manner, maintaining the flap position constant during an interval of 10-minutes and subsequently fully deactivating the flap for another 10-minutes. The interval of 10 minutes was chosen as it is standard for many other wind turbine measurements such as power (a 10-minute interval is a good compromise between including sufficient turbulent variations but excluding wind speed trend variations and is a standard measurement interval in the industry). The AFS is activated

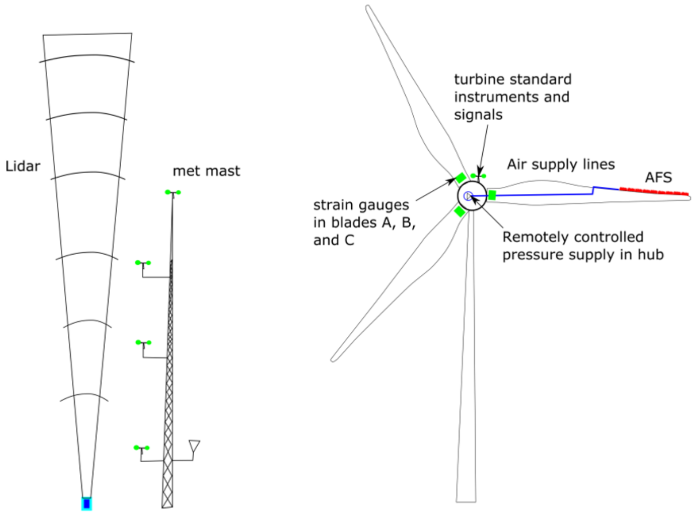

Figure 3: Schematic representation of instrumentation setup

in five discrete states, labelled 0%, 25%, 50%, 75%, and 100%. The lowest and highest activation states correspond to active flap angular deflections of approximately 0 deg and 23 deg (as described in [28], respectively. These on-off activations were performed during several months, collecting data for all activation ranges of the AFS, even though most data was collected for the 75% activation level. The data for the steady state b2b analysis for the AFS is filtered according to low and high wind speeds, for measured hub-height wind speed of less or more than 10 m/s, respectively. This level corresponds approximately with the peak of the load distribution as shown in figure 5 and makes the analysis clearer (the blades operate in quite different aerodynamic conditions before and beyond the peak of bending moment).

The load control authority of the AFS for the different activation states is shown in figure 6 in a b2b manner, and in figure 7 in a relative manner (relative to blade A, without the AFS) as

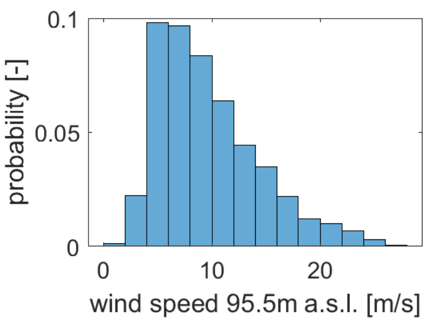

(a) Wind distribution during test phase 3

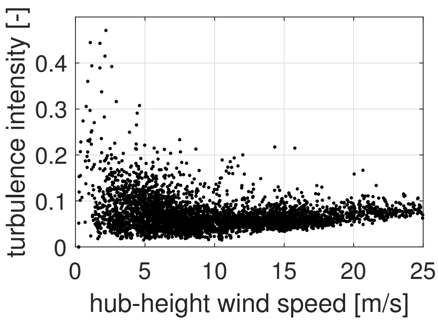

(b) Turbulence intensity - west sector

Figure 4: Wind conditions during test phase 3

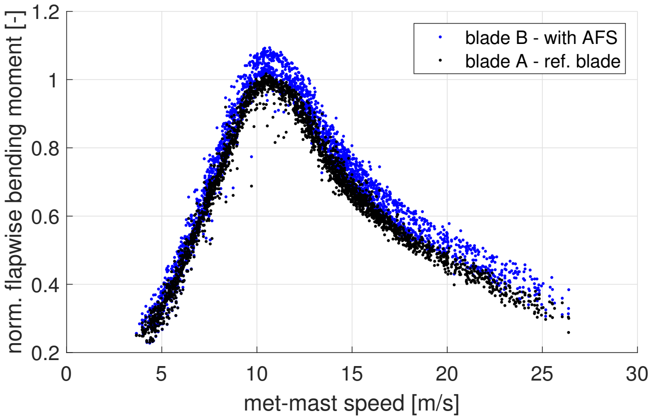

Figure 5: Flapwise bending moment as a function of wind speed measured at the met-mast for phase 3

a function of nacelle wind speed (i.e. the wind speed measured with the nacelle anemometer of the turbine). The steady-state load control authority is seen to range from 3% to 20% depending on the activation state of the flap.

In a further series of tests, the AFS was activated in a feed-forward manner using the azimuth position of the rotor as control signal. The aim of this control strategy was to reduce load variations induced by standard wind shear (i.e. increasing wind speed with increasing height). This simple cyclic approach is a good proxy for the load control authority of the AFS in cyclic conditions. More advanced control strategies are required in order to counteract load imbalance as would occur e.g. from operation in half-wake situations. The reduction in azimuthal load variation of the blades is measured directly by estimating the so-called short term equivalent loads (STEL), which is nothing else than the 1-Hz equivalent load that causes the same amount of damage for a particular Wöhler exponent as the load signal acquired during 10 minutes.

The damage equivalent loads are depicted in figure 8. In this case, for this cyclic 1P feed-forward test periods, the load reduction level measured is approx 10-13% in the range of wind speeds around 12 m/s. The amount of data collected at high wind speeds (higher than approx. 15m/s) is limited.

5.2 Local aerodynamic measurements

Local aerodynamic measurements were performed in a specialized campaign carried out in June 2021 and are reported in [32]. During this campaign, an inflow sensor consisting of a 5-hole Pitot tube and a blade-mounted autonomous data acquisition and transmission system was installed in blade B (including the AFS) in a section in the middle (spanwise) of the AFS extension corresponding to a blade spanwise position of 50m from the hub flange. Furthermore, a pressure belt with 15 taps was installed wrapping around the blade at a spanwise position of 49m. The setup is shown in figure 9a.

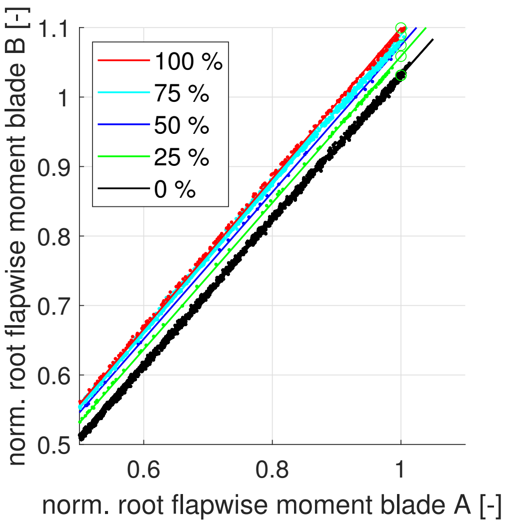

(a) Low wind

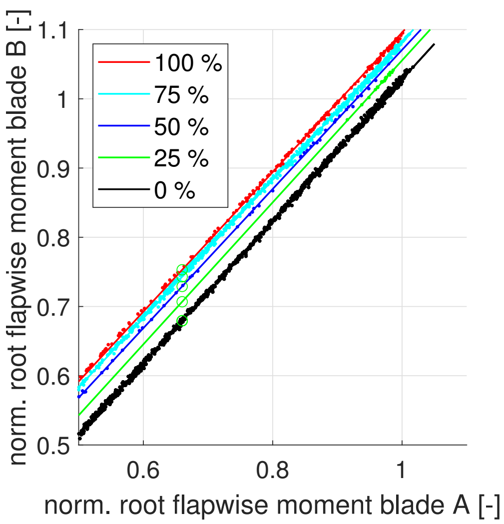

(b) High wind

Figure 6: Blade-2-blade results during test phase 3 and 4

The tests performed consisted in AFS discrete activations at different flap deflection levels (corresponding to the same activation levels as previously described in the b2b method) and different intervals ranging from 3s to 60s. In parallel to the data acquired by the inflow sensor and pressure belt, all operational characteristics of the turbine as well as the same load channels as described in the previous section were recorded. For visual analysis, a GoPro camera was installed to enable the evaluation of the flap deflection directly from video post-processing and to correlate this with the data acquired from the different instruments.

An exemplary pressure distribution assembled using data from the inflow sensor and the pressure belt is shown in figure 9b for binned data sets of the flap actuated at 0% and 75% levels. The resolution of the position of the taps is enough to identify the main characteristics of the pressure distribution of the airfoil, but has been improved in a more recent experiment with a pressure belt with 32 taps with increased accuracy of calculated lift levels [33].

5.3 Aeroelastic simulations

Besides the field validation and the detailed experimental validation of the flap, all test activities were accompanied by aerodynamic or aeroelastic simulations. For the different phases of testing, so-called one-2-one (o2o) simulations were performed. This type of simulations are set up such that for every 10-minute measurement point, there is a corresponding 10-minute aeroelastic simulation reflecting to the extent possible the same atmospheric conditions. The measurements and simulations can then be compared in a statistical manner. The basic setup of these o2o simulations is described in [26] along with the o2o results for phase 1 and 2. The o2o results for phase 4 and part of phase 3 are reported in [34].

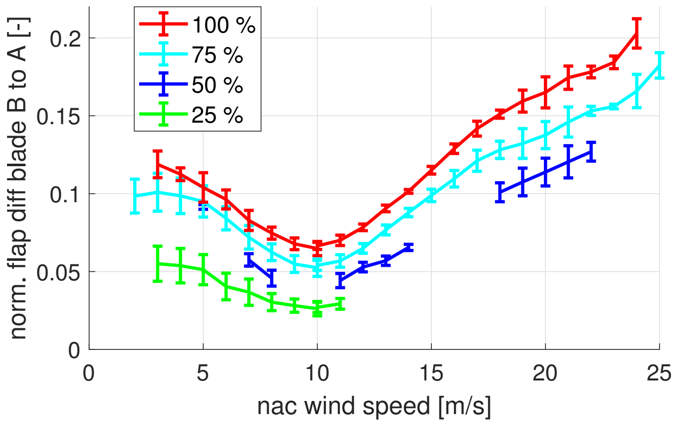

Figure 7: Relative AFS impact as function of nacelle wind speed

The focus of the aeroelastic validation is two-fold. Firstly, it serves to explore the level of accuracy of existing aeroelastic codes for validation of wind turbines with AFS (in this case SGRE's code BHawC and DTU's code HAWC2). Secondly, in combination with the b2b results and detailed aerodynamic measurements described in the previous sections, modelling gaps can be identified in order to increase the fidelity of AFS aeroelastic models. A condensed example showing the measured load control authority level of the AFS as measured on the prototype test turbine (PT) by means of b2b in comparison to the simulated levels with BHawC (BH) and HAWC2 (H2) as shown in figure 10. The figure shows a very good correlation between experiments and aeroelastic simulations, with only a slight overestimation of approximately 1% of the predictions of the aeroelastic codes in comparison with the measurements.

6 CONCLUSIONS AND LESSONS LEARNED

The Active Flap System presented in this article underwent a detailed development and validation process during the Induflap2 and VIAs projects. The main bulk of the field testing took place between 2018 and 2022. The project participants learned that the following aspects were particularly important for a successful development of the technology:

- Experimental and numerical validation work must go hand-in-hand
- Close collaboration between academia and industry is a key element
- Preliminary field validation during early design stages provides very valuable learnings for the successful development of the AFS technology.

For the AFS system developed, the main results can be summarized as follows:

- The steady state load control authority of the actuator (load handle) was measured to be between 3% and 20% depending on wind speed and actuation level of the AFS. For

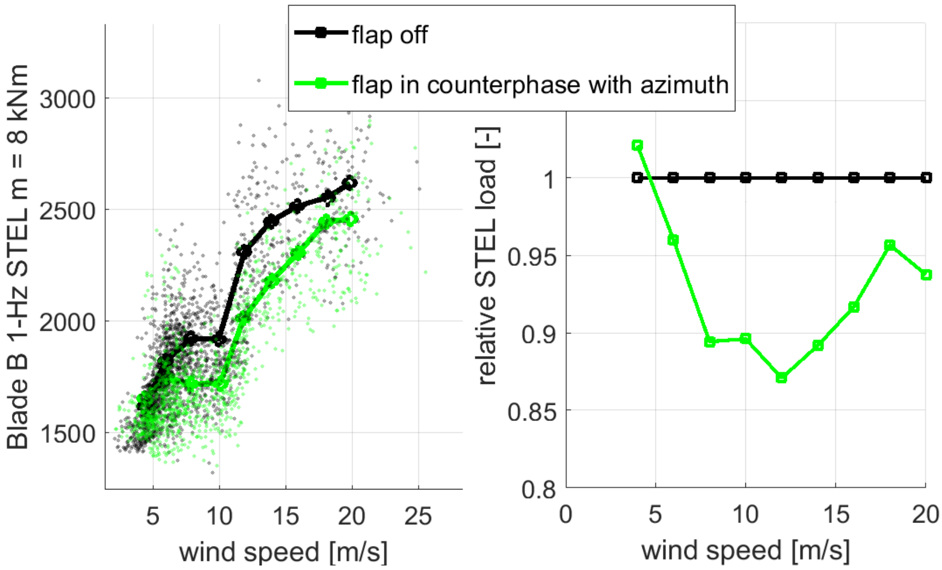

Figure 8: Impact of cyclic flap actuation of damage equivalent loads (fatigue) for a Wöhler slope of m=8 shown in absolute (left) and relative (right) level

azimuth controlled actuation, fatigue load reductions of approximately 10-13% for wind speeds around 12 m/s were measured

- Instrumentation was developed to perform detailed local aerodynamic sectional measurements based on inflow and pressure distribution measurements
- Very good agreement between aeroelastic simulations and measurements was obtained
- The b2b-method proved very beneficial in terms of measuring the load impact of the active flap at full-scale level.

To the author's knowledge, this is the largest (in terms of turbine rated power and rotor diameter) and longest (several years) field validation of an active flap ever documented, and the results collected so far are therefore an important milestone towards the development, improvement, and industrialization of the AFS. There is a need for new technologies to enable future blade designs, and although the active flap technology has not reached yet its full maturity stage, it does have future potential.

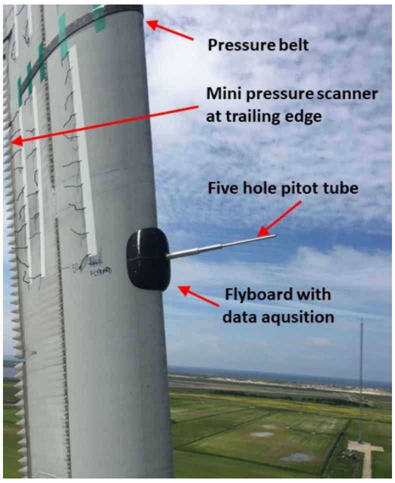

(a) Flyboard setup

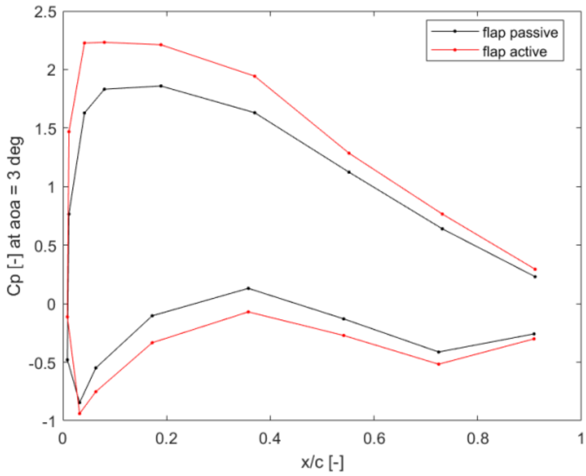

(b) Exemplary pressure distribution obtained from pressure belt

Figure 9: Flyboard setup including inflow sensor and pressure belt (reproduced from [32])

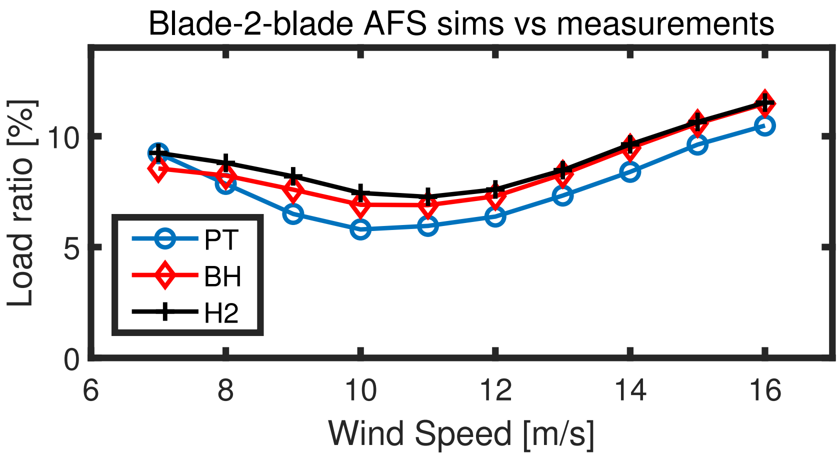

Figure 10: Blade-2-Blade from aeroelastic simulations (reproduced from [34]). Measurements from the prototype turbine are labelled with PT, and the corresponding BHawC and HAWC2 simulations with BH and H2, respectively.

REFERENCES

[1] G. Pechlivanoglou, “Passive and active flow control solutions for wind turbine blades,” Ph.D. dissertation, Technische Universität Berlin, 2013.

[2] T. Barlas and G. van Kuik, “Review of state of the art in smart rotor control research for wind turbines,” *Progress in Aerospace Sciences*, vol. 46, pp. 1–27, 2010.

[3] G. Pechlivanoglou, C. N. Nayeri, and C. O. Paschereit, “Performance optimization of wind turbine rotors with active flow control,” *Proceedings of the ASME Turbo Expo*, vol. 1, pp. 763–775, 2011.

[4] Z. Akhter and F. K. Omar, “Review of Flow Control Devices for Wind Turbine Performance Enhancement,” *Energies*, vol. 14, pp. 1–38, 2021.

[5] J. A. Meijerink and H. W. Hoeijmakersy, “Plasma actuators for active flow control on wind turbine blades,” *29th AIAA Applied Aerodynamics Conference 2011*, no. June, 2011.

[6] H. Matsuda, M. Tanaka, T. Osako, K. Yamazaki, N. Shimura, M. Asayama, and Y. Oryu, “Plasma actuation effect on a MW class wind turbine,” *International Journal of Gas Turbine, Propulsion and Power Systems*, vol. 9, no. 1, pp. 47–52, 2017.

[7] P. Scholz, J. Ortmanns, C. J. Kähler, and R. Radespiel, “Leading edge separation control by means of pulsed jet actuators,” *Collection of Technical Papers - 3rd AIAA Flow Control Conference*, vol. 1, no. June, pp. 147–158, 2006.

[8] S. Shun and N. A. Ahmed, “Wind turbine performance improvements using active flow control techniques,” *Procedia Engineering*, vol. 49, no. mm, pp. 83–91, 2012.

[9] G. Godard and M. Stanislas, “Control of a decelerating boundary layer. Part 3: Optimization of round jets vortex generators,” *Aerospace Science and Technology*, vol. 10, no. 6, pp. 455–464, 2006.

[10] A. G. Oliver, “Air jet vortex generators for wind turbines,” Ph.D. dissertation, City University London, 1997.

[11] V. Maldonado, “Active flow control of wind turbine blades,” in *Wind turbines - design, control and applications*. Intech, 2016, ch. 13, pp. 303–324.

[12] D. J. Heathcote and D. J. Heathcote, “Aerodynamic Loads Alleviation Using Mini-tabs,” Doctoral thesis, University of Bath, 2017.

[13] C. P. Van Dam, R. Chow, J. R. Zayas, and D. E. Berg, “Computational Investigations of Small Deploying Tabs and Flaps for Aerodynamic Load Control,” *Journal of Physics: Conference Series*, vol. 75, pp. 1–10, 2007.

[14] P. H. Jensen, T. Chaviaropolos, and A. Natarajan, "LCOE reduction for the next generation offshore wind turbines: Outcomes from the INNWIND.EU project," *Innwind.eu*, no. October, 2017.

[15] J. Berg, M. Barone, and N. Yoder, "Smart wind turbine rotor: data analysis and conclusions," Sandia National Laboratories, Wind Energy Technologies Department, Tech. Rep. SAND2014-0712, 2014.

[16] J. Berg, B. Resor, J. Paquette, and J. White, "Smart wind turbine rotor: design and field test," Sandia National Laboratories, Wind Energy Technologies Department, Tech. Rep. SAND2014-0681, 2014.

[17] D. Castaignet, I. Couchman, N. Poulsen, T. Buhl, and J. Wedel-Heinen, "Frequency weighted model predictive control of trailing edge flaps on a wind turbine blade," *IEEE Transactions On Control Systems Technology*, vol. 21, no. 4, pp. 1105–1116, 2013.

[18] I. Couchman, D. Castaignet, N. Poulsen, T. Buhl, J. Wedel-Heinen, and N. Olesen, "Active load reduction by means of trailing edge flaps on a wind turbine blade," in *American Control Conference*, Portland, USA, June 2014.

[19] D. Castaignet, T. Barlas, T. Buhl, N. Poulsen, J. Wedel-Heinen, N. Olesen, C. Bak, and T. Kim, "Full-scale test of trailing edge flaps on a vestas v27 wind turbine: active load reduction and system identification," *Journal of Wind Energy*, 2013.

[20] D. Castaignet, J. Wedel-Heinen, T. Kim, T. Buhl, and N. Poulsen, "Results from the first full scale wind turbine equipped with trailing edge flaps," in *Proceedings of the 28th AIAA Applied Aerodynamics Conference*, 2010.

[21] "Induflap2 project website," http://www.induflap.dk, accessed 12.04.2023.

[22] H. A. Madsen, T. Barlas, and T. L. Andersen, "A Morphing Trailing Edge Flap System for Wind," *7th ECCOMAS Thematic Conference on Smart Structures and Materials*, pp. 1–10, 2015.

[23] H. A. Madsen, T. K. Barlas, and T. L. Andersen, "Testing of a new morphing trailing edge flap system on a novel outdoor rotating test rig," *European Wind Energy Association Annual Conference and Exhibition 2015, EWEA 2015 - Scientific Proceedings*, pp. 26–30, 2015.

[24] T. K. Barlas, A. S. Olsen, H. A. Madsen, T. L. Andersen, Q. Ai, and P. M. Weaver, "Aerodynamic and load control performance testing of a morphing trailing edge flap system on an outdoor rotating test rig," *Journal of Physics: Conference Series*, 2018.

[25] J. Frederik, S. Navalkar, J. W. van Wingerden, T. Barlas, H. A. Madsen, A. S. Olsen, T. L. Andersen, L. Lars, V. Riziotis, Q. Ai, P. Weaver, L. Bergami, and J. Kloepfer, "Demonstration and validation of new control concepts by dedicated and scaled turbine experiments," Innwind.eu, EU report, 2017.

[26] A. Gomez Gonzalez, T. Barlas, P. Enevoldsen, and H. Madsen, "Field test of an active flap system on a multi mw wind turbine," in *Presentations of Wind Energy Science Conference WESC2019*, Cork, Ireland, June 2019.

[27] A. Gomez Gonzalez, P. Enevoldsen, T. Barlas, H. Madsen, and A. Olsen, "Consolidated results of the laboratory and full scale field validation of an active flap system," *J. Phys.: Conf. Ser.*, 2020.

[28] A. G. Gonzalez, P. Enevoldsen, T. Barlas, and H. A. Madsen, "Test of an active flap system on a 4.3 mw wind turbine," *Journal of Physics: Conference Series*, vol. 2265, no. 3, p. 032016, may 2022. [Online]. Available: https://dx.doi.org/10.1088/1742-6596/2265/3/032016

[29] T. J. Larsen and A. M. Hansen, *How 2 hawc2, the users manual*, DTU Wind Energy.

[30] R. R. and J. Petersen, "Monopile as part of aeroelastic wind turbine simulation code," in *Proceedings of Copenhagen Offshore Wind*, 2005.

[31] P. Skjoldan, "Aeroelastic modal dynamics of wind turbines including anisotropic effects," Ph.D. dissertation, DTU, 2011.

[32] H. A. Madsen, T. K. Barlas, A. Fischer, A. S. Olsen, and A. G. González, "Inflow and pressure measurements on a full scale turbine with a pressure belt and a five hole pitot tube," *Journal of Physics: Conference Series*, vol. 2265, 2022.

[33] "Wake rake test announcement," https://www.linkedin.com/posts/helge-aagaard-madsen-ba006b93_demonstration-of-an-autonomous-measurement-ugcPost-6970317709028773888-ZeQ2?utm_source=share&utm_medium=member_desktop, accessed 12.04.2023.

[34] A. Gamberini, A. G. Gonzalez, and T. Barlas, "Aeroelastic model validation of an active trailing edge flap system tested on a 4.3 mw wind turbine," *Journal of Physics: Conference Series*, vol. 2265, no. 3, p. 032014, may 2022. [Online]. Available: https://dx.doi.org/10.1088/1742-6596/2265/3/032014

Article 4.

Active Trailing Edge Flap System fault detection via Machine Learning

Under review at the Wind Energy Science journal.

https://doi.org/10.5194/wes-2023-24
Preprint. Discussion started: 11 May 2023

Active Trailing Edge Flap System fault detection via Machine Learning

Andrea Gamberini[1,2] and Imad Abdallah[3]

[1]Siemens Gamesa Renewable Energy A/S, Brande, Denmark
[2]DTU, Dept. of Wind and Energy Systems, Roskilde, Denmark
[3]Chair of Structural Mechanics and Monitoring, ETH Zurich

Correspondence: Andrea Gamberini (andgam@dtu.dk)

Abstract. Active trailing edge flap systems (AFlap) have shown promising results in reducing wind turbine (WT) loads. Once the WT design includes the AFlap, a condition monitoring system will be needed to ensure the flaps provide the expected load reductions. This paper presents two approaches based on machine learning to diagnose the health state of an AFlap system. Both approaches rely only on the sensors commonly available on commercial WTs, avoiding the need and the cost of additional measurement systems. The first approach (MFS) uses manual feature engineering in combination with a random forest classifier. The second approach (AFS) relies on random convolutional kernels to create the feature vectors. The study shows that the MFS method is reliable in classifying all the investigated combinations of AFlap health states in the case of asymmetrical flap faults not only when the WT operates in normal power production but also before startup. Instead, the AFS method can identify some of the AFlap health states for both asymmetrical and symmetrical faults when the WT is in normal power production.

1 Introduction

The pursuit of lower Levelized Cost of Energy has driven a steady increase in the size of utility-scale Wind Turbines (WTs) over the past years, with a consequent increase in the load carried by the WT components. Among the new technologies studied to mitigate this load increase, actively controlled flaps located at the blade trailing edge (AFlap) have shown promising results in reducing fatigue and ultimate loads and increasing annual energy production, see Barlas et al. (2016), and Pettas et al. (2016). Despite the potential benefits of AFlaps, this technology has yet to reach a sufficient level of maturity for its implementation in commercial WTs. To the authors' knowledge, only Siemens Gamesa Renewable Energy (SGRE) has publicly shared data of an AFlap system implemented on two different multi-MW WTs: a 4.0 MW WT prototype and a 4.3 MW WT prototype, both installed in Høvsøre (Denmark), see Gomez Gonzalez et al. (2022).

Once the AFlaps reach a sufficient maturity level to be integrated into the WTs' design, a fault diagnosis and condition monitoring of the AFlap system will be needed to ensure the AFlaps system provides the expected load reductions. This monitoring ability will be critical to ensure the WT's performance and integrity. Until now, the fault diagnosis and condition monitoring of AFlap systems have not been detailed investigated, and to our knowledge, no literature is available on this topic. Nevertheless, we can foresee different approaches for AFlap fault diagnosis and monitoring, following the standard methodologies currently

https://doi.org/10.5194/wes-2023-24
Preprint. Discussion started: 11 May 2023

eawe european academy of wind energy
Open Access WIND ENERGY SCIENCE DISCUSSIONS

applied in the wind energy sector.

First, monitoring and diagnosis can rely on dedicated sensors located in specific mechanical elements, like a temperature sensor in a gearbox. For the AFlap system, position or pressure sensor could be located on the flap surfaces or in their proximity to quantify the AFlap deflection or the AFlap impact on the blade aerodynamic. Due to the expected large blade area covered by the flaps, this monitoring approach will require several sensors distributed along the outer third of the blade length. This system will likely be complex, expensive to deploy and maintain, sensitive to lighting, and affected by the reliability of the sensor operating in the harsh environment of a wind turbine rotating blade.

The second approach is the model-based method that mainly relies on the analyses of the residual signals, signals defined as the difference between the real system outputs and the output from a model of the system created by using, for example, Kalman filter, observers, or model based machine learning techniques. On WTs, the model-based methods have been applied, for example, in the condition monitoring of main bearing (de Azevedo et al., 2016), sensor and actuators (Cho et al., 2018), and generator (Gálvez-Carrillo and Kinnaert, 2011). As a drawback, the model-based methods require a reasonably good model to guarantee the detection of faults. The model generation could be challenging for AFlap fault detection, mainly due to the high nonlinearity of the WT blade dynamic, the high uncertainty on the wind field interacting with the WT rotor, and the limited number of sensor measurements available on a commercial WT. Improved wind field estimations (e.g., from nacelle Lidar) or additional load or pressure sensors on the blade can facilitate the model generations and improve their accuracy at the price of an increased system complexity and cost.

Finally, data-driven methods allow fault detection without needing a detailed system model but by different types of data and signal analysis. These analyses range from the simple detection of changes in mean values, variances, or trends to the more advanced machine learning (ML) methodologies (Badihi et al., 2022). In particular, the study and application of ML methodologies to fault diagnosis and condition monitoring has increased exponentially in the recent years thanks to the technological and computational advances that have allowed to quickly and efficiently analyze the large amount of data needed for the training of the ML models (García Márquez and Peinado Gonzalo, 2022). An overview of the Machine learning methods for wind turbine condition monitoring is provided by (Stetco et al., 2019). ML techniques can be applied for the AFlap fault detection if a sufficient amount of relevant data can be provided for the model training. Currently, the amount of AFlap field data is limited, even more for AFlap faults. Nevertheless, Aeroelastic simulations have been commonly used for WT design, therefore it is reasonable to assume a sufficiently accurate aeroelastic model of a WT equipped with AFlap can be used to train a ML model for the AFlap fault detection. To test this assumption, in this paper we study if a data-driven methods based on ML trained with aeroelastic simulation can properly classify the AFlap fault states.

1.1 Detecting AFlap health state

The detection of the health state of the AFlap is a challenging task. Figure 1a shows the mean blade root moment when the flap is deactivated (AF_Off) or is active without performance degradation (AF_On) in function of the wind speed. As expected, AFlaps have a relevant impact on the WT blade aerodynamic, visible in the two distinct lines of the mean moment binned in function of the wind speed. However, the broad range of environmental conditions where the WT operates causes the moment

https://doi.org/10.5194/wes-2023-24
Preprint. Discussion started: 11 May 2023

Open Access
WIND ENERGY SCIENCE
DISCUSSIONS

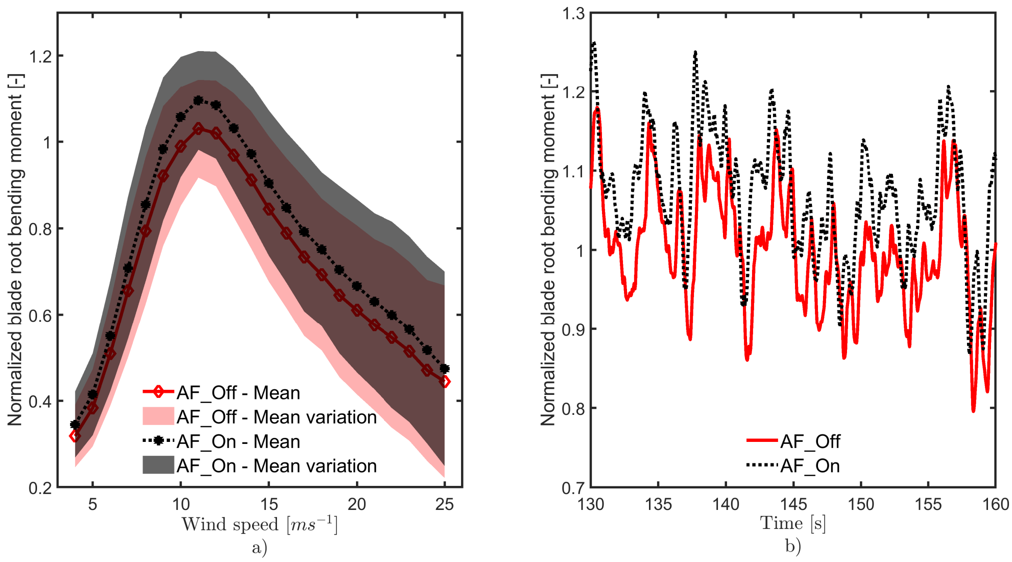

Figure 1. a) Mean value of the normalized blade root bending moment when the AFlap is deactivated (AF_Off) and activated without degradation (AF_On), binned in function of the wind speed. b) Example of time series of the normalized blade root bending moment when the AFlap is deactivated (AF_Off) and activated without degradation (AF_On) for a 10 ms^{-1} turbulent wind

to vary within a wide range of values, range that is shown in the plot by the colored areas. These areas overlap significantly, making it difficult for a detection system to identify the actual AFlap health state. Figure 1b shows the time series of the blade root bending moment for the AFlap active and AFlap not active with the same 10 ms^{-1} turbulent wind. The two lines have a similar highly oscillating behavior with just a small shift due to the increased lift generated by the flap activation.

Furthermore, several faults of the AFlap system can occur in the WT lifetime, which behavior and severity depend on the layout and scope of the AFlap system itself. Wear and tear can slowly degrade the performance of part of the AFlap system; ice or lightning can instead compromise the whole system's functionality. As it is impossible to test all the different combinations of faults, we selected a set of representative conditions we believe can cover a wide range of flap faults. The selected cases cover partial and complete performance degradation happening only on one blade or on all three blades simultaneously. To keep the approach as general as possible, we focus on identifying the AFlap health state in static flap actuation. This approach keeps the detection system independent from any specific AFlap controller strategy, AFlap system design, or Fault dynamics. The idea is to integrate this kind of detection system in an AFlap status check routine running for several minutes where the performance of the stationary flap is verified.

1.2 Research contribution

This paper investigates whether a simple ML algorithm can assess the health of an active trailing edge flap system from the data provided by the sensors commonly available on a commercial WT. The aim is to develop a system that does not require

https://doi.org/10.5194/wes-2023-24
Preprint. Discussion started: 11 May 2023

any additional sensor to be installed on the WTs, making it easy to implement without relevant additional costs for installation or maintenance. This task can be seen as a multivariate time-series classification problem where the ML algorithm aims to estimate if the AFlap is properly operating or is affected by performance degradation. We follow two different approaches for computing the features from the sensors' time series data. In the first approach, we manually select the features based on our knowledge of the impact of AFlaps on the different WTs signals. In the second approach, multiple random convolutional kernels automatically generate the features from all the available signals, without requiring pre-knowledge of the AFlaps' impact on the WT signals. We select the simple but robust random forest classifier for both feature calculation approaches. Aeroelastic simulations are used to train and test the ML models. We use the aeroelastic model developed by (Gamberini et al., 2022) of the 4.3MW WT prototype owned by SGRE, where a 20m AFlap was installed and tested on one blade of the 120 m diameter rotor.

Section 2 describes the aeroelastic model, the environmental conditions, and the flap health states used in the aeroelastic simulations. In Section 3, we describe the ML methodologies used in the study and the two approaches used for AFlap health detection. In Sections 4 and 5, we show the obtained results that we discuss in Section 6.

2 Simulated experiments

The training of the ML models is based on a pool of aeroelastic simulations reproducing the WT aeroelastic response for the combination of wind turbine operative conditions and flap health states of interest.

2.1 Aeroelastic simulations

A set of aeroelastic simulations is computed for every combination of wind turbine operative conditions and flap health state of interest. We computed all sets with the same WT aeroelastic model.

We accounted for the influence of the variability of the environmental conditions on the wind turbine's aeroelastic response by defining the main environmental conditions as random variables of pre-imposed statistical properties.

2.1.1 Environmental conditions

Table 1 shows the environmental conditions modeled as random variables and their parameters, which are:

- **Mean wind speed**: follows a Weibull distribution with the annual average wind speed set to 10 ms^{-1} and the shape parameter to 2. It is equivalent to IEC wind class 1.

- **Wind turbulence intensity**: follows the normal turbulence model described in the IEC 61400-1:2019 (IEC, 2019) for turbulence class A where Iref is set to 0.16 with a lognormal distribution. It is defined as:

$$E[\sigma_U|U] = I_{ref}(0.75U + 3.8) \tag{1}$$

$$Var[\sigma_U|U] = (1.4I_{ref})^2 \tag{2}$$

https://doi.org/10.5194/wes-2023-24
Preprint. Discussion started: 11 May 2023

Table 1. Parameters of the environmental conditions modelled as random variables

Value	Unit	Distribution	Mean	Variance	Min	Max
Turbulence intensity	%	lognormal	Eq.(1)	Eq.(2)	-	-
Wind shear exponent	-	normal	Eq.(3)	Eq.(4)	-0.2	0.4
Air density	$\mathrm{Kg/m^3}$	normal	1.225	0.05	1.103	1.348
Horizontal inflow angle	deg	normal	Eq.(5)	Eq.(6)	-6	6
Vertical inflow angle	deg	normal	3	3	-2	8

- **Wind shear exponent**: the vertical wind profile is modeled with a power law with exponent α. As proposed by Dimitrov et al. (2015), the wind shear exponent is normally distributed and conditionally dependent on the mean wind speed U as follows:

$$E[\alpha|U] = 0.088(ln(U) - 1) \tag{3}$$

$$Var[\alpha|U] = \left(\frac{1}{U}\right)^2 \tag{4}$$

  α values are constrained within realistic limits.

- **Horizontal inflow angle**: Ψ follows a normal distribution, is truncated within realistic limits, and is conditionally dependent on the mean wind speed U as proposed by Duthé et al. (2021):

$$E[\Psi|U] = ln(U) - 3 \tag{5}$$

$$Var[\Psi|U] = \left(\frac{15}{U}\right)^2 \tag{6}$$

- **Vertical inflow angle** and **Air density**: normally distributed, truncated within reasonable limits, with prescribed values of mean and standard deviation.

One example set of environmental condition is sampled for the pre-startup cases, showed in Figure 2, and the normal power production cases, showed in Figure 3.

2.1.2 Aeroelastic model and simulation setup

BHawC is the aeroelastic engineering tool developed internally by SGRE. It is based on the Blade Element Momentum (Fisker Skjoldan, 2011) and models the AFlap's aerodynamic and actuator system with a dedicated flap module.
SGRE provided the BHawC model of the prototype wind turbine (pWT) used for the aeroelastic simulations. It includes the pWT's structural and aerodynamic models and its controller. The AFlap model is also tuned to match the lift increase in the blade region covered by the flap when activated. In Gamberini et al. (2022), one of the authors showed that this model estimates the pWT operational parameters and blade loads with reasonable accuracy, and the AFlap activation increases up to +8% the

https://doi.org/10.5194/wes-2023-24
Preprint. Discussion started: 11 May 2023

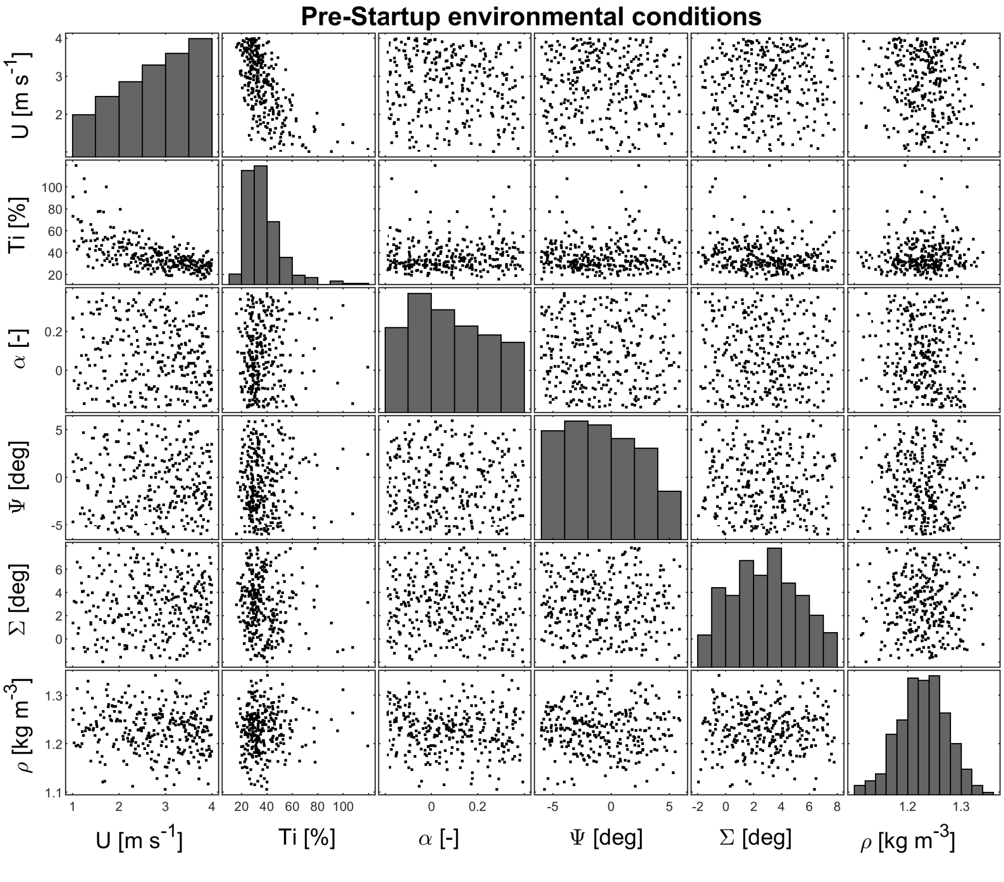

Figure 2. Example of environmental conditions for Pre-Starup simulations: mean wind speed U, wind turbulence intensity TI, wind shear exponent α, horizontal inflow angle Ψ, vertical inflow angle Σ, and air density ρ.

125 mean flapwise bending moment at the blade root. All simulations have the same pWT BHawC model, with only changes in the environmental conditions and the AFlap health state. The simulations are performed with turbulence wind and are 10 minutes long with 0.01 s time step length.

Two operative conditions are simulated: normal power production (NPP) and pre-startup (PS). In the latter cases, the wind turbine is in idling condition with the controller optimizing the blade pitch angle to bring the rotor speed and generator torque to the startup conditions.

For every operative condition, asymmetrical and symmetrical AFlap fault cases are simulated. In the symmetrical flap fault case (3B), the flaps on the three blades have all the same state and performance. This means the three flaps are modeled with the same aerodynamic polars and control signal. In the asymmetrical case (1B), the AFlap is active only on one blade. Even if this is not an expected configuration for future wind turbines, this setup mirrors the pWT setup and in the future it can be

https://doi.org/10.5194/wes-2023-24
Preprint. Discussion started: 11 May 2023

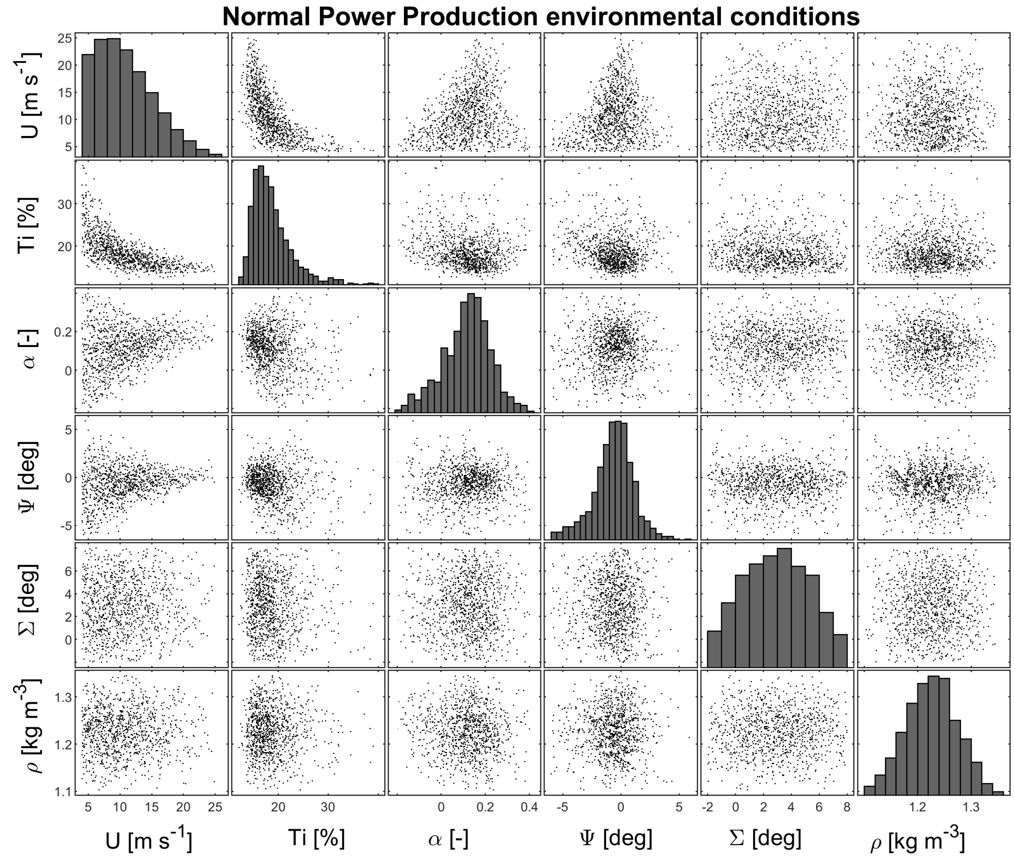

Figure 3. Example of environmental conditions for Normal Power Production simulations: mean wind speed U, wind turbulence intensity TI, wind shear exponent α, horizontal inflow angle Ψ, vertical inflow angle Σ, and air density ρ.

tested with the pWT measurements data. Furthermore, the rotor imbalance due to the flap activated on only one blade is still a good approximation of the imbalance due to a flap on one blade being at a different state or performance than the flaps on the other two blades.

For every case, we simulated seven different AFlap health states:

– **Flap Off (AF_Off)**: AFlap not active, simulated with baseline aerodynamic polar and flap control Off.

– **Flap On (AF_On)**: AFlap active, simulated with active flap aerodynamic polar and flap control On.

– **Flap Off with fault (AF_Off_Fault)**: AFlap active even if the control commands it to be not active. This state can simulate the case when ice formed on the blades prevents the flap from closing. It is simulated with active flap aerodynamic polar and flap control Off.

https://doi.org/10.5194/wes-2023-24
Preprint. Discussion started: 11 May 2023

- **Flap On with fault (AF_On_Fault)**: AFlap not active even if the control commands it to be active. This state can be caused by ice preventing the flap from opening or the flap actuator not working. It is simulated with baseline aerodynamic polar and flap control On.
- **Flap On with degradation**: AFlap active but with degraded performance. Reduced flap deflections due to reduced flap actuator operation, material aging, or extremely low temperature can be associated with these cases. We simulated AFlap performance reduced to 25% (AF_On_25pc), 50% (AF_On_50pc), and 75% (AF_On_75pc) by using a corresponded aerodynamic polar linearly interpolated between the baseline polar and the active flap one meanwhile the flap control is On.

In the simulations, the AFlap's health state is kept constant as this study aims to identify the stationary AFlap health state and not the exact time of the change of state a fault can trigger. Figure 4 shows an example of the normalized lift coefficient of the flap baseline (AF_Off, line with triangle), flap active (AF_On, line with squares),and flap active with performance reduced to 25% (AF_On_25pc, dashed line), 50% (AF_On_50pc, circles), and 75% (AF_On_75pc, dotted line).
For every AFlap health states computed in the NPP case, we make two simulation sets: a Training and Test (TaT) set of 1000 simulations and a Validation (Val) set of 500 simulations. The TaT sets cover a wind speed range from 3.5 and 25 ms^{-1} and share the same sample set of environmental conditions. The Val sets cover the same wind speeds as the TaT sets but share a set of environmental conditions uncorrelated to the TaT set. The PS cases have a similar setup, but they covers wind speeds between 1 and 3.5 ms^{-1}; TaT sets have 300 simulations, and the Val sets 150. Environmental conditions sets used for the PS simulations are also uncorrelated to the NPP ones.
As the input of the ML model, we selected only signals commonly available in the modern commercial wind turbines. These signals are the pitch angle $[\mathrm{deg}]$, the rotor speed $[\mathrm{rpm}]$, the generator power $[\mathrm{kW}]$, flapwise and edgewise bending moments at the root of each of the three blades $[\mathrm{kNm}]$, and linear tower top accelerations $[ms^{-2}]$ together with the flap actuator control signal $[\mathrm{logic}]$.

3 AFlap health state estimation with ML

3.1 Introduction

This paper investigates whether a simple ML algorithm can estimate the health state of an active trailing edge flap from the data provided by the sensors commonly available on a commercial WT. We approached this task as a multivariate time-series classification problem where the ML algorithm aims to estimate the AFlap health state. We followed two different approaches for computing the features from the sensors' time series data. The first approach relies on the manual selection of the channels and their relevant statistics that, from the authors' knowledge, are known to be impacted by the trailing edge flap system. In the second approach, multiple random convolutional kernels automatically generate the features from all the available signals. Based on the MiniRocket algorithm, this approach does not require pre-knowledge of the AFlap system's impact on the WT

https://doi.org/10.5194/wes-2023-24
Preprint. Discussion started: 11 May 2023

WIND ENERGY SCIENCE DISCUSSIONS

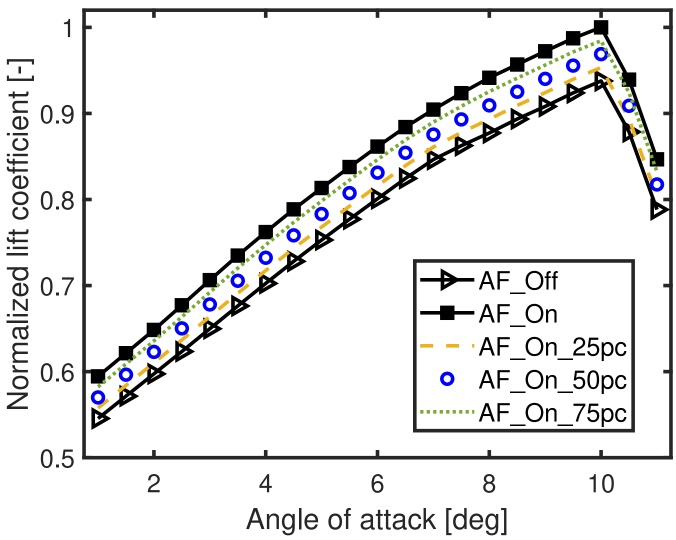

Figure 4. Example of flap normalized lift coefficient of the baseline (AF_Off, line with triangle), flap active (AF_On, line with squares),and flap active with performance reduced to 25% (AF_On_25pc, dashed line), 50% (AF_On_50pc, circles), and 75% (AF_On_75pc, dotted line).

signals and explores possible unknown relations among the different WT channels. As a classifier method, we selected the simple but robust random forest classifier for both feature calculation approaches. For the approach based on the MiniRocket algorithm, we also used the Ridge classifier with Cross Validation.

3.1.1 Random Forest

A Random Forest Classifier (RF) is a supervised discriminative machine learning technique whose objective is to estimate $P\left(Y \,\middle|\, X, \theta\right)$ in which Y: target, X: observable, and θ are the parameters. We assume a multi-class classification problem where each observational sample is assigned to one and only one label, as opposed to the multi-label approach.

The Random Forest classifier is based on a collection of Decision Trees (DT, also called Classification or Prediction Trees), a non-parametric supervised learning method designed for the classification or regression of a discrete category from the data. In the machine learning sense, the goal is to create a classification model (classification tree) that predicts the value of a target variable (also known as label or class) by learning simple decision rules inferred from the data features (also known as attributes or predictors). From Figure 5a, an internal node N denotes a test on an attribute, an edge B represents an outcome of the test, and the Leaf nodes L represent class labels or class distribution. A decision tree is a tree-structured classifier built by starting with a single node that encompasses the entire data and recursively splitting the data within a node, generally into two branches (some algorithms can perform $multiway$ splits). The splitting is obtained by selecting the variable (dimension) that best classifies the samples according to a split criterion, i.e., the one that maximizes the information gain among the random sub-sample of dimensions obtained at every point. The splitting continues until a terminal leaf is created by meeting a stopping

https://doi.org/10.5194/wes-2023-24
Preprint. Discussion started: 11 May 2023

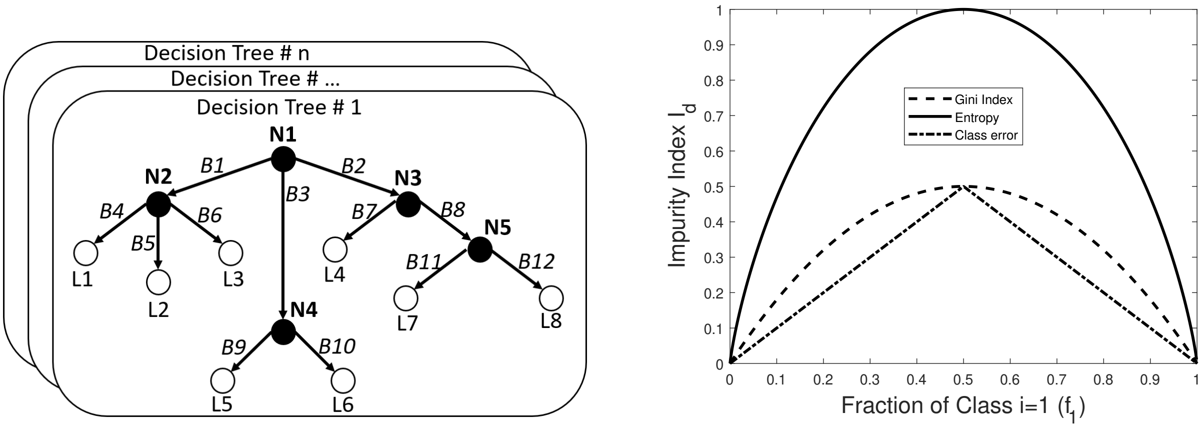

(a) (b)

Figure 5. (a) Graphical representation of a forest of decision tree classifiers. (b) Impurity index I_d for a two-class example as a function of the probability of one of the classes f_1 using the information entropy, Gini impurity and classification error. In all cases, the impurity is at its maximum when the fraction of data within a node with class 1 is 0.5, and zero when all data are in the same category.

criterion, such as a minimum leaf size or a variance threshold. Each terminal leaf contains data that belongs to one or more classes. Within this leaf, a model is applied that provides a reasonably comprehensible prediction, especially in situations where many variables may exist that interact in a nonlinear manner, as is often the case on wind turbines (Carrasco Kind and Brunner, 2013). Several algorithms exist for training decision trees with variations on impurity, pruning, stopping criteria, how to treat missing variables, etc. A top-to-bottom construction of a decision tree begins with a set of objects. Each object has an assigned label and a set of measured features. The dataset is split at each tree node into two subsets, left and right, so the two resulting subsets are more homogeneous than the set in their parent node. To do so, one must define a cost function that the algorithm will minimize. One can use the information entropy, the Gini impurity, or a classification error for the cost function. Formally, the splitting is done by choosing the attribute that maximizes the Information Gain, defined in terms of the impurity degree index I_d as shown in Figure 5b.

By definition, a random forest classifier is a non-parametric classification algorithm consisting of a collection of decision tree-structured classifiers $\{h(\mathbf{x},\Theta_k), k = 1,...\}$ where the Θ_k are independent identically distributed random vectors, and each tree casts a unit vote for the most popular class at input $\mathbf{x}$. The RF prediction consists of the aggregation of the DT results obtained by a majority vote. Furthermore, the fraction of the trees that vote for the predicted class serves as a measure of certainty of the resulting prediction. RF improves prediction accuracy over single decision tree classifiers by injecting randomness that minimizes the correlation $\overline{\rho}$ amongst the grown individual decision trees $h(\mathbf{x},\Theta_k)$ that operate as an ensemble. This is achieved by using bootstrap aggregating (a.k.a. bagging, sample with replacement of the training dataset) in tandem with random feature selection in the process of growing each decision tree in the ensemble Breiman (1996). This forces even more

https://doi.org/10.5194/wes-2023-24
Preprint. Discussion started: 11 May 2023

variation amongst the trees in the model (different conditions in their nodes and different overall structures) and ultimately results in lower correlation across trees and more diversification.

Some of the arguments in favour of using a RF in this research include:

- Random Forests work well with both categorical and numerical data. No scaling or transformation of variables is usually necessary.
- Random Forests implicitly perform feature selection and generate uncorrelated decision trees. It does this by choosing a random set of features to build each decision tree. This also makes it a great model when you have to work with a high number of features in the data.
- Random Forests are not influenced by outliers to a fair degree. It does this by binning the variables.
- Random Forests can handle linear and non-linear relationships well.
- Random Forests generally provide high accuracy and balance the bias-variance trade-off well. Since the model's principle is to average the results across the multiple decision trees it builds, it averages the variance as well.
- Random Forests are fairly interpretable. They provide both feature importance and in certain instances the ability to trace branches to follow the decision making process.

3.1.2 MiniRocket

ROCKET (RandOm Convolutional KErnel Transform) is an algorithm that generates a large number of convolution kernels (10000 by default) with random length, weights, bias, dilation, and padding of the time series provided as input. ROCKET extracts two features for each kernel: the maximum value (an equivalent to the maximum global pooling) and the proportion of positive values (PPV), indicating the proportion of the input matching a given pattern. The PPV is the most critical element of ROCKET for achieving the state of the art accuracy (Dempster et al., 2020).

MiniRocket (MINImally RandOm Convolutional KErnel Transform) is a reformulated version of ROCKET (Dempster et al., 2021), 75 times faster while maintaining the same accuracy. MiniRocket minimizes the number of options for hyperparameters and computes only the PPV, generating half number of features as ROCKET. In addition, it does not require normalization. The v0.3.4 version of the MiniRocket implementation in (Oguiza, 2022) has been used in this paper.

3.1.3 Ridge classifier with Cross Validation

This Ridge classifier uses the Ridge regression to predict the class of a multiclass problem by solving the problem as a multi-output regression where the predicted class corresponds to the output with the highest value. Ridge Regression, also known as Tikhonov regularization, solves a regression model by minimizing the following objective function:

$$\min_{w} ||Xw - y||_2^2 + \alpha ||w||_2^2 \quad (7)$$

https://doi.org/10.5194/wes-2023-24
Preprint. Discussion started: 11 May 2023

Where: X are the training data, y the target values, k the ridge coefficients to be minimized, and α the regularization strength. α controls the amount of shrinkage: the higher the value, the greater the amount of shrinkage, increasing the robustness of the ridge coefficients to collinearity. The addition of the Cross Validation helps to identify the best set of ridge coefficients, reducing the risk of overfitting.

3.2 Manual Feature selection with Random forest classifier

The main effect of the activation or deactivation of a trailing edge flap on a WT is the change of local blade lift that consequently affects the blade's aerodynamic loading. The impact on the blade loading depends significantly on the WT operative conditions, as shown in Gomez Gonzalez et al. (2022). Furthermore, asymmetric activation of the flaps on the three blades leads to a rotor bending moments imbalance that is often associated with tower top vibration. Based on this, we manually select a set of signals to generate the features to train an RF model. In addition, we consider only signals commonly available in all modern commercial wind turbines. The aim is the development of a method that can be implemented on commercial wind turbines without the need of installing additional hardware. Initially, we use simple statistical properties of the signal time series as features. Afterward, we include the Catch22 collection (Lubba et al., 2019) to expand the features pool.

3.2.1 Signal and features selection

The selected WT signals are:

- **Flap actuator control signal** $[\mathrm{logic}]$: control signal of the flap activation state (On or Off).
- **Flapwise and edgewise bending moments at the three blade roots** $[\mathrm{kNm}]$: main signals to detect the impact of the flaps on the blade aerodynamic loading. Load sensors placed at the blade root are commonly available in modern WTs.
- **Pitch angle** $[\mathrm{deg}]$, **rotor speed** $[\mathrm{rpm}]$ and, **generator power** $[\mathrm{kW}]$: main signals to estimate the WT's operative condition to which the flaps' load impact is related. These signals are available in every WT controller.
- **Fore-Aft and side-side tower top accelerations** $[ms^{-2}]$: useful signals in detecting possible rotor imbalances. The WT safety systems commonly monitor these signals to detect WT anomalies.
- **Out of plane rotor bending moments** $[\mathrm{kNm}]$: signals computed from the blade root moments, pitch angle, and azimuth position through the Coleman transformation Bir (2008) equation. These moments help detect possible rotor imbalances.

The initially selected features are the standard deviation, mean, maximum, minimum, range, and maximum absolute value of every signal. Afterward, we add the Catch22 collection (Lubba et al., 2019) to expand the features pool to explore possible unknown correlations between the input signals. We choose the Catch22 (CAnonical Time-series CHaracteristics) collection as it is a high-performing subset of 22 features selected over a pool of over 7000 based on their classification performance across a collection of 93 real-world time-series classification problems. The v0.4 Catch22 Matlab tool is used for this paper. Finally, we include the blade-to-blade difference of the mean and absolute maximum blade root bending moments to help detect possible

https://doi.org/10.5194/wes-2023-24
Preprint. Discussion started: 11 May 2023

flap activation imbalances.

The features generation process computes circa 400 features for each aeroelastic simulation. To reduce complexity, we add two features filtering processes to the algorithm:

- **manual selection** of the desired feature subset in the algorithm pre-processing.
- **automatic features reduction** based on Out-of-bag permuted predictor importance (oobPPI) value. The oobPPI measures how influential a feature is in the model prediction by permuting the value of the feature and measuring the model error. The permutation of an influential feature should have a relevant effect on the model error; little to no effect should come from a permutation of a not influential feature. If this filter is active, the oobPPI of each feature is evaluated after the RF model is trained. Features with an oobPPI value below the threshold specified by the user are removed, and the RF model is trained again with the remaining features subset. The process is repeated until all the remaining features consistently have an oobPPI value above the threshold, simplifying the final model by removing the features not influential on the classification process.

We decided to do not include the wind speed sensor signal in the ML training. This sensor is generally located on the nacelle, behind the rotor, where the complexity of the 3D wind flow can only be correctly estimated by high-fidelity codes, like CFD. In this paper we use a mid-fidelity aeroelastic model that is unable to estimate the wind speed on the nacelle with sufficient accuracy. Therefore, training the ML model with a low-fidelity nacelle wind speed would reduce the model accuracy and performance on a real WT. Furthermore, the ML model can still derive the wind speed data from the rotor speed, pitch angle, and generator power, which strongly correlate to the wind speed. Therefore, omitting the wind speed signal reduces model uncertainties without losing relevant data for the ML training. Instead, we use the mean wind speed for splitting the NPP into different wind speed regions for which a dedicated RF model is trained. Generally, a modern WT operates differently below rated wind speed, where it is power or torque controlled, compared to above rated wind speed, where it is pitch controlled. Therefore, we expect RF models trained for each specific wind region to perform better than a single RF model covering the whole wind speed range.

3.2.2 Algorithm structure and setup

The algorithm has the following structure:

1. Calculation of the features for every simulation. Usually it is done only once, after the aeroelastic simulation is computed.
2. Selection of the AFlap fault symmetry (1B or 3B), WT operative condition (NPP or PS).
3. Selection of the AFlap health states to be used in the classification.
4. For every specified wind speed range:
   (a) Manual selection of the desired feature subset.

https://doi.org/10.5194/wes-2023-24
Preprint. Discussion started: 11 May 2023

(b) Training of the RF model with the TaT set.

(c) If the "automatic features reduction" is enabled, the following steps are repeat until all features have oobPPI above threshold:

i. Evaluation of the oobPPI of every features.

ii. Removal of the features with oobPPI below threshold.

iii. Training of a new RF model with the remaining features.

(d) Validation of the trained RF model with the Val sets.

In the algorithms, three Matlab functions are used: **templateTree** to create the decision tree template; **fitcensemble** to train the Rf model, and **oobPermutedPredictorImportance** to compute the oobPPI value for each feature.
We use the setup proposed by (Abdallah, 2019) as default RF setup: number of trees of 100, learning rate of 0.25, maximum number of split of 12, test rate of 30% and impOOB threshold of 0.01.

3.3 Automatic Feature Generation with Random Forest or Ridge classifier

The AFS approach relies on the same signals used for the manual feature selection approach: pitch position, rotor speed, generator power, flapwise and edgewise bending moments at the root of each of the three blades, linear tower top accelerations, and the flap actuator control signal. As described in Section 3.2, these signals are relevant to detect the flap impact on the WT and are provided with the standard sensors available on commercial WT. Instead of generating a set of features for each signal based on statistical properties, the AFS approach utilizes ML techniques developed for image processing to create features of the whole simulation. We implement two different algorithms for the classification: a RF classifier, similarly on what we used for the MFS, and a Ridge classifier with Cross Validation (Ridge) suggested by (Dempster et al., 2020) for application with MiniRocket.

3.3.1 Feature generation with MiniRocket

MiniRocket works by first combining the time series of the relevant signals of a single simulation in a single matrix, aligning them in function of time. Then it processes the resulting matrix like an image utilizing a kernel from which the proportion of positive values is computed. A set of 10000 kernels of random length, weights, bias, dilation, and padding, are used, generating 10000 features per simulation. This process is repeated for all the simulations. For consistency, the same kernel set must be used for all the simulations used in the RF models' training, testing, and validation.

3.3.2 Algorithm structure and setup

The algorithm has the following structure:

1. Calculation of the features with MiniRocket.

2. Selection of the AFlap fault symmetry (1B or 3B) and WT operative condition (NPP or PS).

https://doi.org/10.5194/wes-2023-24
Preprint. Discussion started: 11 May 2023

3. Selection of the AFlap health states to be used in the classification.
4. Selection of the classifier: RF or Ridge.
5. For every specified wind speed range:
   (a) Training of the classification model:
      i. Training of one (or more) classification model.
      ii. If more than one classification model is trained, select the model with higher F1-score.
   (b) Validation of the trained classification model with the Val sets.

In the AFS method, we used the following sklearn python codes (Pedregosa et al., 2011): **StratifiedShuffleSplit** to create multiple Test and Training subsets from the TaT sets; **RandomForestClassifier** to train, test and validate the RF models; **RidgeClassifierCV** to train, test and validate the Ridge classifier models; **f1_score** to compute the F1-score; **StandardScaler** to standardize features by removing the mean and scaling to unit variance.

Starting from the setup proposed by (Abdallah, 2019), we investigate the optimal RF setup for the different scenarios, obtaining as optimal values: test rate of 30%, number of trees of 100, Shannon entropy as the criterion to measure the quality of a split, maximum depth of the tree of 5, minimum number of samples required to split an internal node of 5, and all features included. For the Ridge setup, the regularization strength parameter was set to an evenly spaced vector in log space of 1000 values between 1 and 10^6, and the cross-validation set to Leave-One-Out Cross-Validation that handles efficiently the case of the number of features higher than the number of samples.

4 Manual feature selection results

The potential of the MFS approach in detecting a flap system's fault is investigated for several AFlap fault scenarios. These scenarios cover different combinations of AFlap fault symmetry (1B or 3B), WT operative conditions (NPP or PS), the possible split in different wind speed ranges, and different initial features selection (All or Reduced). The initial features option allows the reduction of the features used in training. We set the features subset without the Catch22 collection as the default Reduced setup. Instead, the wind speed ranges option enables the training of a dedicated ML model for every specified wind speed range. The default ranges used in this paper are Below Rated (BR: wind speed between 3.5 and 9.5 ms^{-1}), Around Rated (Rt: wind speed between 9.5 and 16.5 ms^{-1}), and Above Rated (AR: wind speed between 16.5 to 25 ms^{-1}).

Furthermore, we investigate three different fault detection levels:

– **Primary**: the model is trained to detect only the four primary health states: flap not active (AF_Off), active (AF_On), not active with fault (AF_Off_Fault), and active with fault (AF_Off_Fault).

– **Degraded**: the model is trained to detect if the flap has degraded performance but without identifying the performance degradation level. The three health states of flap with degraded performance are merged in a single state, called active with degradation (AF_On_Degr), that is included in the training with the four primary health states.

https://doi.org/10.5194/wes-2023-24
Preprint. Discussion started: 11 May 2023

- **Detailed**: the model is trained to identify the flap performance reduced to 25% (AF_On_25pc), 50% (AF_On_50pc), and 75% (AF_On_75pc) in addition to the primary health states.

Table 2 collects the list of the MFS scenarios and shows their setup. Scenarios stated within parenthesis have a customized setup detailed described in the following chapters.

The selection of the models' performance metrics is strictly related to the requirements of the detection system. If one (or more) flap fault is critical for the WT integrity, the detection of this fault would be prioritized over the other AFlap health states. In this case, a good metric would be the Recall of the critical fault. For an opposite scenario, where it would be more critical to avoid false fault detections and keep the WT operating, the Precision of the different faults should be considered. In this paper, we are not considering any particular requirement for the fault detection system, and we aim to correctly detect all the different classes equally without prioritizing anyone specifically. Therefore we select the F1-score, a trade-off between Recall and Precision that rewards the reduction of both false positives and false negatives. In detail, we use the weighted F1-score: the average of the F1-score of each class weighted by the ratio of the number of samples of each class over the total sample number. This metric is consistent between balanced and unbalanced classification tasks, allowing us to properly evaluate the few scenarios where the classes are not balanced.

4.1 Detection of asymmetric fault

Table 3 collects the performance of the RF models trained for the asymmetric fault scenarios described in Table 2. In addition to the weighted F1-score, the number of features obtained after the automatic feature reduction in the model training is shown. We use this number as an estimate of the model complexity: where more features are needed, more complex is to implement and execute the model. In addition, Precision and Recall values of the AFlap health states for some specific asymmetric fault scenario models are collected in Table 4.

As the first step, scenario 1BN_A1 trains a single RF model for all the wind speeds to detect the Primary flap health states in normal power production, starting the training with all the available features. The trained model needs only 3 features (out of 400) to achieve an F1-score of 1, meaning it can perfectly classify the Primary health states. To understand how this trained model would perform with AFlap degradation (that will occur during the normal lifetime of the flap, also as a partial fault), we test it with all the degraded AFlap health states classified as AF_On_Fault (scenario 1BN_A1c). Under this condition, the model F1-score decreases to 0.79 due to the misclassification of the flap fault (AF_On_Fault) as normal flap operation (AF_On). This misclassification is expressed numerically by a low value of AF_On Recall (0.33) and AF_On_Fault Precision (0.48). We obtain similar results in scenario 1BN_A2, where the wind speeds are split into three different wind speed ranges, and an independent RF model is trained for each range. The models trained in this scenario detect well the Primary health states (F1-score of 1) but cannot distinguish the degraded AFlap states (scenario 1BN_A2c).

As the second step, we unify the degraded AFlap health states under a single category (AF_On_Degr). Scenario 1BN_B1 trains a single RF model for all the wind speeds to detect the Degraded fault health states in NPP. The trained model requires 17 features for an F1-score of 0.90, mainly due to the low Recall (0.56) of the AF_On class. Removing the Catch22 features

https://doi.org/10.5194/wes-2023-24
Preprint. Discussion started: 11 May 2023

Table 2. Compact description of the setup of the AFlap fault scenarios.

Fault scenario names for detection level:			Fault scenario setup:			
Primary	**Degraded**	**Detailed**	**Features**	**Wind speed ranges**	**WT operation**	**Fault symmetry**
1BN_A1 (1BN_A1c)	1BN_B1	1BN_C1	All	No	NPP	Asymmetric (1B)
-	1BN_B1r	-	Reduced			
1BN_A2 (1BN_A2c)	1BN_B2	1BN_C2	All	Yes		
-	1BN_B2r	1BN_C2r	Reduced			
-	1BP_B1	1BP_C1	All	No	PS	
1BP_A1r (1BP_A1rc)	1BP_B1r	1BP_C1r	Reduced			
3BN_A01	-	-	All	No	NPP	Symmeatric (3B)
3BN_A02 (3BN_A02c)	3BN_B2 (3BN_B2b)	3BN_C2 (3BN_C2b)	All	Yes		
-	3BN_B3	3BN_C3	All	Yes		
3BP_A1 (3BN_A01c)	3BP_B1 (3BP_B1b)	3BP_C1 (3BP_C1b)	All	No	PS	

to simplify the model (scenario 1BN_B1r) leads to a lower F1-score (0.82), poor AF_Off_Fault class Recall (0.41), and poor AF_On class Precision (0.37). Splitting the training for the tree wind speed ranges (scenario 1BN_B2) generates three high-performing models (F1-score higher than 0.95) even in the scenario where the Catch22 features are removed (1BN_B2r).

As the last step for the NPP case, we test if a model could individually identify the degraded AFlap health states. Scenario 1BN_c1 trains a single RF model for all the wind speeds for a Detailed detection level in NPP. The trained model requires 16 features for an F1-score of 0.70 and can almost not distinguish the AF_Off_Fault from the other classes. Splitting the training for the tree wind speed ranges (scenario 1BN_c2) dramatically improves the performance of the models with an F1-score of 0.91 BR, 0.95 around rated, and 0.98 AR obtained with 14 features or less. In detail, the BR model is imprecise in classifying the AF_Off_Fault and has a low Recall for AF_On. Removing the Catch22 features leads to models with similar performance but fewer features (10 or less).

After the NPP scenarios, we investigated if the AFlap health states can be correctly classified in pre-startup conditions where the WT is idling due to low wind speed. For the scenarios aiming at the Primary flap health states (1BP_A1r and 1BP_A1rc) in the PS condition, the performance follows the same pattern as the previous similar scenarios in NPP. When the AF_On_Degr class is included (scenario 1BP_B1), the trained model shows a high F1-score (0.94) with 20 features. A high F1-score of 0.95

https://doi.org/10.5194/wes-2023-24
Preprint. Discussion started: 11 May 2023

eawe european academy of wind energy
Open Access WIND ENERGY SCIENCE DISCUSSIONS

Table 3. F1-score of the asymmetric flap fault scenarios evaluated with MFS and AFS approaches. The number of features used for the MFS is also specified.

Blade Fault	WT operation	Wind speed range $[ms^{-1}]$	Basic				Degraded					Detailed				
				MFS				MFS			AFS		MFS			AFS
			Case name	RF F1-Score	-	# Features	Case name	RF F1-Score	-	# Features	RF F1-score	Case name	RF F1-Score	-	# Features	RF F1-score
1B	NPP	3.5 - 25.5	1BN_A1 (1BN_A1c)	1 (0.79)	-	3	1BN_B1	0.90	-	17	0.67	1BN_C1	0.70	-	16	0.55
							1BN_B1r	0.82	-	11						
	NPP	3.5 - 9.5 (BR)	1BN_A2 (1BN_A2c)	1 (0.80)	-	10	1BN_B2	0.96	-	10	0.59	1BN_C2	0.91	-	14	0.52
		9.5 - 16.5 (RT)		1 (0.82)	-	5		0.98	-	9	0.78		0.95	-	14	0.73
		16.5 - 25.5 (AR)		1 (0.80)	-	4		0.99	-	5	0.62		0.98	-	4	0.56
		3.5 - 9.5 (BR)					1BN_B2r	0.95	-	6		1BN_C2r	0.90	-	10	
		9.5 - 16.5 (RT)						0.90	-	7			0.94	-	10	
		16.5 - 25.5 (AR)						0.98	-	3			0.99	-	6	
	PS	0 - 3.5					1BP_B1	0.94	-	20	0.45	1BP_C1	0.92	-	27	0.38
			1BP_A1r (1BP_A1rc)	1 (0.80)	-	5	1BP_B1r	0.95	-	9		1BP_C1r	0.93	-	14	

is also achieved with only 9 features starting from a reduced set of features (scenario 1BP_B1r). Finally, when we analyze the Detailed detection level (scenario 1BP_C1), the trained model achieves an F1-score of 0.92 with 27 features. Omitting the Catch22 features in training (scenario 1BP_C1r) brings an equivalent F1-score with only 14 features.

4.2 Detection of symmetric fault

Table 5 collects the performance of the RF models trained for the symmetric fault scenarios described in Table 2. Precision and Recall values of the AFlap health states for some specific symmetric fault scenario models are collected in Table 6.

Similarly to the asymmetric faults cases, we start with a scenario (3BN_A1) that trains a single RF model for all the wind speeds to detect the Primary health cases in NPP, using all the available features initially. The trained model achieves an F1-score of 0.75 with 32 features. When tested with the degraded flap health states bundled together as AF_On_Fault (scenario 3BN_A1c), the F1-score decreased to 0.71 due to the misclassification of the fault (AF_On_Fault) as normal flap operation (AF_On). This misclassification is expressed numerically by a low value of AF_On Recall (0.33) and low Precision (0.61) of both AF_Off_Fault and AF_On_Fault. We obtained similar results in scenario 3BN_A2, where we trained an independent RF model for each of the three different wind speed ranges. The models trained in this scenario detect better than the previous scenario the Primary flap health states, especially for AR (F1-score of 0.92) but cannot correctly distinguish the degraded AFlap states (scenario 1BN_A2c).

As the second step, we include the degraded AFlap health states under a single category (AF_On_Degr). Scenario 3BN_B2 trains an independent RF model to detect the Degraded flap cases in NPP for each of the three different wind speed ranges. The

https://doi.org/10.5194/wes-2023-24
Preprint. Discussion started: 11 May 2023

eawe european academy of wind energy
Open Access WIND ENERGY SCIENCE DISCUSSIONS

Table 4. Precision and Recall values of each AFlap health state of a selection of scenarios of asymmetric flap fault evaluated with MFS and AFS approaches.

Approach		**MFS**								**AFS**			
WT operation		**NPP**						**PS**		**NPP**			**PS**
Scenarios		**1BN_A1c**	**1BN_B1**	**1BN_B1r**	**1BN_C1**	**1BN_C2**		**1BP_B1r**	**1BP_C1r**	**1BN_B1**	**1BN_C1**	**1BN_B2**	**1BP_B1**
Wind speed range		All	All	All	All	BR	AR	All	All	All	All	RT	All
F1 score		0.79	0.90	0.82	0.70	0.91	0.98	0.95	0.93	0.67	0.55	0.78	0.45
Precision	AF_Off	1.00	1.00	0.98	0.97	1.00	1.00	0.95	0.98	0.81	0.80	0.99	0.66
	AF_Off_Fault	1.00	0.77	0.70	0.00	0.53	0.95	0.84	0.78	0.89	0.93	1.00	0.63
	AF_On	1.00	0.95	0.37	0.68	0.92	0.97	0.90	0.93	0.50	0.59	0.61	0.28
	AF_On_Fault	0.48	1.00	1.00	0.98	1.00	0.98	0.95	0.98	0.47	0.49	0.55	0.27
	AF_On_Degr	-	0.81	0.87	-	-	-	0.98	0.96	0.73	-	0.90	0.62
	AF_On_25pc	-	-	-	0.88	1.00	0.98	-	-	-	0.40	-	-
	AF_On_50pc	-	-	-	0.66	0.88	0.99	-	0.90	-	0.30	-	-
	AF_On_75pc	-	-	-	0.97	1.00	1.00	-	0.95	-	0.42	-	-
Recall	AF_Off	1.00	1.00	1.00	1.00	1.00	1.00	1.00	0.97	0.90	0.95	1.00	0.59
	AF_Off_Fault	1.00	0.95	0.41	0.00	1.00	1.00	1.00	1.00	0.79	0.76	0.99	0.70
	AF_On	0.33	0.56	0.56	0.44	0.65	0.99	0.88	0.83	0.71	0.58	0.85	0.41
	AF_On_Fault	1.00	0.97	0.96	0.92	1.00	0.98	0.99	0.95	0.60	0.54	0.93	0.50
	AF_On_Degr	-	0.98	0.99	-	-	-	0.90	-	0.56	-	0.57	0.35
	AF_On_25pc	-	-	-	0.84	0.99	0.99	-	0.90	-	0.21	-	-
	AF_On_50pc	-	-	-	0.47	0.84	0.94	-	0.87	-	0.48	-	-
	AF_On_75pc	-	-	-	1.00	1.00	0.98	-	0.99	-	0.32	-	-

trained model shows a low F1-score of 0.41 for BR, 0.51 at rated, and 0.64 for AR. To improve the performance of the models, we explore the RF model hyperparameters setup. One of the most successful results is scenario 3BN_B2b, where we increase the number of trees from 100 to 300 and the maximum number of slit from 12 to 30. These changes lead to an increase of the F1-score of around 0.08, with the highest value achieved in the AR wind sped range with an F1-score of 0.72. This model still shows low Recall for AF_On and AF_On_Fault flap states and a low Precision for AF_On_Degr. As a final try to increase the models' performance, we reduce the width of the wind speed ranges, obtaining: BRa (3.5 to 6.5 ms^{-1}), BRb (6.5 to 9.5 ms^{-1}), RTa (9.5 to 12.5 ms^{-1}), RTb (12.5 to 15.5 ms^{-1}), ARa (15.5 to 20.5 ms^{-1}), and ARb (20.5 to 25.5 ms^{-1}). This scenario (3BN_B3) leads to RF models with higher performance but only ARa and ARb models have the F1-scores higher than 0.7 (0.75 and 0.83, respectively). Both RF models have good Precision except for the AF_On_Degr class but a low Recall for AF_On, AF_On_Fault and AF_On_Degr.

Finally, we investigate if an RF model could individually identify the Detailed flap health states, obtaining models with poor

https://doi.org/10.5194/wes-2023-24
Preprint. Discussion started: 11 May 2023

Table 5. F1-score of the symmetric flap fault scenarios evaluated with MFS and AFS approaches. The number of features used for the MFS is also specified.

Blade Fault	WT operation	Wind speed range [ms^{-1}]	Basic				Degraded					Detailed				
				MFS				MFS			AFS		MFS			AFS
			Case name	RF F1-Score	-	# Features	Case name	RF F1-Score	-	# Features	RF F1-score	Case name	RF F1-Score	-	# Features	RF F1-score
3B	NPP	3.5 - 25.5	3BN_A1 (3BN_A1c)	0.75 (0.71)	-	32										
	NPP	3.5 - 9.5 (BR)	3BN_A2 (3BN_A2c)	0.74 (0.69)	-	27	3BN_B2 (3BN_B2b)	0.41 (0.49)	-	20 (23)	0.53	3BN_C2 (3BN_C2b)	0.24 (0.35)	-	21 (22)	0.49
		9.5 - 16.5 (RT)		0.85 (0.75)	-	31		0.51 (0.63)	-	18 (25)	0.61		0.30 (0.40)	-	15 (16)	0.55
		16.5 - 25.5 (AR)		0.92 (0.81)	-	15		0.64 (0.72)	-	8 (9)	0.63		0.50 (0.61)	-	7 (7)	0.58
	NPP	3.5 - 6.5 (BRa)					3BN_B3	0.61	-	7	0.49	3BN_C3	0.48	-	7	0.43
		6.5 - 9.5 (BRb)						0.55	-	16	0.55		0.39	-	17	0.49
		9.5 - 12.5 (RTa)						0.67	-	20	0.55		0.48	-	15	0.49
		12.5 - 15.5 (RTb)						0.62	-	9	0.64		0.45	-	8	0.59
		15.5 - 20.5 (ARa)						0.75	-	8	0.67		0.58	-	9	0.60
		20.5 - 25.5 (ARb)						0.83	-	7	0.49		0.77	-	9	0.50
	PS	0 - 3.5	3BP_A1 (3BP_A1c)	0.80 (0.71)	-	12	3BP_B1 (3BP_B1b)	0.55 (0.55)	-	11 (22)	0.50	3BP_C1 (3BP_C1b)	0.30 (0.38)	-	7 (7)	0.43

performance in the symmetric fault case during NPP. Scenario 3BN_C2 trains an independent RF model to detect the Degraded fault cases in NPP for each of the three different wind speed ranges. The trained model has an F1-score below 0.50. Increasing the number of trees to 300 and the maximum number of slit to 30 (scenario 3BN_C2b) improves the F1-score of around 0.1. The Precision and Recall values show that the models cannot correctly detect most AFlap health states. Adding the reduction of the size of the wind ranges (scenario 3BN_C3) does slightly improve the F1-score, but with the best performing model (ARb) reaching only an F1-score of 0.77. For the PS wind turbine operation, the scenario aiming at the Degraded flap health states (scenario 3BP_B1) trains a model with a low F1-score (0.55) unable to classify all the different AFlap health states correctly. Increasing the number of trees and split (3BP_B1b) does not lead to better performance. Also, for the Detailed detection level (scenario 3BP_C1), the trained model achieves a poor F1-score of 0.30 that is only marginally improved (0.38) by increasing the number of trees and split (3BP_C1b).

5 Automatic feature selection results

The AFS approach is investigated with most of the scenarios used for the MFS approach and collected in Table 2. An initial preliminary investigation shows that a model trained only to detect the Primary flap health states will most likely perform poorly when the AFlap starts to have degraded performance, similar to what we obtain in the MFS analysis. Since this performance degradation is likely to happen, there is a low interest in a model that cannot account for it properly, and the Primary fault detection level is therefore omitted in the AFS analyses. Furthermore, the initial feature reduction does not apply to the AFS

https://doi.org/10.5194/wes-2023-24
Preprint. Discussion started: 11 May 2023

Table 6. Precision and Recall values of each AFlap health state of a selection of scenarios of symmetric flap fault evaluated with MFS and AFS approaches.

Approach		**MFS**									**AFS**			
WT operation		**NPP**								**PS**	**NPP**			**PS**
Scenarios		**3BN_A1c**	**3BN_B2b**		**3BN_B3**		**3BN_C2b**		**3BP_C3**	**3BP_B1**	**3BN_B2**	**3BN_B3**	**3BP_C3**	**3BP_B1**
Wind speed range		All	BR	AR	ARa	ARb	BR	AR	ARb	All	AR	ARa	ARa	All
F1 score		0.71	0.49	0.72	0.75	0.83	0.35	0.61	0.77	0.55	0.63	0.67	0.60	0.50
Precision	AF_Off	0.84	0.44	0.68	0.80	0.94	0.37	0.81	0.78	0.06	0.94	0.90	0.93	0.74
	AF_Off_Fault	0.61	0.58	0.77	0.74	0.94	0.39	0.44	0.78	0.15	0.95	0.98	0.98	0.78
	AF_On	0.71	0.71	0.82	0.80	0.89	0.50	0.71	0.78	0.15	0.40	0.40	0.54	0.29
	AF_On_Fault	0.62	0.73	0.94	0.84	1.00	0.15	0.41	0.78	0.10	0.42	0.53	0.53	0.35
	AF_On_Degr	-	0.16	0.54	0.65	0.61	-	-	-	0.97	0.67	0.76	-	0.65
	AF_On_25pc	-	-	-			0.09	0.49	0.78	-	-	-	0.38	-
	AF_On_50pc	-	-	-			0.21	0.47	0.61	-	-	-	0.33	-
	AF_On_75pc	-	-	-			0.63	0.78	0.83	-	-	-	0.29	-
Recall	AF_Off	0.69	0.94	0.97	1.00	1.00	0.63	0.97	0.93	1.00	0.95	0.98	0.98	0.79
	AF_Off_Fault	0.79	0.82	1.00	1.00	1.00	0.67	1.00	1.00	1.00	0.94	0.89	0.92	0.72
	AF_On	0.32	0.30	0.51	0.52	0.64	0.37	0.53	0.74	0.60	0.79	0.85	0.78	0.55
	AF_On_Fault	0.89	0.28	0.52	0.60	0.58	0.20	0.41	0.70	0.70	0.85	0.80	0.62	0.66
	AF_On_Degr	-	0.58	0.78	0.77	0.91	-	-	-	0.45	0.22	0.35	-	0.26
	AF_On_25pc	-	-	-			0.20	0.51	0.82	-	-	-	0.28	-
	AF_On_50pc	-	-	-			0.20	0.40	0.58	-	-	-	0.31	-
	AF_On_75pc	-	-	-			0.29	0.63	0.68	-	-	-	0.22	-

approach, and the scenarios with the Reduced feature setup are not included. Regarding the RF hyperparameters setup, we ran an initial study using several randomly generated subsets of features to identify the values of the hyperparameters optimizing the F1-score. This study shows an optimal hyperparameters setup with the number of trees of 100 (an increase up to 300 does not improve the performance), the maximum depth of the tree of 5 (lower values tend to cause overfitting), the minimum number of samples required to split an internal node of 5, and Shannon entropy as a criterion to measure the quality of a split. The final model training is instead performed including all the features. This configuration showed better performance compared to the random pick of a subset of features of the size of square root or $log2$ of the total number of features.

Having a number of features considerably higher than the number of samples, a condition not ideal for the RF method, we investigate if another classifier can perform better than RF. We selected the Ridge regression classifier with Cross Validation, a linear classifier tested in the development of both ROCKET (Dempster et al., 2020) and MiniRocket (Dempster et al., 2021).

https://doi.org/10.5194/wes-2023-24
Preprint. Discussion started: 11 May 2023

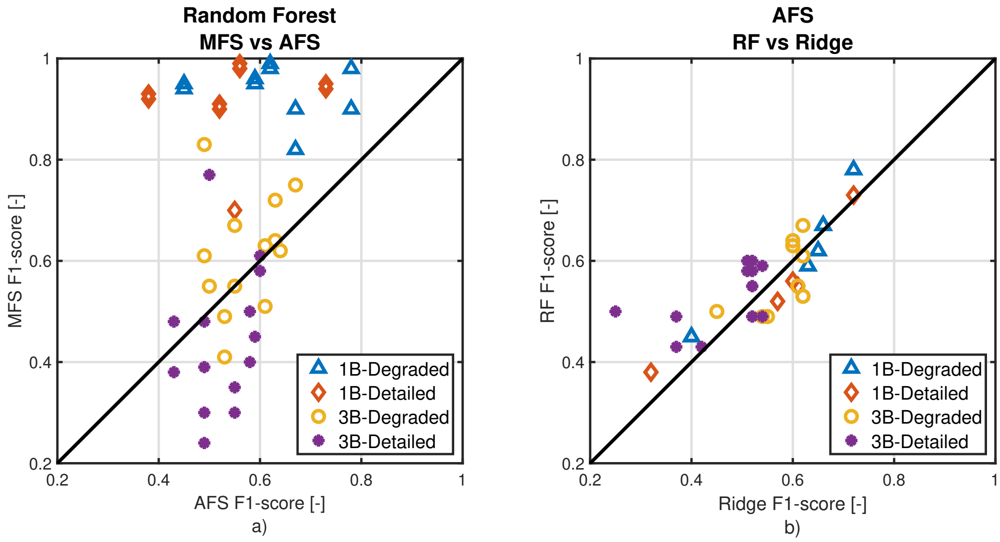

Figure 6. a) Comparison between the MFS RF F1-scores and the MFS RF F1-scores of the different Degraded and Detailed flap health scenarios. b) Comparison between the AFS RF F1-scores and the AFS Ridge F1-scores of the different Degraded and Detailed flap health scenarios.

5.1 Detection of asymmetric fault

The performances of models trained with the RF classifier for the asymmetric fault scenarios described in Table 2 are shown in Table 3, together with the results from the MFS approach. Table 4 collects Precision and Recall values of the AFlap health states for some specific asymmetric fault scenarios of the RF models.

In NPP, AFS RF shows low performance when trained to detect the Degraded health states for all the wind speeds (scenario 1BN_B1) with an F1-score of 0.67. The model can correctly classify the AF_Off and AF_Off_Fault states but cannot classify the other AFlap health states, as indicated by the Recall and Precision values. When we train the classifiers for the Detailed health states (scenario 1BN_C1), performance decreases with an F1-score of 0.55. Also, for this scenario, the models can adequately classify AF_Off and AF_Off_Fault states but fail with the other states. Performances slightly increase when we split the training into different wind speed ranges. AFS RF achieves the highest performance in evaluating the Degraded health states (scenario 1BN_B2) around rated wind speed with an F1-score of 0.78. For the other wind speed ranges, the F1-score stays around 0.6. Similar results are achieved for the Detailed health states (scenario 1BN_C2), where AFS RF achieves a max F1-score of 0.73 at RT and not higher than 0.56 in the other wind speed ranges. Looking at the results in PS, the RF classifier performs poorly in identifying Degraded and Detailed health states (scenario 1BP_B1 and 1BP_C1, respectively) with a max F1-score of 0.45.

Figure 6 compares the F1-scores from AFS RF with the scores from AFS Ridge. The Ridge classifier achieves similar results

https://doi.org/10.5194/wes-2023-24
Preprint. Discussion started: 11 May 2023

compared to RF for Degraded and Detailed flap health states in the 1B case. Also, the Precision and Recall values of the Ridge models are close to the values of the RF models of the corresponding scenarios. For brevity, we have not included them in this paper.

5.2 Detection of symmetric fault

The performances of models trained with the RF classifier for the symmetric fault scenarios described in Table 2 are shown in Table 5, together with the results from the MFS approach. Precision and Recall values of the AFlap health states for some specific asymmetric fault scenario models are collected in Table 6.

In NPP, AFS RF shows low performance when trained to detect the Degraded health states (scenario 3BN_B2) for different wind speed ranges. The F1-score is between 0.53 at BR and 0.63 at AR. Similarly to what was observed in the asymmetric fault, the models can detect most of the AF_Off and AF_Off_Fault states properly but cannot classify the other AFlap health states. Reducing the width of the wind speed ranges (scenario 3BN_B3) mainly reduces the performance, especially for low and high wind speeds, except at ARa, where the F1-score increases up to 0.67. Looking at the Detailed health states for the three wind seed ranges (scenario 3BN_C2), the F1-score rises from 0.49 at BR to 0.58 at AR. Similarly to the Degraded flap health states, reducing the width of the wind speed ranges (scenario 3BN_C3) does reduce the performance, especially for low or high wind speeds. Like the previous scenarios, the models have high Recall and Precision values for AF_Off and AF_Off_Fault states and low values for the other health states.

Looking at the results in PS, AFS RF classifiers perform poorly in identifying Degraded and Detailed health states (scenario 1BP_B1 and 1BP_C1 respectively) with a max F1-score of 0.5. Also, the ability to correctly classify AF_Off and AF_Off_Fault states is consistently reduced with both Recall and Precision below 0.8.

Similarly to the asymmetrical case, the Ridge classifier achieves similar results to RF for both Degraded and Detailed flap health states in the 3B case. Figure 6 shows that AFS RF performs slightly better than the Ridge classifier for the Detailed flap health states.

6 Discussion

6.1 Manual feature selection with random forest

The results described in Section 4.1 show that the manual feature selection approach with a random forest classifier can correctly classify the AFlap health states in the case of asymmetric flap fault 1B. In normal power production, Degraded and Detailed health states are correctly classified, and the performance increases when splitting the training into three wind speed ranges. This result supports our initial hypothesis that as a WT operates differently at different wind speed ranges, models trained for specific wind ranges perform better than a single model trained for all wind speeds. Notably, less than 20 features are needed for the models, a small fraction of the around 400 provided at the beginning of the training. This number can be further reduced to 10 or less by removing the Catch22 features without significantly reducing the models' performance. Even

https://doi.org/10.5194/wes-2023-24
Preprint. Discussion started: 11 May 2023

if few features are specific to some scenarios, all scenarios share the blade-to-blade differences of the mean blade root bending moment (mainly of flapwise bending moment), followed by the mean value of WT performance indicators like pitch angle, generator power, rotor speed, or blade root bending moments. This sounds logical since an asymmetrical flap fault among the different blades should result in a relevant difference in the blades' loading. The blade-to-blade load difference channels should collect this load imbalance. Furthermore, the blade imbalance is a function of the WT operational working state that the models most probably identify with the WT performance indicator features. Also, the models need fewer features at above rated wind speed, where generator power and rotor speed are almost constant, and the blade-to-blade load difference is most likely less impacted by them. Looking at pre-startup operation, both Degraded and Detailed health states are correctly classified and the Catch22 features can be omitted without reducing performance, as experienced in NPP. The models need more features than the NPP scenarios, with still blade-to-blade load difference as main features followed by mean values of the blade loads. Generator power and rotor speed are no longer relevant, being almost null in the idling state.

Regarding the Primary health states detection, the models obtained with MFS show, on one side, high performance in identifying the four Primary health states in both NPP and PS, but on the other side, they cannot account properly for the degradation of the AFlap performance. Since this degradation is likely to happen in the WT lifetime, we think these models can lead to some significant misclassification and we do not recommend them for field application.

In the case of a symmetric flap fault 3B, the MFS approach fails to correctly classify all the tested AFlap health states in both NPP and PS operation states. Increasing the model complexity or reducing the wind range width improves the performance negligibly, and the only case with an acceptable F1-score is the Degraded health states at high wind speeds (ARb). Looking at the selected features helps to understand the reasons for the misclassification. The blade-to-blade features are no longer present, replaced by several features related to single-blade loading, tower top accelerations, and rotor speed. This result confirms that the blade-to-blade loads no longer contain any flap fault information in the symmetric fault scenario, where the flap fails symmetrically in all three blades. Therefore, the RF models try to estimate the AFlap health states from the features of other channels, like blade loads. The failure to obtain good performance means the channels used in training do not have sufficient information to identify the AFlap health states, and more signals are needed to achieve it. A possible solution to properly detect and classify AFlap health states in the 3B condition is to transform it into an asymmetrical case. This transformation can be achieved with a flap check routine that activates the flap one blade at a time, which is like a 1B condition where the RF models can accurately estimate the flap health states.

6.2 Automatic feature selection with random forest and ridge classifier

The results described in Section 5 show that the automatic feature selection approach with a random forest classifier cannot correctly classify the AFlap health states for both asymmetric and symmetric flap fault cases. The trained models do not reach an F1-score higher than 0.8 in 1B scenarios and higher than 0.7 in 3B scenarios. Figure 6 compares the F1-scores between MFS and AFS RF models, with the MFS models outperforming the AFS models in the 1B scenarios. In the 3B scenarios, AFS RF models perform slightly better, especially for the Detailed flap health states. As shown in Figure 6, for the 1B scenarios, AFS Ridge models perform similarly to the AFS RF models in 1B cases and slightly worst in the 3B cases. The overall

https://doi.org/10.5194/wes-2023-24
Preprint. Discussion started: 11 May 2023

performances of the AFS models need to be improved for the AFS models to be implemented in detecting all the AFlap health states. However, for the NPP operation state, the AFS models can correctly identify the AF_Off and AF_OFF_Fault flap health states from the other states with Precision and Recall above 0.9. If these two states are relevant to the WT design, the AFS models can be implemented to detect these two specific flap health states. Furthermore, this capability shows that the AFS approach has some potential that can be further explored with other ML techniques like, for example, Multirocket (MiniRocket evolution) or HYDRA.

7 Conclusions

In this paper, we investigated two approaches to identify the health state of a WT's active trailing edge flaps. These approaches do not rely on specific sensors designated for AFlap's health monitoring but only on sensors commonly available on all commercial wind turbines. Both approaches are based on multivariate time-series classification methods. The first method (MFS) uses manual feature engineering in combination with a random forest classifier. The second method (AFS) creates the feature vectors from MTS data by passing the inputs through multiple random convolutional kernels in combination with a random forest classifier. We trained both methods to classify combinations of seven AFlap health states for a WT operating in normal power production and pre-startup. We analyzed asymmetrical flap faults, with the flap health states applied to only one blade, and symmetrical flap faults, where the flap health states were applied to all three blades. The study is based on a pool of aeroelastic simulations of a WT equipped with an active flap. These simulations were performed with a broad set of environmental conditions to account for the variability due to external weather conditions in the model's training. To keep the approach as general as possible, we focused on identifying the AFlap health state when the flap is in stationary actuation positions. This approach keeps the detection system independent from any specific AFlap controller strategy, AFlap system design, or fault dynamics. The underlying idea is to integrate the monitoring system in an AFlap status check routine running for several minutes where the performance of the stationary flap is verified.

In this paper, we showed that the MFS method could classify the different combinations of AFlap health states in the case of asymmetrical flap faults. The MFS method is reliable when the WT operates in normal power production and pre-startup, achieving an F1-score higher than 0.9. Essential features to achieve this result are the blade-to-blade differences of the mean blade root loads.

Instead, the MFS method failed to classify the AFlap health states in the case of symmetrical flap fault. This failure is likely due to the channels used for the training not providing sufficient information about the flap fault. To avoid adding other sensor signals to the model, we suggest transforming the symmetrical flap fault detection into an asymmetrical one. For example, a flap check routine can activate the flap one blade at a time, generating a temporary asymmetrical flap activation that the MFS methodology can monitor.

Furthermore, we showed that the AFS method fails to classify most AFlap health states in asymmetrical and symmetrical flap faults. However, for both cases, with the wind turbine in normal power production, the AFS method can be used to identify two specific flap health states.

https://doi.org/10.5194/wes-2023-24
Preprint. Discussion started: 11 May 2023

We also tested a Ridge classifier in the AFS method, obtaining a similar performance to the random forest classifier with a consistently lower training time.

As future developments, we suggest further exploring the AFS method by applying different and more performing convolutional techniques. It is also of extreme interest to validate the capability of the MFS method with data from an actual wind turbine, to which the models can be adapted via transfer learning techniques.

Author contributions. AG and IA conceptualized and designed the study. AG designed the objectives, performed analysis, and wrote the original draft paper. AI supported the methodology, the analysis and reviewed and edited the whole paper.

Competing interests. AG is hired by Siemens Gamesa Renewable Energy, company that is developing the flap technology used as reference in the paper.

Acknowledgements. The authors thank Gregory Duthé and Eleni Chatzi for their support. This research was partially funded by Danmarks Innovationsfond, Case no. 9065-00243B, PhD Title: "Advanced model development and validation of Wind Turbine Active Flap system" and by Otto Mønsteds Fond, application file number 22-70-0210. The authors also thank xxx and xxx anonymous reviewers whose comments and suggestions helped improve and clarify this manuscript.

References

Abdallah, Imad Chatzi, E.: Probabilistic fault diagnostics using ensemble time-varying decision tree learning, https://doi.org/10.5281/zenodo.3474633, 2019.

Badihi, H., Zhang, Y., Jiang, B., Pillay, P., and Rakheja, S.: A Comprehensive Review on Signal-Based and Model-Based Condition Monitoring of Wind Turbines: Fault Diagnosis and Lifetime Prognosis, Proceedings of the IEEE, 110, 754–806, https://doi.org/10.1109/JPROC.2022.3171691, 2022.

Barlas, T., Pettas, V., Gertz, D., and Madsen, H. A.: Extreme load alleviation using industrial implementation of active trailing edge flaps in a full design load basis, in: Journal of Physics: Conference Series, vol. 753, Institute of Physics Publishing, https://doi.org/10.1088/1742-6596/753/4/042001, 2016.

Bir, G.: Multi-blade coordinate transformation and its application to wind turbine analysis, 46th Aiaa Aerospace Sciences Meeting and Exhibit, pp. 2008–1300, 2008.

Breiman, L.: Bagging predictors, Mach. Learn., 24, 123–140, 1996.

Carrasco Kind, M. and Brunner, R.: TPZ : Photometric redshift PDFs and ancillary information by using prediction trees and random forests, Monthly Notices of the Royal Astronomical Society, 432, 1483–1501, 2013.

Cho, S., Gao, Z., and Moan, T.: Model-based fault detection, fault isolation and fault-tolerant control of a blade pitch system in floating wind turbines, Renewable energy, 120, 306–321, 2018.

de Azevedo, H. D. M., Araújo, A. M., and Bouchonneau, N.: A review of wind turbine bearing condition monitoring: State of the art and challenges, Renewable and Sustainable Energy Reviews, 56, 368–379, 2016.

Dempster, A., Petitjean, F., and Webb, G. I.: ROCKET: exceptionally fast and accurate time series classification using random convolutional kernels, Data Mining and Knowledge Discovery, 34, 1454–1495, 2020.

Dempster, A., Schmidt, D. F., and Webb, G. I.: Minirocket: A very fast (almost) deterministic transform for time series classification, in: Proceedings of the 27th ACM SIGKDD conference on knowledge discovery & data mining, pp. 248–257, 2021.

Dimitrov, N., Natarajan, A., and Kelly, M.: Model of wind shear conditional on turbulence and its impact on wind turbine loads, Wind Energy, 18, 1917–1931, https://doi.org/10.1002/we.1797, 2015.

Duthé, G., Abdallah, I., Barber, S., and Chatzi, E.: Modeling and Monitoring Erosion of the Leading Edge of Wind Turbine Blades, Energies, 14, https://doi.org/10.3390/en14217262, 2021.

Fisker Skjoldan, P.: Aeroelastic modal dynamics of wind turbines including anisotropic effects, Risø National Laboratory, 2011.

Gamberini, A., Gomez Gonzalez, A., and Barlas, T.: Aeroelastic model validation of an Active Trailing Edge Flap System tested on a 4.3 MW wind turbine, Journal of Physics. Conference Series, 2265, 032 014, https://doi.org/10.1088/1742-6596/2265/3/032014, 2022.

García Márquez, F. P. and Peinado Gonzalo, A.: A Comprehensive Review of Artificial Intelligence and Wind Energy, Archives of Computational Methods in Engineering, 29, 2935–2958, https://doi.org/10.1007/s11831-021-09678-4, 2022.

Gomez Gonzalez, A., Enevoldsen, P. B., Madsen, H. A., and Barlas, A.: Test of an active flap system on a 4.3 MW wind turbine, TORQUE 2022, 2022.

Gálvez-Carrillo, M. and Kinnaert, M.: Sensor fault detection and isolation in doubly-fed induction generators accounting for parameter variations, Renewable Energy, 36, 1447–1457, https://doi.org/https://doi.org/10.1016/j.renene.2010.10.021, 2011.

IEC: Standard IEC 61400-1: 2019, Wind Energy Generation System—Part 1: Design Requirements, 1, 2019.

https://doi.org/10.5194/wes-2023-24
Preprint. Discussion started: 11 May 2023

Lubba, C. H., Sethi, S. S., Knaute, P., Schultz, S. R., Fulcher, B. D., and Jones, N. S.: catch22: CAnonical Time-series CHaracteristics: Selected through highly comparative time-series analysis, Data Mining and Knowledge Discovery, 33, 1821–1852, https://doi.org/10.1007/s10618-019-00647-x, 2019.

Oguiza, I.: tsai - A state-of-the-art deep learning library for time series and sequential data, Github, https://github.com/timeseriesAI/tsai, 2022.

Pedregosa, F., Varoquaux, G., Gramfort, A., Michel, V., Thirion, B., Grisel, O., Blondel, M., Prettenhofer, P., Weiss, R., Dubourg, V., Vanderplas, J., Passos, A., Cournapeau, D., Brucher, M., Perrot, M., and Duchesnay, E.: Scikit-learn: Machine Learning in Python, Journal of Machine Learning Research, 12, 2825–2830, 2011.

Pettas, V., Barlas, T., Gertz, D., and Madsen, H. A.: Power performance optimization and loads alleviation with active flaps using individual flap control, in: Journal of Physics: Conference Series, vol. 749, p. 012010, Institute of Physics Publishing, https://doi.org/10.1088/1742-6596/749/1/012010, 2016.

Stetco, A., Dinmohammadi, F., Zhao, X., Robu, V., Flynn, D., Barnes, M., Keane, J., and Nenadic, G.: Machine learning methods for wind turbine condition monitoring: A review, Renewable Energy, 133, 620–635, https://doi.org/10.1016/j.renene.2018.10.047, 2019.